

อิทธิพลของพีระโคเซอร์ต่อการสังเคราะห์และสมบัติการดูดซับโลหะของซิลิกาโดยดัวซีฟเบส



นางสาวกนกกาญจน์ สกุลณี

สถาบันวิทยบริการ

จุฬาลงกรณ์มหาวิทยาลัย

วิทยานิพนธ์นี้เป็นส่วนหนึ่งของการศึกษาตามหลักสูตรปริญญาวิทยาศาสตรมหาบัณฑิต

สาขาวิชาปิโตรเคมีและวิทยาศาสตร์พอลิเมอร์

คณะวิทยาศาสตร์ จุฬาลงกรณ์มหาวิทยาลัย

ปีการศึกษา 2550

ลิขสิทธิ์ของจุฬาลงกรณ์มหาวิทยาลัย

**INFLUENCE OF PRECURSORS ON SYNTHESIS AND METAL SORPTION
PROPERTIES OF SCHIFF'S BASE DOPED SILICA**


Miss Kanokkarn Skulnee



**A Thesis Submitted in Partial Fulfillment of the Requirements
for the Degree of Master of Science Program in Petrochemistry and Polymer Science
Faculty of Science
Chulalongkorn University
Academic Year 2007
Copyright of Chulalongkorn University**


Thesis Title INFLUENCE OF PRECURSORS ON SYNTHESIS AND
METAL SORPTION PROPERTIES OF SCHIFF'S BASE
DOPED SILICA.
By Miss Konokkarn Skulnee
Field of study Petrochemistry and Polymer Science
Thesis Advisor Amarawan Intasiri, Ph.D.


Accepted by the Faculty of Science, Chulalongkorn University in
Partial Fulfillment of the Requirements for the Master's Degree


.....Dean of the Faculty of Science
(Professor Supot Hannongbua, Ph.D.)

THESIS COMMITTEE


.....Chairman
(Professor Pattarapan Prasassarakich, Ph.D.)


.....Thesis Advisor
(Amarawan Intasiri, Ph.D.)


.....Member
(Associate Professor Wimonrat Trakarnpruk, Ph.D.)


.....Member
(Assistant Professor Yongsak Sritana-anant, Ph.D.)

กนกกาญจน์ สกุลณี : อิทธิพลของพรีเคอร์เซอร์ต่อการสังเคราะห์และสมบัติการดูดซับโลหะของซิลิกาโดปด้วยชิฟเบส (INFLUENCE OF PRECURSORS ON SYNTHESIS AND METAL SORPTION PROPERTIES OF SCHIFF'S BASE DOPED SILICA.)
 อ.ที่ปรึกษา : ดร.อมรราวรณ อินทศิริ, 98 หน้า.

งานวิจัยนี้มีวัตถุประสงค์เพื่อศึกษาอิทธิพลของสารตั้งต้นซิลิกาต่อการสังเคราะห์และสมบัติในการดูดซับโลหะของเมโซพอร์ซิลิกาโดปด้วยชิฟเบส พรีเคอร์เซอร์ชนิดต่างๆที่ทำการศึกษา ได้แก่ เทตระเอทอกซีไฮเลน (TEOS), เมโซพอร์ซิลิกาที่ผ่านการเผาที่อุณหภูมิสูง, ซิลิกาเจล 60, ไวนิลไตรเอทอกซีไฮเลน (VTES), โพรพิลไตรเมทอกซีไฮเลน (PTMS) และ เอทิลไตรเอทอกซีไฮเลน (ETES) ชิฟเบสหลายชนิดชื่อว่า salen, saltn และ haen ถูกใช้เป็นโมเลกุลในการโดป ซิลิกาโดปด้วยชิฟเบสที่สังเคราะห์จาก TEOS, เมโซพอร์ซิลิกาที่ผ่านการเผาที่อุณหภูมิสูง, VTES, PTMS และ ETES มีพื้นที่ผิวสูง มีการกระจายของรูพรุนในช่วงที่แคบ มีโครงสร้างเป็นผลึก และมีรูปร่างเป็นทรงกลม สมบัติด้านการสกัดของซิลิกาที่ปรับปรุงแล้วต่อ Cu(II), Fe(III) และ Ni(II) ได้รับการตรวจหา อิทธิพลของอัตราส่วนของชิฟเบสต่อ TEOS ที่มีต่อการสังเคราะห์และสมบัติด้านการดูดซับโลหะได้รับการตรวจสอบ ปริมาณสูงสุดของชิฟเบสที่สามารถใส่เข้าไปได้พบว่ามีค่า 1.00, 0.86 และ 0.96 มิลลิโมลต่อกรัม สำหรับซิลิกาโดปด้วย salen, saltn และ haen ตามลำดับ การสกัด Fe(III) เพิ่มขึ้นตามการเพิ่มของปริมาณชิฟเบสที่อยู่ในซิลิกา การศึกษาการสกัดขั้นลึกได้ทำกับซิลิกาโดปด้วย salen ที่สังเคราะห์จาก TEOS และซิลิกาที่ผ่านการเผาที่อุณหภูมิสูงเนื่องจากสมบัติทางกายภาพและทางเคมีที่ดีเยี่ยมของซิลิกาเหล่านี้ การศึกษาจลนพลศาสตร์การดูดซับของซิลิกาเหล่านี้พบว่าสอดคล้องกับแบบจำลอง pseudo-second-order ไอโซเทอมของการดูดซับสอดคล้องที่สุดกับแบบจำลอง Langmuir ความสามารถสูงสุดในการสกัด Cu(II) และ Fe(III) ของซิลิกาโดปด้วย salen ที่สังเคราะห์จากซิลิกาที่ผ่านการเผาที่อุณหภูมิสูงพบว่ามีค่า 18.42 และ 20.70 มิลลิกรัมต่อกรัมตามลำดับ การนำกลับมาใช้ใหม่ของซิลิกาเหล่านี้ได้ถูกประเมินการดูดซับและการคายโลหะต่อเนื่องกันสามารถรอบด้วยเช่นกัน

สาขาวิชา..ปิโตรเคมีและวิทยาศาสตร์พอลิเมอร์...ลายมือชื่อนิสิต.....กนกกาญจน์ สกุลณี
 ปีการศึกษา.....2550.....ลายมือชื่ออาจารย์ที่ปรึกษา.....อมรราวรณ อินทศิริ

477 25831 23 : MAJOR PETROCHEMISTRY AND POLYMER SCIENCE

KEY WORD: SCHIFF'S BASE / MESOPOROUS SILICA / DOPED SILICA / METAL EXTRACTION

KANOKKARN SKULNEE : INFLUENCE OF PRECURSORS ON SYNTHESIS AND METAL SORPTION PROPERTIES OF SCHIFF'S BASE DOPED SILICA. THESIS ADVISOR : AMARAWAN INTASIRI, Ph.D., 98 PP.

This work is aimed at investigating the influence of silica precursor on the synthesis and metal sorption properties of Schiff's base doped mesoporous silica. Different silica precursors including TEOS, calcined mesoporous silica, silica gel 60, VTES, PTMS and ETES were used. Various Schiff's bases namely, salen, saltn and haen were used as doping molecules. The Schiff's base doped mesoporous silica synthesized from TEOS, calcined mesoporous silica, VTES, PTMS, and ETES had large surface area, narrow pore size distribution, crystalline structure, and spherical shape. The extraction properties of the modified silica towards Cu(II), Fe(III) and Ni(II) were determined. The influence of the ratio of Schiff's base/TEOS on the synthesis and extraction properties were investigated. The maximum amounts of incorporating Schiff's base were found to be 1.00, 0.86, and 0.96 mmol g⁻¹ for salen, saltn, and haen doped mesoporous silica, respectively. The extraction of Fe(III) was increased with the increase of amount of incorporated Schiff's base. The profound extraction studies were performed on the salen doped mesoporous silica synthesized from TEOS or calcined mesoporous silica due to their excellent physical and chemical properties. Adsorption kinetic of these sorbents was consistent with the pseudo-second order model. The adsorption isotherm was best fitted to the Langmuir model. The Cu(II) and Fe(III) maximum extraction capacity of salen doped mesoporous silica synthesized from calcined mesoporous silica was found to be 18.42 and 20.70 mg g⁻¹ respectively. The reusability of the modified silica was also assessed for three successive adsorption-desorption cycles.

Field of study..Petrochemistry and Polymer Science..Student's signature *Kanokkarn Skulnee*
Academic year.....2007.....Advisor's signature *Amarawan Intasiri*

ACKNOWLEDGEMENTS

I would like to express my sincerest appreciation and deepest thankfulness to my thesis advisor, Dr. Amarawan Intasiri for her discerning suggestion, encouragement, sacrifice, and forbearance through my course of study. Thanks are also extended to Prof. Dr. Pattarapan Prasassarakich, Assoc. Prof. Dr. Wimonrat Trakarnpruk and Asst. Prof. Dr. Yongsak Sritana-anant for being members of the thesis committee and for their worthy comments and suggestions.

I gratefully acknowledge the Office of Commission for Higher Education-CU Graduate Thesis Grant for their financial supports. Research facilities provided by the Solid-Phase Extraction Research Group and the Organic Synthesis Research Unit (OSRU) of Chulalongkorn University are greatly appreciated.

Finally, I would like to express my gratitude to family members for their love, understanding and great support throughout my study. Also, special thanks are expanded to my friends for friendship, encouragements and cheerful moral support.



สถาบันวิทยบริการ
จุฬาลงกรณ์มหาวิทยาลัย

CONTENTS

	PAGE
ABSTRACT (IN THAI)	iv
ABSTRACT (IN ENGLISH)	v
ACKNOWLEDGEMENTS	vi
CONTENTS	vii
LIST OF FIGURES	xi
LIST OF TABLES	xvi
LIST OF ABBREVIATION	xviii
CHAPTER I : INTRODUCTION	1
CHAPTER II : THEORY AND LITERATURE REVIEWS	2
2.1. Silica.....	2
2.1.1. Generality.....	2
2.1.2. Synthesis of silica.....	3
2.1.3. Mesoporous silica.....	4
2.1.4. Functionalization of silica.....	6
2.2. Characterization of materials.....	6
2.2.1. Characterization of porous structure.....	6
2.2.1.1. Generality.....	6
2.2.1.2. Classification of adsorption isotherm.....	7
2.2.1.3. Adsorption hysteresis.....	8
2.2.1.4. Application of Brunauer-Emmett-Teller method (BET).....	9
2.2.1.5. Pore volume and pore size distribution.....	9
2.2.2. X-ray diffraction.....	10
2.2.3. Scanning electron microscope.....	10
2.3. Determination of metal sorption properties of materials.....	12
2.4. Schiff's base molecules.....	13
2.5. Literature reviews.....	14
2.6. Objective.....	16
CHAPTER III : EXPERIMENTS	17
3.1. Reagents.....	17
3.2. Apparatus.....	17

	PAGE
3.3. Experimentals.....	18
3.3.1. Synthesis of materials.....	18
3.3.2. Characterization of materials.....	18
3.3.2.1. Determination of organic matters in silica.....	18
3.3.2.2. Determination of accessible Schiff's bases.....	19
3.3.2.3. Determination of crystallinity.....	19
3.3.2.4. Determination of morphology.....	19
3.3.2.5. Investigation of functional group of organic and inorganic molecules in mesoporous silica	19
3.3.2.6. Determination of surface area and pore size.....	19
3.4. Extraction properties of materials.....	20
CHAPTER IV : RESULTS AND DISCUSSION.....	21
4.1. Synthesis and properties of silica synthesized from single silica precursor.....	21
4.1.1. Characterization of materials.....	22
4.1.1.1. Organic matters contents in silica.....	22
4.1.1.2. Determination of accessible Schiff's base.....	24
4.1.1.3. Investigation of organic molecules using FTIR spectroscopy.....	25
4.1.1.4. Determination of crystallinity.....	28
4.1.1.5. Morphology of materials.....	30
4.1.1.6. Determination of surface area and pore size.....	32
4.1.2. Extraction properties of materials.....	36
4.1.2.1. Extraction of Cu(II).....	36
4.1.2.2. Extraction of Fe(III).....	37
4.1.2.3. Extraction of Ni(II).....	38
4.2. Synthesis and properties of silica synthesized from TEOS and co- precursor.....	39
4.2.1. Characterization of materials.....	40
4.2.1.1. Organic matters contents in silica.....	40

	PAGE
4.2.1.2. Determination of accessible Schiff's base.....	41
4.2.1.3. Investigation of organic molecules using FTIR spectroscopy.....	42
4.2.1.4. Determination of crystallinity.....	44
4.2.1.5. Morphology of materials.....	46
4.2.1.6. Determination of surface area and pore size.....	48
4.2.2. Extraction properties of materials.....	51
4.2.2.1. Extraction of Cu(II).....	51
4.2.2.2. Extraction of Fe(III).....	53
4.2.2.3. Extraction of Ni(II).....	54
4.3. Influence of Schiff's base content on the extraction properties of materials of Schiff's base doped silica.....	55
4.3.1. Synthesis of materials.....	55
4.3.2. Characterization of materials.....	56
4.3.2.1. Organic matters contents in silica.....	56
4.3.3. Extraction properties of materials.....	56
4.3.3.1. Extraction of Fe(III).....	56
4.4. Profound extraction study on appropriated Schiff's base modified sorbents.....	57
4.4.1. Reproducibility.....	58
4.4.2. Kinetic extraction.....	59
4.4.3. Effect of salt presence in metal solution.....	62
4.4.4. Determination of sorbent capacity.....	64
4.4.5. Selectivity.....	67
4.4.6. Effect of amount of silica.....	68
4.4.7. Desorption and reusability.....	69
CHAPTER V : CONCLUSION.....	71
REFERENCES.....	73
APPENDICES.....	79
APPENDIX I Synthesis of Schiff's base ligands.....	80
APPENDIX II ¹ H NMR spectra of Schiff's base ligand.....	82

	PAGE
APPENDIX III Synthesis of calcined mesoporous silica.....	84
APPENDIX IV The XRD pattern and N ₂ sorption of calcined mesoporous silica and silica gel 60.....	85
APPENDIX V Calculation of organic matter contents in mesoporous silica.....	87
CURRICULUM VITAE.....	98



สถาบันวิทยบริการ
จุฬาลงกรณ์มหาวิทยาลัย

LIST OF FIGURES

FIGURES	PAGE
2.1 Structure of silica	2
2.2 Phase formation of mesoporous materials.....	5
2.3 Proposed formation mechanistic pathways.....	5
2.4 Types of pores.....	7
2.5 Types of adsorption isotherm.....	8
2.6 The four hysteresis shapes of adsorption isotherm.....	8
2.7 Diffraction of X-ray by a crystal.....	10
2.8 The schematic for a generic SEM.....	11
2.9 Structure of Schiff's bases used in this research.....	14
3.1 The heating program for the calcinations process.....	19
4.1 The percentage of incorporated Schiff's base in Schiff's base doped mesoporous silica synthesized by different type of single silica precursors.....	22
4.2 Percentage of accessible Schiff's base in modified silica synthesized from various silica precursors when C ₂ H ₅ OH : H ₂ O equal 9:1 was used as extracted solvent.....	25
4.3 FT-IR spectra of CTAB and non-doped mesoporous silica synthesized from various silica precursors: (a) TEOS, (b) calcined mesoporous silica and (c) silica gel 60.....	26
4.4 FT-IR spectra of salen and salen doped mesoporous silica synthesized from various precursors: (a) TEOS, (b) calcined mesoporous silica and (c) silica gel 60.....	26
4.5 FT-IR spectra of salth and saltn doped mesoporous silica synthesized from various precursors: (a) TEOS, (b) calcined mesoporous silica and (c) silica gel 60.....	27
4.6 FT-IR spectra of haen and haen doped mesoporous silica synthesized from various precursors: (a) TEOS, (b) calcined mesoporous silica and (c) silica gel 60.....	27
4.7 XRD patterns of silica synthesized from various single silica precursors: (A) TEOS, (B) calcined mesoporous silica and (C) silica gel 60.....	29

FIGURES	PAGE
4.8 SEM images of silica synthesized from TEOS:(a) non-doped, (b) salen doped, (c) saltn doped and (d) haen doped mesoporous silica.....	31
4.9 SEM images of silica synthesized from calcined mesoporous silica: (a) non-doped, (b) salen doped, (c) saltn doped and (d) haen doped mesoporous silica.....	31
4.10 SEM images of silica synthesized from silica gel 60: (a) non-doped, (b) salen doped, (c) saltn doped and (d) haen doped mesoporous silica.....	32
4.11 Nitrogen sorption isotherms of silica synthesized from various precursors: (a) TEOS (b) calcined mesoporous silica and (c) silica gel 60	34
4.12 Pore size distribution of silica synthesized from various precursors: (a) TEOS (b) calcined mesoporous silica and (c) silica gel 60.....	35
4.13 The amount of Cu(II) extracted by Schiff's base doped mesoporous silica: (a) salen doped, (b) saltn doped and (c) haen doped mesoporous silica.....	36
4.14 The amount of Fe(III) extracted by Schiff's base doped mesoporous silica: (a) salen doped, (b) saltn doped and (c) haen doped mesoporous silica.....	38
4.15 The amount of Ni(II) extracted by Schiff's base doped mesoporous silica: (a) salen doped, (b) saltn doped and (c) haen doped mesoporous silica.....	39
4.16 The percentage of incorporated Schiff's base in Schiff's base doped mesoporous silica synthesized by TEOS and different type of co-precursors.....	40
4.17 Percentage of accessible Schiff's base in modified silica synthesized from TEOS and various co-precursors.....	42
4.18 FT-IR spectra of CTAB and non-doped mesoporous silica synthesized from TEOS and various co-precursors: (a) VTES, (b) ETES and (c) PTMS.....	42
4.19 FT-IR spectra of salen and salen doped mesoporous silica synthesized from TEOS and various co-precursors: (a) VTES, (b) ETES and (c) PTMS.....	43

FIGURES	PAGE
4.20 FT-IR spectra of salt _n and salt _n doped mesoporous silica synthesized from TEOS and various co-precursors: (a) VTES, (b) ETES and (c) PTMS.....	43
4.21 FT-IR spectra of haen and haen doped mesoporous silica synthesized from TEOS and various co-precursors: (a) VTES, (b) ETES and (c) PTMS.....	43
4.22 XRD patterns of silica synthesized from TEOS and various co-precursors: (A) VTES, (B) PTMS and (C) ETES.....	45
4.23 SEM images of silica synthesized from TEOS and VTES: (a) non-doped, (b) salen doped, (c) salt _n doped and (d) haen doped mesoporous silica....	46
4.24 SEM images of silica synthesized from TEOS and PTMS: (a) non-doped, (b) salen doped, (c) salt _n doped and (d) haen doped mesoporous silica.....	47
4.25 SEM images of silica synthesized from TEOS and ETES: (a) non-doped, (b) salen doped, (c) salt _n doped and (d) haen doped mesoporous silica....	47
4.26 Nitrogen sorption isotherm of silica synthesized from TEOS and various co-precursors: (a) VTES, (b) PTMS and (c) ETES.....	49
4.27 Pore size distribution of silica synthesized from TEOS and various co-precursors: (a) VTES, (b) PTMS and (c) ETES.....	50
4.28 The Cu(II) extracted by Schiff's base doped mesoporous silica synthesized from TEOS and various co-precursor: (a) salen doped, (b) salt _n doped and (c) haen doped.....	52
4.29 The Fe(III) extracted by Schiff's base doped mesoporous silica synthesized from TEOS and various co-precursor: (a) salen doped, (b) salt _n doped and (c) haen doped.....	53
4.30 The Ni(II) extracted by non-doped and Schiff's base doped mesoporous silica synthesized from TEOS and various co-precursor: (a) salen doped, (b) salt _n doped and (c) haen doped.....	54

FIGURES	PAGE
4.32 The Fe(III) extractability of Schiff's base doped mesoporous silica synthesized from various Schiff's base/TEOS mole ratios.....	57
4.33 The sorption rate of metal onto salen doped mesoporous silica synthesized from TEOS or calcined mesoporous silica: (a) Cu(II) extraction and (b) Fe(III) extraction.....	59
4.34 The intra-particle diffusion kinetic for adsorption of metals onto salen doped mesoporous silica synthesized from TEOS or calcined mesoporous silica: (a) Cu(II) extraction and (b) Fe(III) extraction.....	60
4.35 The pseudo-first-order kinetic for metal sorption of salen doped mesoporous silica synthesized from TEOS or calcined mesoporous silica: (a) Cu(II) extraction and (b) Fe(III) extraction.....	61
4.36 The pseudo-second-order kinetic for metal sorption of salen doped mesoporous silica synthesized from TEOS or calcined mesoporous silica: (a) Cu(II) extraction and (b) Fe(III) extraction.....	61
4.37 Effect of salt presence in the metal solution on the metal extraction: (a) Cu(II) extracted and (b) Fe(III) extracted.....	63
4.38 The amounts of metal extracted by the modified silica as a function of initial concentration of metal: (a) Cu(II) extracted and (b) Fe (III) extracted.....	64
4.39 Equilibrium adsorption isotherm of metal adsorption on salen doped mesoporous silica synthesized from TEOS or calcined mesoporous silica: (a) Cu (II) and (b) Fe(III).....	65
4.40 The linearization of Langmuier adsorption isotherm for metal adsorption by salen doped mesoporous silica synthesized from TEOS or calcined mesoporous silica: (a) Cu(II) adsorption and (b) Fe(III) adsorption.....	65
4.41 The linearization of Freundlich adsorption isotherm for metal adsorption by salen doped mesoporous silica synthesized from TEOS or calcined mesoporous silica: (a) Cu(II) adsorption and (b) Fe(III) adsorption.....	66
4.42 Effect of amount of salen doped mesoporous silica synthesized from different precursor on the metal extraction: (a) Cu(II) extracted and (b) Fe(III) extracted.....	68

FIGURES	PAGE
I.1 The structure of Schiff's base ligand.....	81
II.1 ¹ H NMR spectrum of Salen in CDCl ₃ at 400 MHz.....	82
II.2 ¹ H NMR spectrum of Saltn in CDCl ₃ at 400 MHz.....	82
II.3 ¹ H NMR spectrum of Haen in CDCl ₃ at 400 MHz.....	83
IV.1 The XRD patterns of (a) calcined mesoporous silica and (b) silica gel 60.	85
IV.2 N ₂ adsorption-desorption isotherms and pore-size distribution plot (insert) of (a) Calcined mesoporous silica and (b) Silica gel 60.....	85



สถาบันวิทยบริการ
จุฬาลงกรณ์มหาวิทยาลัย

LIST OF TABLES

TABLES	PAGE
4.1 The amount of incorporated Schiff's bases in each Schiff's base doped mesoporous silica synthesized from various types of single silica precursors.....	22
4.2 Organic matter contents in materials prepared from difference single silica precursors.....	23
4.3 The amount of accessible Schiff's base extracted from the Schiff's base doped mesoporous synthesized from TEOS.....	24
4.4 The XRD results of as-synthesized silica and their corresponding calcined silica.....	30
4.5 Characterizations results of the Schiff's base doped mesoporous silica synthesized from various precursors.....	33
4.6 The amount of incorporated Schiff's base in each Schiff's base doped mesoporous silica synthesized from TEOS and various co-precursors.....	39
4.7 Organic matter content in mesoporous silica prepared from TEOS and various co-precursors.....	41
4.8 XRD results of materials synthesized from TEOS and various co-precursors.....	44
4.9 Characterizations results of the materials synthesized from TEOS and various co-precursors.....	51
4.10 The amount of incorporated Schiff's bases in each Schiff's base doped mesoporous silica synthesized from various mole ratios of Schiff's base/TEOS.....	55
4.11 The organic matter contents in silica synthesized from different mole ratios of Schiff's base/TEOS.....	56
4.12 The reproducibility results of Fe(III) extracted by salen doped mesoporous silica synthesized from TEOS or calcined mesoporous silica	58
4.13 The comparison of kinetic models for the adsorption of Cu(II) onto the salen doped mesoporous silica synthesized from TEOS or calcined mesoporous silica.....	62

TABLES	PAGE
4.14 The comparison of kinetic models for the adsorption of Fe(III) onto the salen doped mesoporous silica synthesized from TEOS or calcined mesoporous silica.....	62
4.15 The experimental value of amount of adsorbed metal at equilibrium (q_e) by the salen doped mesoporous silica synthesized from TEOS or calcined mesoporous silica.....	62
4.16 Langmuir and Freundlich constants for the metal sorption of salen doped mesoporous silica synthesized from TEOS or calcined mesoporous silica	66
4.17 The amounts of each metal ion extracted from mixture solution using salen doped mesoporous silica synthesized from TEOS or calcined mesoporous silica as a sorbent.....	67
4.18 Effect of concentration of HNO_3 on the desorption of Fe(III) from salen doped mesoporous silica synthesized by TEOS	69
4.19 The amount of Fe(III) extracted by salen doped silica synthesized from TEOS or calcined mesoporous silica in each cycle	70
I.1 Starting substrate used for the synthesis of various Schiff's bases.....	80
IV.1 The textural properties of calcined mesoporous silica and silica gel 60....	86
V.1 The amount of starting materials for the synthesis of silica using TEOS as silica precursor.....	87
V.2 The amount of starting materials for the synthesis of silica using calcined mesoporous silica as silica precursor.....	89
V.3 The amount of starting materials for the synthesis of silica using silica gel 60 as silica precursor.....	90
V.4 The amount of starting materials for the synthesis of silica using TEOS and VTES as silica precursors.....	92
V.5 The amount of starting materials for the synthesis of silica using TEOS and PTMS as silica precursors.....	94
V.6 The amount of starting materials for the synthesis of silica using TEOS and ETES as silica precursors.....	96

LIST OF ABBREVIATIONS

APD	average pore diameter
BET	Brunauer-Emmet-Teller
BJH	Barrett-Joyner-Halenda
CTAB	cetyltrimethylammonium bromide
FT-IR	fourier-transform infrared spectroscopy
haen	2,2'-{ethane-1,2-diylbis[nitrilo(1 <i>E</i>)eth-1-yl-1-ylidene]}diphenol
salen	2,2'-{ethane-1,2-diylbis[nitrilo(<i>E</i>)methylidene]}diphenol
saltn	2,2'-{propane-1,3-diylbis[nitrilo(<i>E</i>)methylidene]}diphenol
IUPAC	International Union of Pure and Applied Chemistry
SEM	Scanning electron microscopy
SPE	solid-phase extraction
TEOS	tetraethylorthosilicate
XRD	X-ray diffraction



สถาบันวิทยบริการ
จุฬาลงกรณ์มหาวิทยาลัย

CHAPTER I

INTRODUCTION

Silica gel or silica is the most abundant material in the earth [1]. Silica is also widely used as sorbent material in chromatography and solid-phase extraction due to its several advantages which are superior to other materials. These features are including high chemical and thermal stability, good mechanical strength and strain or not swell in aqueous solution [2-3]. However, traditional silica has some common limitation such as lack of selectivity especially for trace metal extraction. Therefore, the modification of silica surface in order to be used as a sorbent for serving this purpose is a subject of considerable interest.

There are various synthetic routes to modified silica such as chemical immobilization (grafting), impregnation techniques and chemical doping. Among these methods, doping technique has gained much interest in the recent years. This method possesses several advantages such as easy preparation, low synthesis temperature, many delicate organic compounds could be entrapped and reduction of leaching of organic molecules [4]. For doping molecules, Schiff's bases are the attractive ligand due to their stable complex with various metals and they are also used as selective extraction reagents for several kinds of metal ions [5-7]. However the improvement of silica surface could be performed by the type of silica source as well. The many researchers reveal that the silica precursor can be influenced the physico-chemical and sorption properties of silica [8-9].

From the previous study on the synthesis of Schiff's base doped mesoporous silica, it was found that the amount of Schiff's base incorporated in the silica was limited. Furthermore, the synthesis was performed using only one type of silica source. Thus in this work, various parameters such as the type of silica precursor and the amount of Schiff's base used for the synthesis of such Schiff's base doped mesoporous silica were performed. Also, the physical and sorption properties of the synthesized silica were investigated. The most effective sorbent was then subjected to profound studies including kinetic extraction, selectivity, and reusability.

CHAPTER II

THEORY AND LITERATURE REVIEWS

2.1 Silica

2.1.1 Generality

Silica gel or silica is the most abundant material in the earth crust. The general formula of silica is $\text{SiO}_2 \cdot x\text{H}_2\text{O}$. Due to its properties such as chemical resistant, high thermal and mechanical stability, silica is thus the most widely used material in chromatography and separation technique.

The structure of silica shown in Fig. 2.1 contains siloxane bond (Si-O-Si) and silanol group (Si-OH). The latter can be divided into three types: vicinal, geminal and isolated silanol. Silica is hydrophilic since its silanol groups can form hydrogen bonding with water molecules. The adsorbed water can be removed by heating at 150 °C under vacuum for several hours [3].

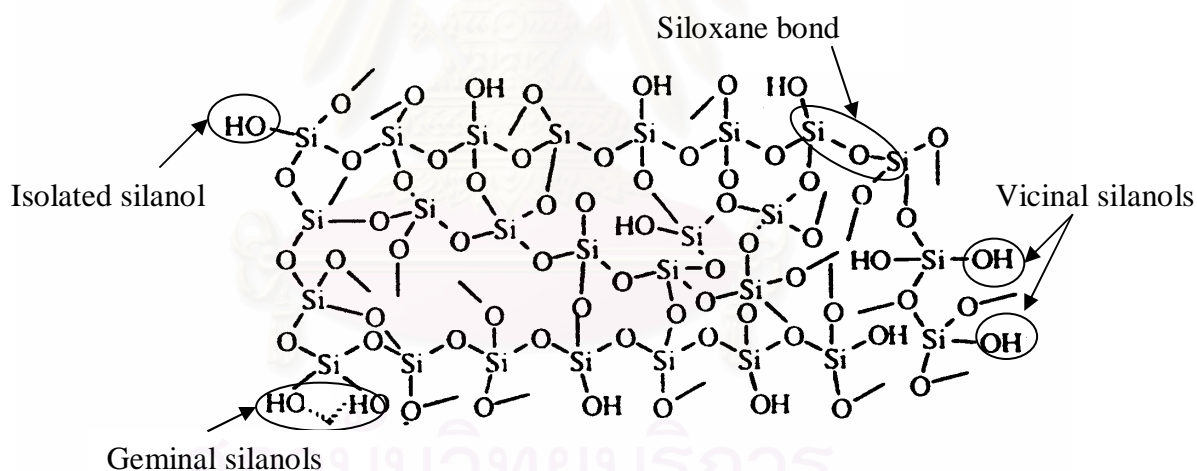
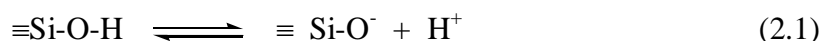


Figure 2.1 Structure of silica [10]

The hydroxyl groups on the silica surface have also an acidic character which the reaction is displayed in equation (2.1). The pKa value of this reaction is about 6.8 ± 0.5 [3]. The hydronium ions of silanol groups can exchange with cations in the solution which creates the ion-exchange property of silica. This property is highly dependent on pH of solution, surface area and silanol concentration.



The point of zero charge (pzc) and the isoelectric point (iep) of silica have been variously reported to be from 0.5 to 3.7. However, a pH around 2 ± 0.5 appeared to be an average for various types of silica ranging from purified ground quartz to colloidal silica depending on the structure of silica, particle size and the presence of impurities. [1]

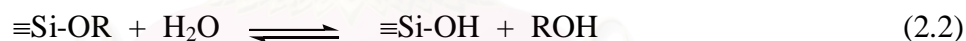
The porous silica can be classified in three types depending on their pore size according to IUPAC [11].

1. Microporous silica with pore diameter smaller than 2 nm.
2. Mesoporous silica with pore diameter between 2 and 50 nm.
3. Macroporous silica with pore diameter larger than 50 nm.

2.1.2 Synthesis of silica

Silica is usually made by acidification of sodium silicate or polymerization of silicic acid [1]. Also, this material could be synthesized by the use of sol-gel process. This technique is based on the exceptional properties of organosilicon compounds to form siloxane polymer. Hydrolysis and condensation of monomeric silicon alkoxide precursors upon addition of water can be described by the following three equations [12]:

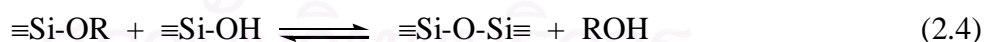
Hydrolysis:



Water condensation:



Alcohol condensation:



where R is an alkyl group.

Both hydrolysis and condensation reactions are occurred by acid or base catalyst. The most widely used alkoxides are alkoxy silanes, such as tetramethoxysilane (TMOS) or tetraethoxysilane (TEOS). However, the organosilane such as organotrialkoxysilane and organotrihalosilane monomers can also be used as silica precursor. The hydrolysis and condensation reaction of silica synthesized from organosilane is displayed as follow [9]:



where R' = methyl, ethyl; R = H, methyl, ethyl, *n*-propyl, *n*-butyl, isobutyl, *tert*-butyl, *n*-hexyl, *n*-octyl, *n*-dodecyl, *n*-hexadecyl, octadecyl, cyclohexyl, vinyl, phenyl, benzyl, phenethyl, chloromethyl, (*p*-chloromethyl)phenyl, tridecafluoro-1,1,2,2-tetrahydrooctyl.

The modified silica synthesized from organosilane has several advantages [13-15]. First, the materials combine the properties of inorganic framework (rigidity, three-dimensional structure, mechanical stability) and the specific chemical reactivity of the organic component. Second, the accessibility of organic functional group can be enhanced due to the homogeneous distribution of the organic groups in the framework. Finally, the materials are easy to synthesize.

The characteristic and properties of a particular sol-gel inorganic network are related to a number of factors that affect the rate of hydrolysis and condensation reactions. Examples of these factors are pH, temperature, reaction time, reagent concentration, type of catalyst, H₂O/Si molar ratio, and method of drying [12].

2.1.3 Mesoporous silica

The periodic mesostructure materials have been reported in early 1990s by the team of Mobil scientist [16]. These materials possess the large uniform pore structure, high specific surface area, specific pore volumes, high thermal stability and mechanical stability. Since then, these materials have been paid much attention in both scientific researcher and practical applications. These materials have found applications in various fields such as catalysis, adsorption, separation, sensing, medical usage, ecology and nanotechnology [17]. The mesoporous materials were basically prepared through silica formation around template micelle assemblies. The use of the different types of the surfactant templates results in numerous silicate mesophase. According to phase formation, there are five main categories of silicate mesophase (Figure 2.2) including disorder rods, hexagonal, cubic, lamellar phase and octomer [18].

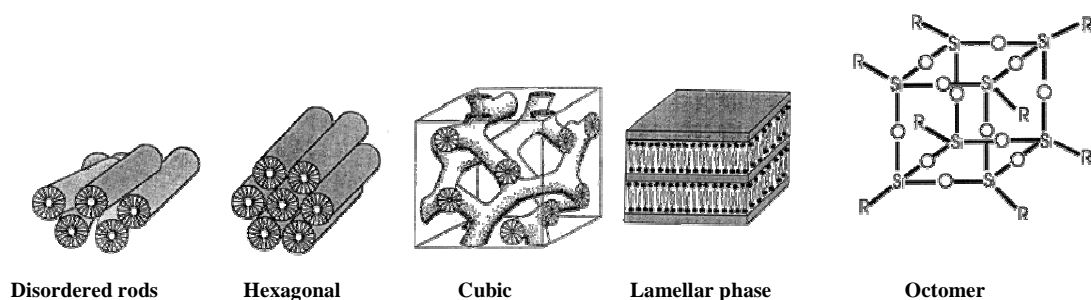


Figure 2.2 Phase formation of mesoporous materials [18]

The formation mechanism of ordered mesoporous silica-surfactant materials is illustrated in Fig. 2.3. This mechanism was proposed by Huo and co-workers [19] and Inagaki and co-workers [20]. They observed the formation of a layered silica-surfactant phase upon mixing the reactants that, with time, produced an MCM-41 structure (pathway 3 in figure Figure2.3). Davis and Burkett [21] proposed a somewhat similar mechanism (pathway 2 in Figure2.3) where, depending on the reaction temperature, the formation of MCM-41 occurs via a disordered or lamellar structure.

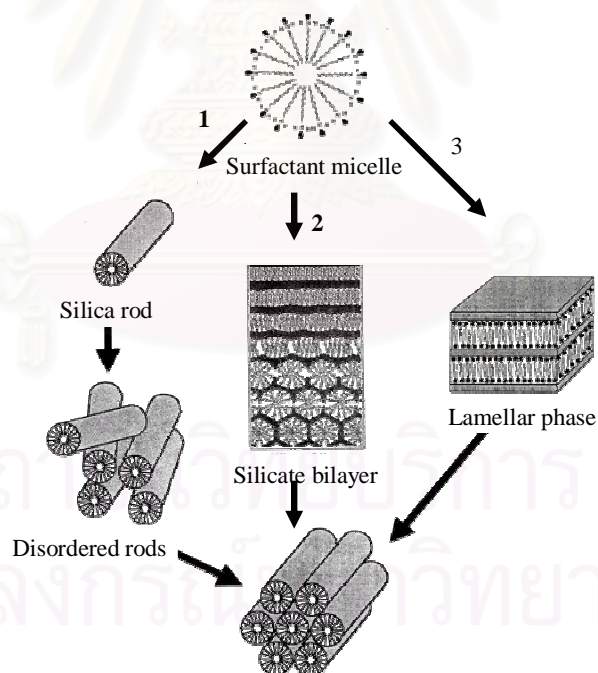


Figure 2.3 Proposed formation mechanistic pathways by (1) stacking of silicate surfactant rods via the formation of an initial (2) lamellar intermediate and (3) silicate bilayer. [18]

The crystallinity and pore size of the mesoporous silica was depended on the alkyl chain length of surfactant molecules, pH and temperature of the synthesis gel. Careful control of these factors, the well-defined geometry of materials will be achieved.

2.1.4 Functionalization of silica

Various techniques can be used for the modification of silica surface. These techniques are impregnation, grafting and doping [4]. The impregnation technique deals with physical interaction between a modifier and a solid support. However, the adhesion of the modifier to the solid support is rather weak. Consequently, leaching of modifier molecule is frequently found and the lifetime of the support is short. The second modification method is grafting. In this technique, the functional group is chemically bonding onto the silica surface. This technique has found in many applications due to the high stability of material. However, this technique is a time-consuming process and requires a specific reaction condition and precursor for each case. Furthermore, a limit loading level of the functional groups can be grafted because of the limited density of the reactive surface silanols. The last modification technique is doping technique. In this system, the organic, inorganic or biological moieties are mixed with the silica precursor. After gel formation, the dopants remain entrapped in the porous gel. Since sol-gel polymerization can be conducted under mild condition and using a process that does not involve free radical formation, so the sol-gel doping technique provides a convenient way to incorporate many delicate organic compounds and even active proteins or sensitive biological entities into or onto inorganic matrices [22]. The doping technique is used in various applications such as catalysis, sensor and separation [23-25].

2.2 Characterization of materials

2.2.1 Characterization of porous structure

2.2.1.1 Generality

Quantitative evaluation of the pore structure in porous solid is crucial aspect of processes involved in the design and application of materials for adsorption or catalysis. Gas adsorption measurements are widely used for determining the surface area and pore size distribution of a variety of different porous materials. There are many uniform of pore structure. Pore can be closed (not accessible from the

external), blind, or through. Each pore can be isolated or, more frequently, connected to other pores to form a porous network (Figure 2.4).

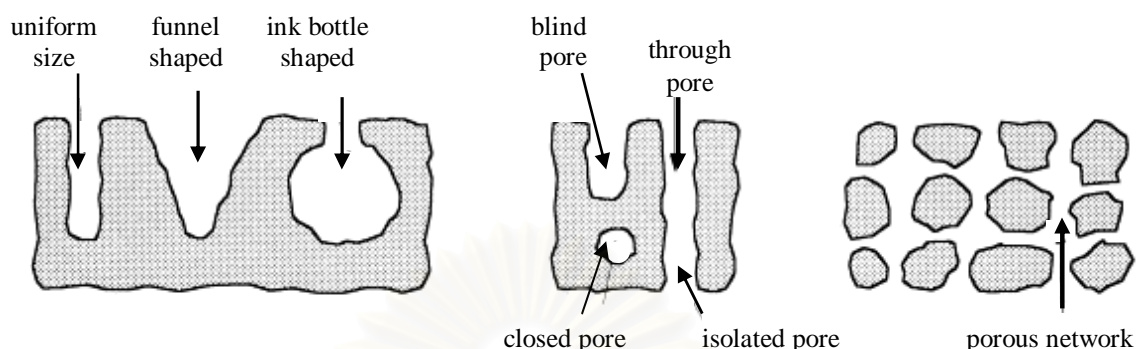


Figure 2.4 Types of pores [26]

2.2.1.2 Classification of adsorption isotherm

Isotherm shape depends on the solid porous texture. According to IUPAC classification, six types can be distinguished (Figure 2.5) [11]. The type I isotherm is given by the microporous solids having relatively small external surface (e.g. activated carbons, zeolites). Type II isotherm is the normal form of the isotherm obtained with a non-porous or macroporous adsorbent. Type II isotherm represents unrestricted monolayer-multilayer adsorption. Type III isotherm is convex to P/P_0 axis over its entire range. Isotherms of this type are not common, but there are a number of systems (e.g. nitrogen on polyethylene) which give isotherms with gradual curvature and an indistinct. Type IV isotherm are its hystereses loop and the limiting uptake at high P/P_0 . Type IV isotherm is attributed to monolayer-multilayer adsorption. For mesoporous industrial sorbents, the isotherm typical measurements follow this type. Type V isotherm is related to the type III isotherm in that the adsorbent-adsorbate interaction is weak. Type VI isotherm represents stepwise multilayer adsorption on a uniform non-porous surface.

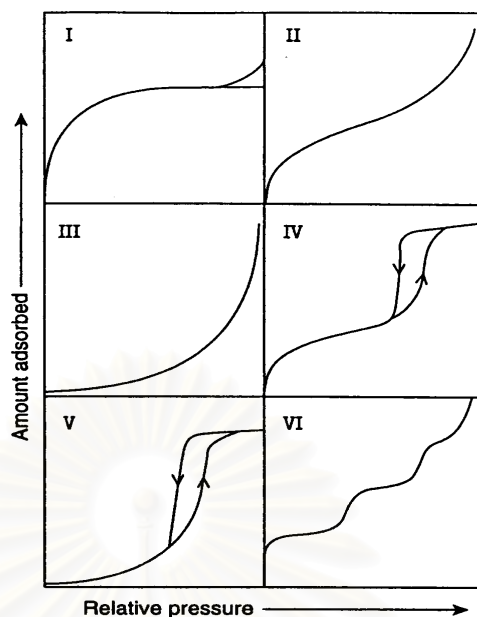


Figure 2.5 Types of adsorption isotherm [11]

2.2.1.3 Adsorption hysteresis

Hysteresis appearing in the multilayer range of physisorption isotherms is usually associated with capillary condensation in mesopore structures. According to IUPAC classification there are four types of hysteresis (Figure 2.6) [11].

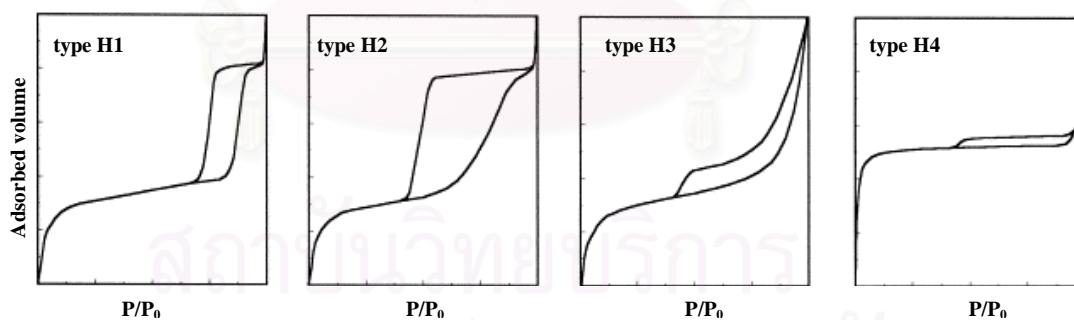


Figure 2.6 The four hysteresis shapes of adsorption isotherm [26]

Types H1 and H2 hysteresis are characteristic of solid consisting of particles crossed by nearly cylindrical channels or made by aggregates (consolidated) or agglomerates (unconsolidated) of spheroidal particles. In both cases, pores can have uniform size and shape (type H1) or nonuniform size or shape (type H2).

Types H3 and H4 hysteresis are usually found on solids consisting of aggregates or agglomerates of particles forming slit shaped pores (plates or edged

particles like cubes), with uniform (type H4) or nonuniform (type H3) size and/or shape. Hysteresis are usually due to a different behavior in adsorption and desorption. For example in pore formed by parallel plates the meniscus is flat (radius= ∞) during adsorption (condensation does not take place at any relative pressure) and cylindrical (radius=half the distance between plates) during desorption. Typical examples of this class are active carbons and zeolites.

No hysteresis is observed in the case of blind cylindrical, cone-shaped and wedge-shaped pores.

2.2.1.4 Application of Brunauer-Emmett-Teller method (BET)

The Brunauer-Emmett-Teller (BET) gas adsorption method has become the most widely used standard procedure for the determination of the surface area of finely-divided and porous materials. The BET equation is usually expressed in the linear form [11].

$$\frac{P}{n(P_0 - P)} = \frac{1}{n_m C} + \frac{(C-1)}{n_m C} \frac{P}{P_0} \quad (2.6)$$

where P/P_0 is the equilibrium relative pressure and P_0 is the saturation pressure of the pure adsorptive at the temperature of the measurement, n is the amount adsorbed at the relative pressure P/P_0 and n_m is the monolayer capacity. According to the BET theory, C is a constant which is related exponentially to the heat of adsorption for the first layer. The surface area is determined from equation

$$A_s = n_m \cdot L \cdot a_m \quad (2.7)$$

where A_s is surface area of adsorbent, L is the Avogadro's number and a_m is the area covered by one nitrogen molecule. The a_m value generally accepted is 0.162 nm^2 .

2.2.1.5 Pore volume and pore size distribution

The established method for the determination of pore size is based on the Barrett-Joyner-Halenda (BJH) method [26]. The BJH method is widely used also by commercial instruments to perform calculation on mesopores. This model is simple. In the capillary condensation region ($P/P_0 > 0.4$), each pressure increase causes an increase of the thickness of layer adsorbed on pore walls and capillary condensation in pores having a core size r_c (i.e. the empty space of pores) defined by Kelvin equation:

$$r_c = \frac{-2\gamma w_m \cos\theta}{RT \ln(P_0/P)} \quad (2.8)$$

where r_c represents the radius for cylindrical pores or the distance between walls for slit shape pores, γ is the surface tension, w_m is molar volume of the liquid condensate, θ is the contact angle and P_0/P is the relative pressure at which condensation occurs.

2.2.2 X-ray diffraction

X-ray diffraction is a very important method to characterize the structure of crystalline material. The technique can typically be used for the lattice parameters analysis of single crystals or interplanar spacing. When X-ray beam hit the atom, the electrons around the atom start to oscillate with the same frequency as the incoming beam. The interference of the secondary waves leads to scattering of X-rays by the atoms. Since the interatomic distances in the crystal are comparable with the wavelength of the primary X-rays, interference occurs between the X-ray waves scattered by the individual atoms, reflected in particular directions, leading to the formation of the diffraction pattern for the crystal.

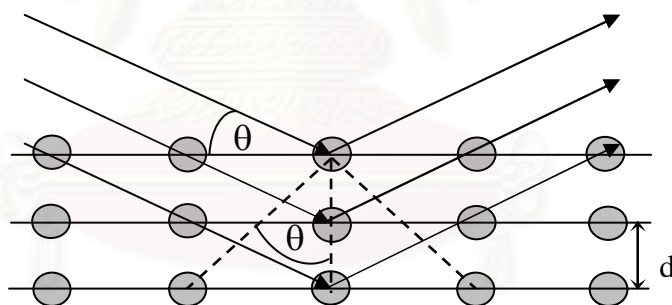


Figure 2.7 Diffraction of X-ray by a crystal [27]

Bragg's equation which expressed the relation between wavelength (λ), atomic spacing (d) and the diffraction angle (θ), is displayed as following:

$$n\lambda = 2d \sin\theta \quad (2.7)$$

where quantity n is corresponded to the diffraction order.

2.2.3 Scanning electron microscope (SEM)

The scanning electron microscope (SEM) provides the images of surface features, morphology and the crystallographic information. Unlike the conventional

light microscopy, SEM is capable of magnification of 100,000 times and extreme resolution. SEM operates by scanning an electron beam over the sample and measuring the electrical interactions with the surface. When the electrons hit the surface, weakly bound electrons will be ejected to produce secondary electrons. These secondary electrons can then be measured by a detector, and used to calculate the color for each pixel of an SEM image. Since these secondary electrons are of low energy, their trajectories can be easily influenced by electromagnetic fields. In order to avoid a charge build-up on the surface of the sample which would alter the path of the secondary electrons, the surface must be conducting. However, shadowing methods have been developed for coating non-conductive samples with a thin layer of metal so that SEM measurements become possible. The generic SEM is displayed in Figure 2.8.

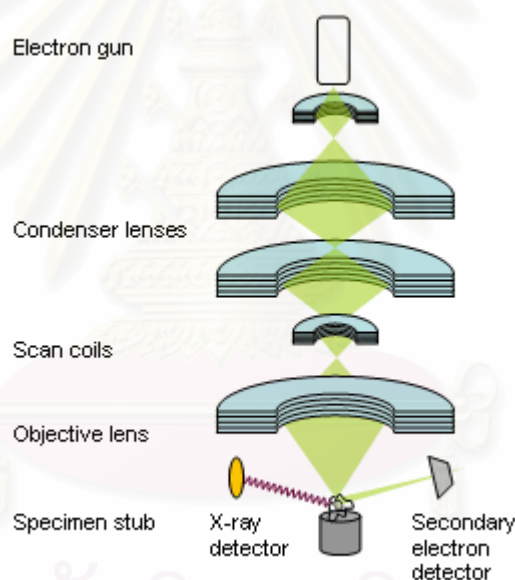


Figure 2.8 The schematic for a generic SEM [28]

From the figure above, the electron gun is producing a stream of monochromatic electrons. The beam of electron is condensed by the first condenser lens. Then the scan coils scan or sweep the beam in a grid fashion, dwelling on points for a period of time determined by the scan speed. The final lens, the objective lens focus the scanning beam onto the part of the specimen desired. When the beam irradiates the specimen, the signal in the form of x-ray fluorescence, secondary or

backscattered electrons are produced. These produced electrons are detected, then the image is determined [29].

2.3 Determination of metal sorption properties of materials

The calculation of the amount of metal ions sorped on the sorbent and the distribution ratio of the metal are shown following [30]:

$$q = (C_i - C_e) \times L/W \quad (2.10)$$

$$D = q/C_e \quad (2.11)$$

where q is the amount of metal on the sorbents (mol kg^{-1} or mg g^{-1})

D is the distribution ratio of the metal (L kg^{-1})

C_i is the initial metal concentration in aqueous solution
(mol L^{-1} or mg L^{-1})

C_e is the metal concentration in aqueous solution at equilibrium
(mol L^{-1} or mg L^{-1})

L is the volume of aqueous solution (L)

W is the weight of sorbents (g)

Adsorption isotherm studies provide information on the capacity of sorbent which is a most important parameter for an adsorption system. When the adsorption reaches the equilibrium at a constant temperature, the adsorption isotherm can be obtained by the relationship between the concentration of adsorbate remaining in solution and adsorbed extent. There are the several isotherm equations describing the equilibrium and the most common of them are Langmuir and Freundlich isotherm [31].

The most important model of monolayer adsorption is Langmuir isotherm [32]. The assumptions of the Langmuir isotherm are: (1) adsorption energy is constant over all sites; (2) adsorbed atoms or molecules are adsorbed at definite, localized sites; (3) each site can accommodate only one molecule or atom; (4) there is no interaction between adsorbates. This isotherm is given as

$$q_e = \frac{q_m K_i C_e}{1 + K_i C_e} \quad (2.12)$$

The linear form of equation 2.12 is:

$$\frac{C_e}{q_e} = \frac{C_e}{q_m} + \frac{1}{K_i q_m} \quad (2.13)$$

where q_e is amounts of adsorbed at equilibrium (mg g^{-1}), q_m is the maximum capacity of the adsorbent (mg g^{-1}) and K_L is the equilibrium constant for the adsorption reaction. The value of q_m and K_L are obtained from the slope and intercept of the plot of C_e/q_e versus C_e .

The empirical Freundlich isotherm is used to describe multilayer adsorption isotherm for heterogeneous surface and expressed by the following equation [33]:

$$q_e = K_f C_e^{1/n} \quad (2.4)$$

where K_f and n are the Freundlich constant related to adsorption capacity and intensity, respectively. Equation 2.14 is generally used in the linear form, represented by:

$$\log q_e = \log K_f + \frac{1}{n} \log C_e \quad (2.15)$$

2.4 Schiff's base molecules

Schiff's base is an important class of ligand that is well known as coordinating agent [34]. Schiff's base is an imine product which is derived from an amine and an aldehyde or ketone. Since Schiff's base containing O, N, S or P donor atoms, it is then able to form a complex with several metal ions such as Al(II), Ca(II), Cd(II), Co(II), Cu(II), Fe(II), Fe(III), Ga(III), Mg(II), Mn(II), Mn(III), Ni(II), Pb(II) and Zn(II). [35-38]. Schiff's base has been found extensive use in catalyst, sensor, separation and preconcentration [39-41].

In this research, three Schiff's base ligands namely, 2,2'-{ethane-1,2-diylbis[nitrilo(*E*)methylylidene]}diphenol (salen), 2,2'-{propane-1,3-diylbis[nitrilo(*E*)methylylidene]}diphenol (saltn) and 2,2'-{ethane-1,2-diylbis[nitrilo(1*E*)eth-1-yl-1-ylidene]}diphenol (haen) are used as doping molecules. These ligands are chosen because they are easily synthesized and they are able to form the stable complex with various metals. In addition, these ligands are used as selective extraction reagent for several kinds of metal [42]. Their chemical structures are shown as below:

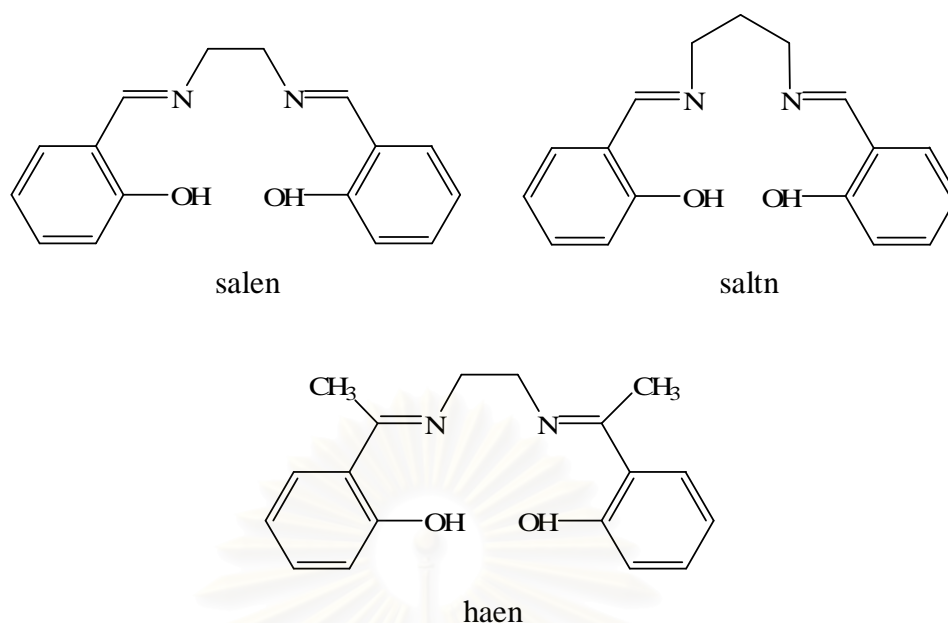


Figure 2.9 Structures of Schiff's bases used in this research.

2.5 Literature reviews

Since the ordered mesostructure silica materials were introduced by Mobil researchers in 1992 [16], the functionalization/modification of mesoporous silica has played an important role in various application such as catalyst, sensor and separation technology. There are several researches related to the synthesis of such materials and some works were described below.

Mokaya [43] studied the restructure of mesoporous silica by performing the secondary synthesis (recrystallisation) in which the calcined MCM-41 silica is used as a silica source. The factors investigated are (1) the time allowed for hydrothermal recrystallisation at 150°C, (2) the amount of amorphous silica available during the recrystallisation and (3) the use of large pore MCM-41 as a silica source. The results had shown that the extended recrystallisation time can be used to prepare purely MCM-41 materials with good long-range structural ordering and thicker pore walls. The pore wall thickness can be increased by more than 70% without any significant structural degradation. Restructuring to larger elongated and sheet particles is most effective when there is only a limited amount of amorphous silica available in the recrystallisation gel. The recrystallisation can be used, not only to tailor the particle morphology but also to prepare highly thermally stable MCM-41 materials.

For research related to the surface modification of silica with organosilane, Chong and coworker [44] prepared mesoporous silica SBA-15 functionalized with

organosilane by co-condensation method in the presence of nonionic triblock copolymer P123 as a template under acidic condition. The mesoporous silica were synthesized using tetraethoxysilane (TEOS) and one of the following organosilane namely, 3-aminopropyltriethoxysilane (APTES), 3-mercaptopropyltrimethoxysilane (MPTMS), phenyltrimethoxysilane (PTMS), vinyltriethoxysilane (VTES) and 4-(triethoxysilyl)butyronitrile (TSBN) as silica co-precursor. The functionalized SBA-15 materials exhibited long-range ordering of two-dimensional hexagonal pore arrays of size ranging from 66 to 90 Å. The obtained materials were used as the supports for immobilization of enzyme penicillin acylase (PA). The functionalized materials displayed improved properties for immobilization of PA in comparison with pure-silica SBA-15. This improvement is due to the enhanced surface hydrophobicity and electrostatic interactions of the functional groups with the PA. Also, Wu and coworkers [45] prepared the hybrid mesoporous silica gel from the TEOS, methyltriethoxysilane (MTES), vinyltriethoxysilane (VTES), propyltriethoxysilane (PTES) or phenyltriethoxysilane (PhTES). The adsorption of organic dyes alizarin red S and phenol red on hybrid mesoporous silica were investigated. The experimental results demonstrate that the adsorption capacity of hybrid gels is much higher than that of the pure silica gel and increases as the gel surface becomes more hydrophobic. This suggests that the organic dye adsorption is governed mainly by the hydrophobic interaction between the organic dyes and the gel surface.

For the research concerning the functionalization of silica by chemical doping, Boos and coworker [48] proposed the preparation of HPMSP doped mesoporous silica to be used as a sorbent. The Cu(II) sorption capacity of HPMSP modified silica was approximately 5 times greater than that of microporous silica. The influence of parameter on the synthesis of HPMSP doped mesoporous silica was also investigated.

For the research related to the functionalization of silica with Schiff's base ligand, Khorrami and coworkers [46] reported the preparation of the octadecyl-bonded silica (OBDS) membrane disk functionalized with *N,N'*-bis (3-methylsalicylidene) ortho phenylene diamine (MSOPD) using impregnation technique. This modified silica membrane disk was used as a sorbent for the separation and preconcentration of Ni(II). The study result found that the bare membrane disk did not show any tendency for the adsorption of Ni(II), while the modified disk with MSOPD are capable to retain Ni(II) ion in the sample solution.

The maximum adsorption of Ni(II) onto membrane disk modified by 3 mg of MSOPD was found to be $146 \pm 4 \mu\text{g}$.

Khamloet [47] reported the synthesis of Schiff's base doped mesoporous silica. These modified silicas were synthesized using Schiff's base namely, salen, saltn, salophen and haen as doping molecules, tetraethoxysilane as a silica precursor and CTAB as a template. The maximum amounts of Schiff's base that could be incorporated in 1 mole of the synthesized mesoporous silica were found to be 90.6, 43.5, 58.6 and 67.0 mmole for salen, saltn, salophen and haen, respectively. All synthesized silica had good ordered arrangement of mesopore with narrow pore size distribution. These materials had large surface area and pore volume. These silica could extract Co(II), Cu(II), Fe(II), Fe(III) and Mn(II). In addition, all Schiff's base doped mesoporous silica had high selectivity to the extraction of Cu(II) and Fe(III).

According to these reviews, only few papers reported on the modification of silica with Schiff's base using doping technique. Furthermore, the study on parameters affected the physical and chemical properties of such Schiff's base doped silica was still limited. Thus, in this work, the crucial synthesis factors including the type of silica precursor and the amount of Schiff's base used are investigated in order to attain the optimum parameter for the preparation of this effective sorbent. Also, the physical and metal sorption properties of the synthesized silica are determined.

2.6 Objective

1. To synthesize Schiff's base doped mesoporous silica using various silica precursors.
2. To investigate the influence of precursors on the physical and metal sorption properties of the Schiff's base doped mesoporous silica.

CHAPTER III

EXPERIMENTS

3.1 Reagents

Tetraethoxysilane (TEOS, 98%) ethyltriethoxysilane ($\text{CH}_3\text{CH}_2\text{Si}(\text{OCH}_2\text{CH}_3)_3$ ETES, 98%), vinyltriethoxysilane ($\text{CH}_2=\text{CHSi}(\text{OCH}_2\text{CH}_3)_3$, VTES, 98%), propyltrimethoxysilane ($\text{CH}_3(\text{CH}_2)_2\text{Si}(\text{OCH}_3)_3$, PTMS, 98%) and cetyltrimethylammonium bromide (CTAB, 98%) were received from Fluka. The calcined mesoporous silica was synthesized as describing in Appendix III. The silica gel 60 (0.063-0.200 mm, 70-230 mesh) was purchased from Merck. The reagents for synthesizing Schiff's base ligands: salicylaldehyde, ethylenediamine, 2-hydroxyacetophenone and 2-propylenediamine, were from Fluka and were used without further purification. $\text{Cu}(\text{NO}_3)_2 \cdot 3\text{H}_2\text{O}$ (99%), $\text{Fe}(\text{NO}_3)_3 \cdot 9\text{H}_2\text{O}$ (98%) and $\text{Ni}(\text{NO}_3)_2 \cdot 6\text{H}_2\text{O}$ (99%) from Fluka were used to prepare metal ion solution. Sodium hydroxide (NaOH) was obtained from Carlo Erba Reagenti. Ethanol ($\text{C}_2\text{H}_5\text{OH}$) and nitric acid (HNO_3) were from Merck. Deionized water ($>18 \text{ M}\Omega \text{ cm}^{-1}$) from Millipore system (Milli Q, model Millipore ZMQS5V00Y) was used throughout.

3.2 Apparatus

UV spectra were obtained on a HP8453 UV-Visible spectrophotometer. The FT-IR spectra were recorded on a Nicolet fourier transform infrared spectrophotometer model Impact 410 using KBr pellet technique. X-ray diffraction was determined using a Rigaku DMAX 2200/Ultima⁺ X-ray diffractometer ($\text{Cu-K}_{\alpha 1}$ radiation, $\lambda = 1.5406 \text{ \AA}$). The nitrogen adsorption-desorption isotherms were carried out using a Belsorp-mini II nitrogen adsorptometer. The temperature in the extraction was controlled by thermoregulated bath (JULABO model F10). Atomic absorption measurement of metal ions was performed with a Perkin Elmer AAnalyst 100 atomic absorption spectrometer. The morphology of material was observed using a JEOL JSM 5410LV scanning electron microscope.

3.3 Experiments

3.3.1 Synthesis of silica

The synthesis of silica was divided into two parts depending on the number of silica precursors. For the first part, each type of silica precursor including TEOS, calcined mesoporous silica and silica gel 60 was used for the synthesis of materials. And in the second part, the silica were prepared from TEOS and one of these co-precursors: VTES, ETES or PTMS. The synthesis method was based on the procedure reported by Boos and co-workers [48]. The molar composition of silica precursor : (co-precursor) : H₂O (0.1 M NaOH as catalyst) : CTAB : C₂H₅OH : Schiff's base was 1 : (0.25) : 140 : 0.18 : 13 : 0.12. The synthesis method was described below.

Schiff's base and ethanol were mixed and stirred at 60 °C for 1 h. CTAB and NaOH were then added to the solution and the mixture was stirred at 60 °C for 4 h. The silica precursor was subsequently added. The mixture was continued on stirring at 60 °C for 1 h and at room temperature for 23 h. The product was recovered by vacuum filtration and washed copiously with deionized water and 10⁻³ M HNO₃. All filtrates were then collected to determine the quantity of doping molecules that might be leached out during the synthesis and washing processes. The obtained silica was dried at 110 °C overnight. Control non-doped silica was also prepared for comparison according to the above procedure without adding Schiff's base.

3.3.2 Characterization of silica

3.3.2.1 Determination of organic matters in silica

The organic matter content in materials was determined using calcination method as described below.

300 mg of as-synthesized silica were dehydrated at 110 °C overnight. Then the sample was placed in a muffle furnace and heated from room temperature to 100 °C at a rate of 1 °C/minute and hold at this temperature for 1 h. Then the modified silica was heated to 540 °C at a rate of 1 °C/minute and hold at this temperature for 10 h. After calcination process, the sample was again weighed. The silica weight difference indicated the organic matters in material. The heating program could be summarized in Figure 3.1

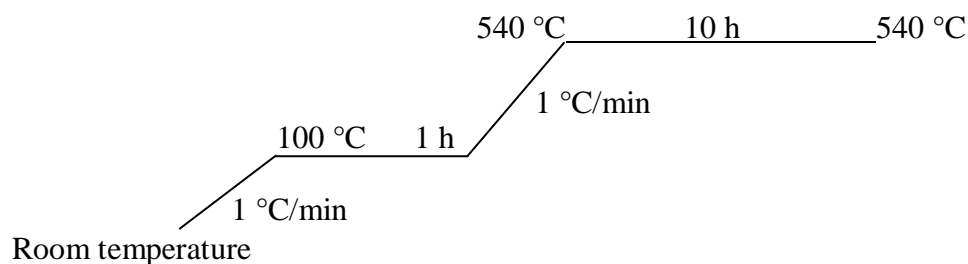


Figure 3.1 The heating program for the calcination process

3.3.2.2 Determination of accessible Schiff's bases

The amount of active Schiff's base molecules in the Schiff's base doped mesoporous silica could be indicated by the amount of accessible Schiff's base. The experimental process was conducted as follow unless stated otherwise.

10 mL of ethanol : H₂O (1:1, v/v) were added to 100 milligrams of the dried Schiff's base doped mesoporous silica. The mixture was stirred for 3 hours at room temperature. The liquid phase was then separated by centrifugation. The amounts of accessible Schiff's bases in the solution were analyzed by UV-visible spectroscopy.

3.3.2.3 Determination of crystallinity

The structure of silica was investigated by X-ray diffraction technique (XRD) using CuK α radiation ($\lambda = 1.5406 \text{ \AA}$) at 40 kV, 30 mA. The spectra of powder sample were recorded from 1.0° to 10.0° (2 θ) with a scan time of 2° (2 θ) per minute.

3.3.2.4 Determination of morphology

The morphology of silica was investigated by a scanning electron microscope using conductive coating technique. The sample was held on cylindrical mount with adhesive tape. The specimen surface was coated with gold in order to make them conductive.

3.3.2.5 Investigation of functional group of organic and inorganic molecules in mesoporous silica

The present of organic and inorganic functional groups in modified silica were determined by FTIR spectroscopy. The sample was analyzed in the range of 400 – 4000 cm⁻¹ using the KBr pellet technique. The spectra were collected with 32 scans.

3.3.2.6 Determination of surface area and pore size

20 mg of calcined sample were outgassed at 200 °C for 3 h. The sorption of nitrogen was recorded using equilibrium time approximately 10 min per point. The specific surface area was then calculated using the Brunauer-Emmett-Teller (BET) model. The pore size distribution and pore volume were evaluated from the desorption branch of the nitrogen isotherm via the Barrer-Joyner-Halenda (BJH) method.

3.4. Extraction properties of silica

The extraction properties of Schiff's base doped silica towards Cu(II), Fe(III) and Ni(II) were investigated using batch equilibrium technique. The method was described as follow.

25 mL of 100 ppm of metal solution were added to 100 mg of dried silica. The mixture was stirred at 25 °C in thermoregulated bath for 24 hours. Then the slurry was centrifuged and the amount of unextracted metal ions in solution was determined using flame atomic absorption spectroscopy.

CHAPTER IV

RESULTS AND DISCUSSION

4.1 Synthesis and properties of silica synthesized from single silica precursor

All types of silica precursor including TEOS, calcined mesoporous silica and silica gel 60 could be successfully used for the preparation of non-doped and Schiff's base doped mesoporous silica. The control non-doped silica was white solid while all Schiff's base modified silica were yellowish. However, the yellow coloration of Schiff's bases, confirmed by the presence of their UV characteristic peaks, was still observed in the supernatant and washing solution. These results meant that only some Schiff's base molecules could be achievedly incorporated in the silica. The percentage of incorporated Schiff's base and the amount of incorporated Schiff's base in mmol g^{-1} of each Schiff's base doped silica on three replicated syntheses are shown in Fig. 4.1 and Table 4.1, respectively.

From Table 4.1 and Fig. 4.1, it was found that the amount of incorporated Schiff's base was highest when TEOS was used as silica precursor. These results were probably due to the homogeneous solution obtained after the addition of TEOS to the Schiff's base solution, hence rendered the incorporation facility of Schiff's base molecules into the framework of silica. On the contrary, when the precursor was calcined mesoporous silica or silica gel 60, the mixture between these precursors and the Schiff's base solution was heterogeneous. Consequently, the Schiff's base ligand preferred to be in solution. In case of the silica synthesis by using silica gel 60 as precursor, the obtained silica had the lowest amount of incorporated Schiff's base. This result may be explained by the structure of silica gel 60 which is amorphous as evidence by XRD (see Appendix IV).

Concerning the effect of Schiff's base ligand, the percentage of incorporated Schiff's base was found to be in this order: salen > haen > saltn. This result might be explained in terms of structure of saltn, which had propyl group between two imine-N atoms. The propyl group was increased the hydrophobic. Consequently, the lowest amount of incorporated Schiff's base was obtained. While the amount of incorporated haen lower than salen since haen had methyl substituent groups on the imine-C atoms. These methyl groups cause steric hindrance and had effect on the amount of

incorporated haen. This result was in accordance with the previous work reported by Khamloet [47]

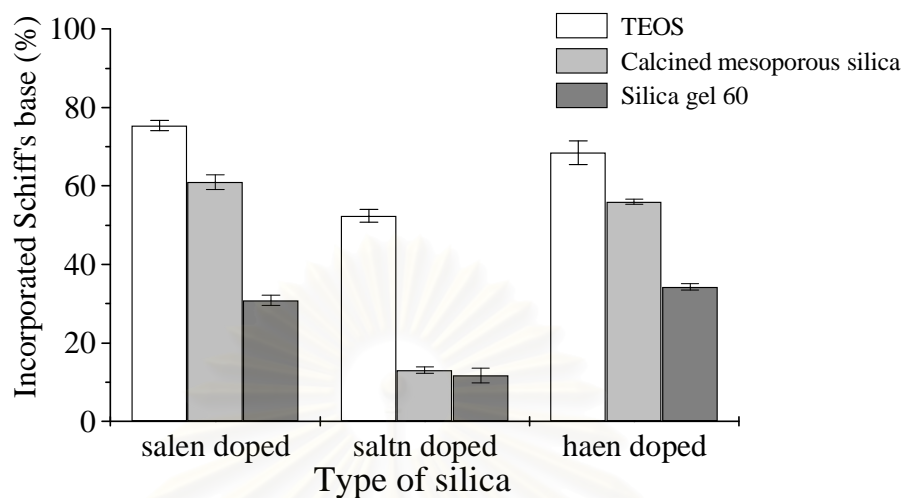


Figure 4.1 The percentage of incorporated Schiff's base in Schiff's base doped mesoporous silica synthesized by different type of single silica precursors.

Table 4.1 The amount of incorporated Schiff's bases in each Schiff's base doped mesoporous silica synthesized from various types of single silica precursors

Type of precursor	Amount of incorporated Schiff's base in silica (mmol g^{-1})		
	Salen doped	Saltn doped	Haen doped
TEOS	0.670 ± 0.009	0.490 ± 0.013	0.608 ± 0.022
Calcined mesoporous silica	0.560 ± 0.014	0.136 ± 0.009	0.513 ± 0.005
Silica gel 60	0.306 ± 0.012	0.121 ± 0.018	0.333 ± 0.007

4.1.1 Characterization of materials

4.1.1.1 Organic matters contents in silica

The organic matter contents in all as-synthesized materials were determined by a calcination technique. The values obtained from the experiment were collected to compare with the theoretical values which were calculated from the mole composition of starting materials used in the synthesis (see Appendix V for the calculation). The results from three replicated experiments are presented in Table 4.2.

Table 4.2 Organic matter contents in materials prepared from difference single silica precursors.

precursor	Type of silica	Organic matters (%)		$\frac{\text{Experimental value}}{\text{Theoretical value}} \times 100$
		Experimental value	Theoretical value	
TEOS	non-doped	48.16 ± 0.12	46.05	104.57
	salen doped	55.52 ± 0.38	55.61	99.83
	saltn doped	51.73 ± 0.54	53.67	96.39
	haen doped	54.09 ± 0.13	55.88	96.80
Calcined mesoporous silica	non-doped	50.04 ± 0.41	45.93	108.96
	salen doped	50.92 ± 0.90	54.01	94.27
	saltn doped	39.84 ± 0.55	49.77	80.04
	haen doped	48.56 ± 0.48	55.76	87.09
Silica gel 60	non-doped	45.17 ± 0.76	45.97	98.25
	salen doped	32.98 ± 1.09	50.51	65.30
	saltn doped	24.54 ± 0.85	47.85	51.29
	haen doped	29.00 ± 0.81	50.41	57.52

As seen from Table 4.2, the experimental value of all non-doped silica was close to the theoretical value. For some experimental results which were slightly higher than the theoretical values, these might be due to the physisorbed water and chemisorbed water remained in the silica framework before the beginning of calcination process. In fact, the elimination of physisorbed water and chemisorbed water is achieved at 170 °C and 400 °C, respectively [49].

In the case of Schiff's base doped silica, it was found that the organic matters obtained from experimental values of silica synthesized from TEOS or calcined mesoporous silica were close to the theoretical value. For the silica obtained from silica gel 60, the experimental values were lower than the theoretical values. These results probably are losing of some surfactant during the washing step. Actually these leaching of surfactant were observed in the form of bubbles.

4.1.1.2 Determination of accessible Schiff's base

The amount of active Schiff's base molecules in the modified silica is significant for the silica's extraction properties. In order to determine the amount of active Schiff's base in the silica, the accessible Schiff's base was performed by solvent extraction method and the amounts of extracted Schiff's base were determined by UV-visible spectroscopy. The C₂H₅OH/H₂O mixtures were used as solvent. To find out the suitable solvent ratio, the preliminary experiment was carried out with Schiff's base doped mesoporous silica synthesized from TEOS. The ratio of C₂H₅OH : H₂O was varied. The results are shown in Table 4.3 below.

Table 4.3 The amount of accessible Schiff's base extracted from the Schiff's base doped mesoporous silica synthesized from TEOS

Type of silica	C ₂ H ₅ OH : H ₂ O Ratio (v/v)	Amount of accessible Schiff's base (%)	% RSD
Salen doped	1 : 1	55.81 ± 2.49	4.47
	9 : 1	63.92 ± 1.16	1.81
Saltn doped	1 : 1	43.17 ± 0.50	1.16
	9 : 1	57.51 ± 2.02	3.52
Haen doped	1 : 1	12.87 ± 0.29	2.26
	9 : 1	18.51 ± 0.83	4.47
	1 : 9	5.66 ± 0.29	5.07

The experimental results show that mole ratio of C₂H₅OH : H₂O equal 9:1 had highest extractability of Schiff's base. Thus, this ratio was applied to further experiments on the Schiff's base doped silica synthesis from other silica sources. Their results are presented in Figure 4.2.

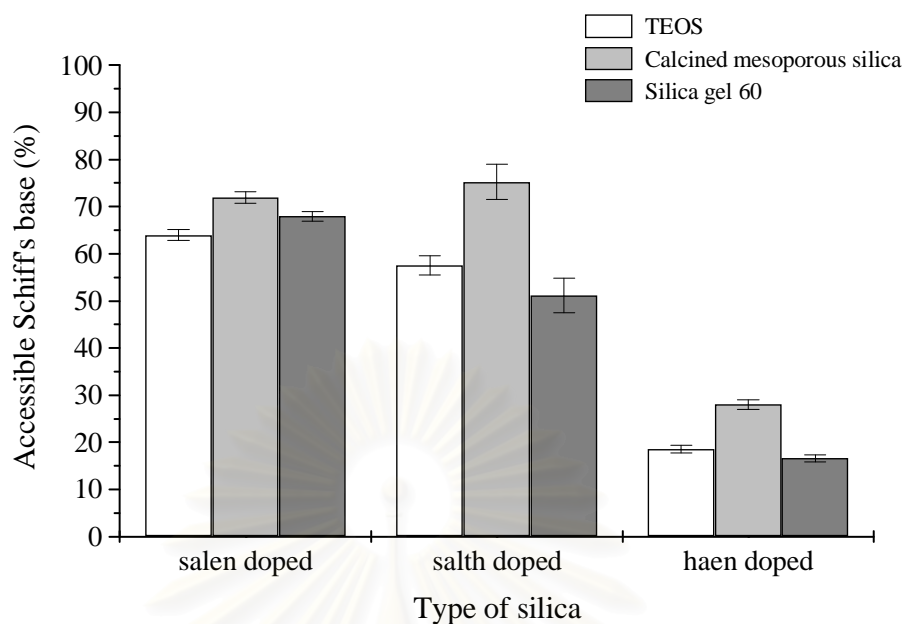


Figure 4.2 Percentage of accessible Schiff's base in modified silica synthesized from various silica precursors when $C_2H_5OH : H_2O$ equal 9:1 was used as extracted solvent.

The result shows that all of modified silica synthesized from calcined mesoporous silica had the highest amount of accessible Schiff's base. Comparison on the type of Schiff's base doped mesoporous silica, the amount of accessible Schiff's base was found to be in this order: salen > saltn > haen doped mesoporous silica. These results were in accordance with the preliminary study. However, the amount of accessible Schiff's base could not achieve 100% therefore the some Schiff's base molecules are located in the close pore of silica.

4.1.1.3 Investigation of organic molecules using FTIR spectroscopy

The presence of organic molecules in the as-synthesized silica could be demonstrated using FTIR technique. The spectra of non-doped and Schiff's base doped silica were shown in Figure 4.3-4.6, respectively. As seen, the characteristic band of silica framework was observed in all spectra of silica. The vibration of Si-OH group was observed at 3424 cm^{-1} and 962 cm^{-1} . The bands at 1061 cm^{-1} and 794 cm^{-1} were related to asymmetric and symmetric stretching band of Si-O-Si, respectively. The spectrum band at 450 cm^{-1} was associated with the O-Si-O vibration. In addition, the characteristic bands of CTAB were also present at about 2924 cm^{-1} , 2854 cm^{-1} and

1480 cm^{-1} for C-H stretching. These evidences indicated the presence of surfactant on the silica framework.

For the IR spectra of Schiff's base doped silica, the characteristic bands of the corresponding Schiff's base were also observed (1594($\nu\text{C}=\text{N}$) cm^{-1}). These results confirmed the existing of doping molecules in the modified silica.

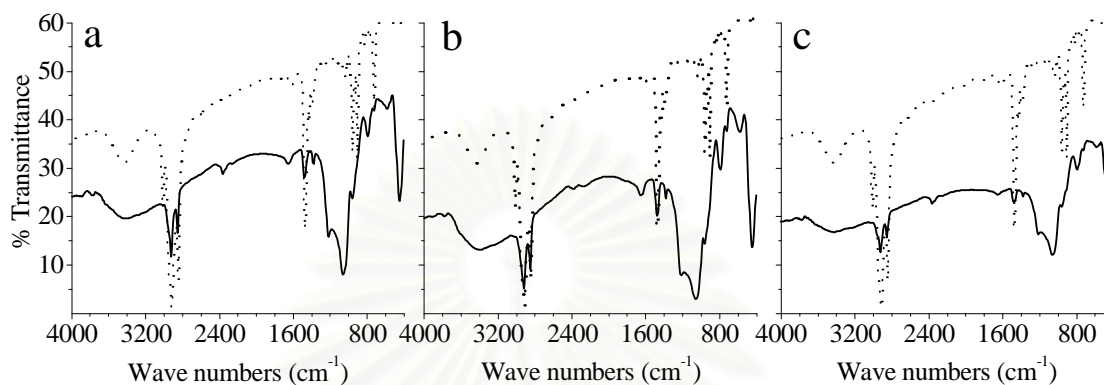


Figure 4.3 FT-IR spectra of CTAB and non-doped mesoporous silica synthesized from various silica precursors: (a) TEOS, (b) calcined mesoporous silica and (c) silica gel 60. (Solid line: mesoporous silica, dot line: CTAB)

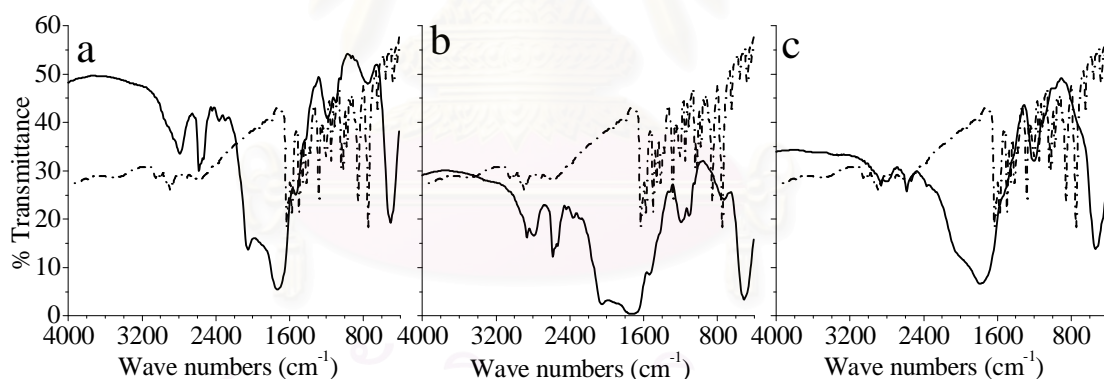


Figure 4.4 FT-IR spectra of salen and salen doped mesoporous silica synthesized from various precursors: (a) TEOS, (b) calcined mesoporous silica and (c) silica gel 60. (Solid line: mesoporous silica and dash dot line: salen)

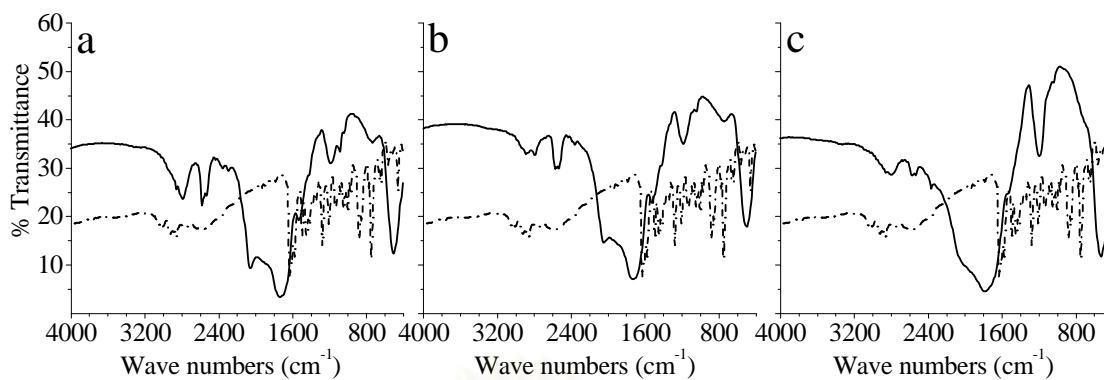


Figure 4.5 FT-IR spectra of salth and saltn doped mesoporous silica synthesized from various precursors: (a) TEOS, (b) calcined mesoporous silica and (c) silica gel 60. (Solid line: mesoporous silica and dash dot line: saltn)

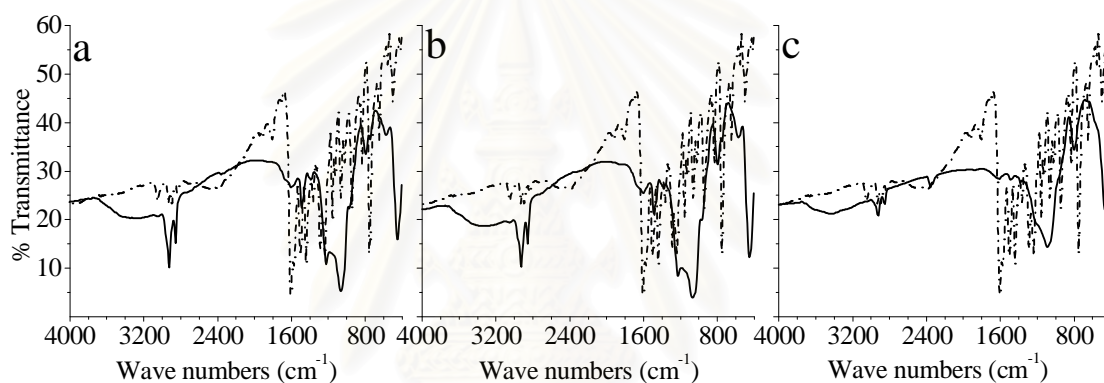


Figure 4.6 FT-IR spectra of haen and haen doped mesoporous silica synthesized from various precursors: (a) TEOS, (b) calcined mesoporous silica and (c) silica gel 60. (Solid line: mesoporous silica and dash dot line: haen)

สถาบันวิทยบริการ
จุฬาลงกรณ์มหาวิทยาลัย

4.1.1.4 Determination of crystallinity

The structure and crystallinity of as-synthesized and calcined silica were investigated by X-ray diffraction technique. The obtained XRD patterns are shown in Figure 4.7. The d-spacing values of all modified silica are also summarized in Table 4.4. The crystal structure of all synthesized and calcined silica were obtained when using TEOS or calcined mesoporous as silica source, whereas the structure of silica prepared from silica gel 60 was amorphous. Indeed, all silica synthesized from TEOS or calcined mesoporous silica was observed (100) diffraction peak around $2\theta = 2^\circ$, indicated the presence of order mesostructure. These results were consistent with previous study that had investigated the silica prepared from calcined mesoporous silica [43]. The comparison of the silica prepared from TEOS with the silica prepared from calcined mesoporous show that the silica prepared from TEOS was more structural ordered than those of silica prepared from calcined mesoporous silica.

Considering the XRD patterns and d-spacing data of as-synthesized and calcined silica, it was found that after calcination process the peak intensity was increased with the decreasing of the d-space for all modified silica except the salt-doped silica synthesized from TEOS. These results indicate better structural ordering and the shrinkage of pore size. This phenomenon was probably due to removal surfactant and organic molecule which were promoted the condensation of the silanol group. Therefore, the ordering of the silica frameworks was improved [50]. In case of salt-doped mesoporous silica synthesized from TEOS, the intensity of XRD decrease after calcination process. This might be due to the destruction of the some structure of silica framework during the calcination process. This suggested that the template of this material was unstable towards calcination.

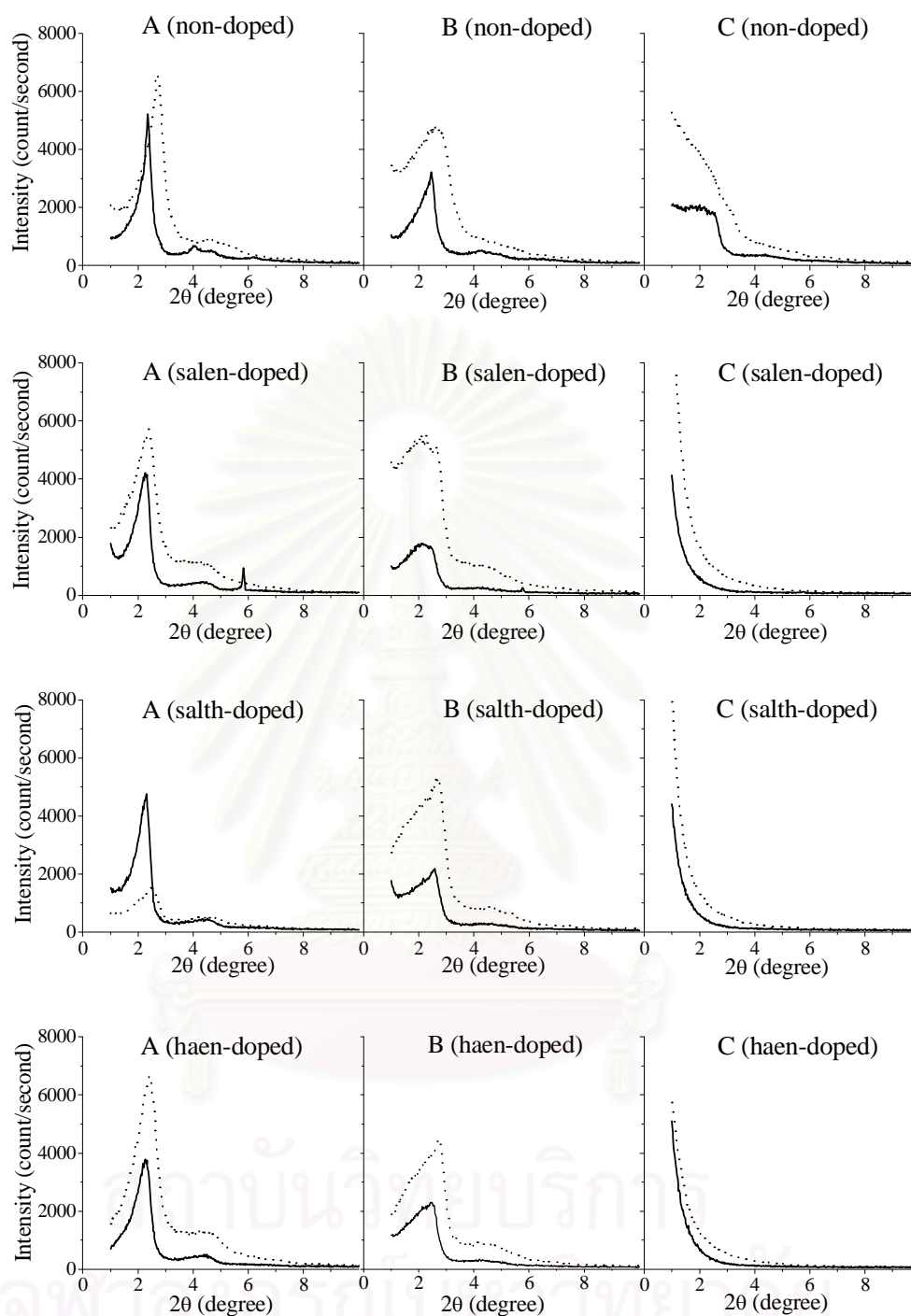


Figure 4.7 XRD patterns of silica synthesized from various single silica precursors: (A) TEOS, (B) calcined mesoporous silica and (C) silica gel 60. The text in the parenthesis referred to the type of the Schiff's base doped silica (Solid line: as-synthesized silica, dot line: calcined silica).

Table 4.4 The XRD results of as-synthesized silica and their corresponding calcined silica

Silica precursor	Type of silica	As-synthesized silica		Calcined silica	
		2 θ (degree)	d-spacing (nm)	2 θ (degree)	d-spacing (nm)
TEOS	Non-doped	2.360	3.74	2.700	3.27
	Salen doped	2.260	3.91	2.399	3.68
	Saltn doped	2.300	3.84	2.499	3.53
	Haen doped	2.280	3.87	2.440	3.62
Calcined mesoporous silica	None-doped	2.460	3.59	2.719	3.25
	Salen doped	2.160	4.09	2.120	4.16
	Saltn doped	2.579	3.42	2.660	3.32
	Haen doped	2.479	3.56	2.700	3.27

4.1.1.5 Morphology of materials

The morphology of as-synthesized silica observed from scanning electron microscopy (SEM) technique are shown in Figure 4.8-4.10. The SEM data indicated that the silica prepared from TEOS or calcined mesoporous silica show agglomerates of spherical particles. The particle sizes as estimated from SEM images were found in the range of 0.84 – 2.86 μm . On the contrary, all silica synthesized from silica gel 60 seemed to be a glass-like particle. These results suggested that the morphology of silica was affected by the types of silica precursors.

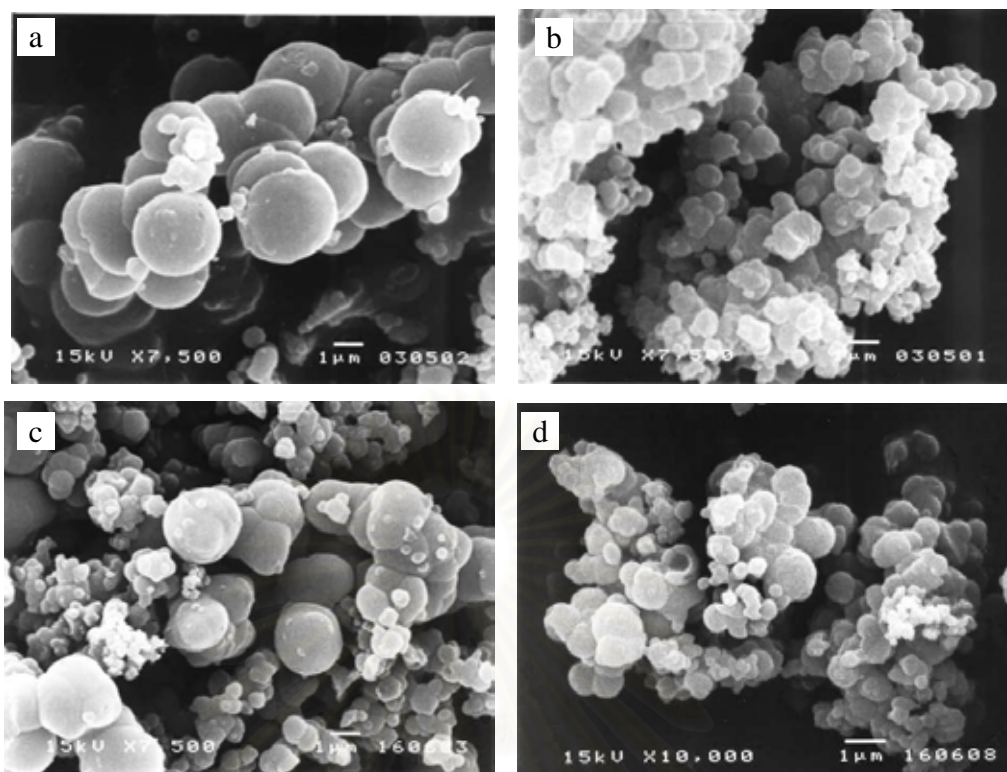


Figure 4.8 SEM images of silica synthesized from TEOS:(a) non-doped, (b) salen doped, (c) saltn doped and (d) haen doped mesoporous silica

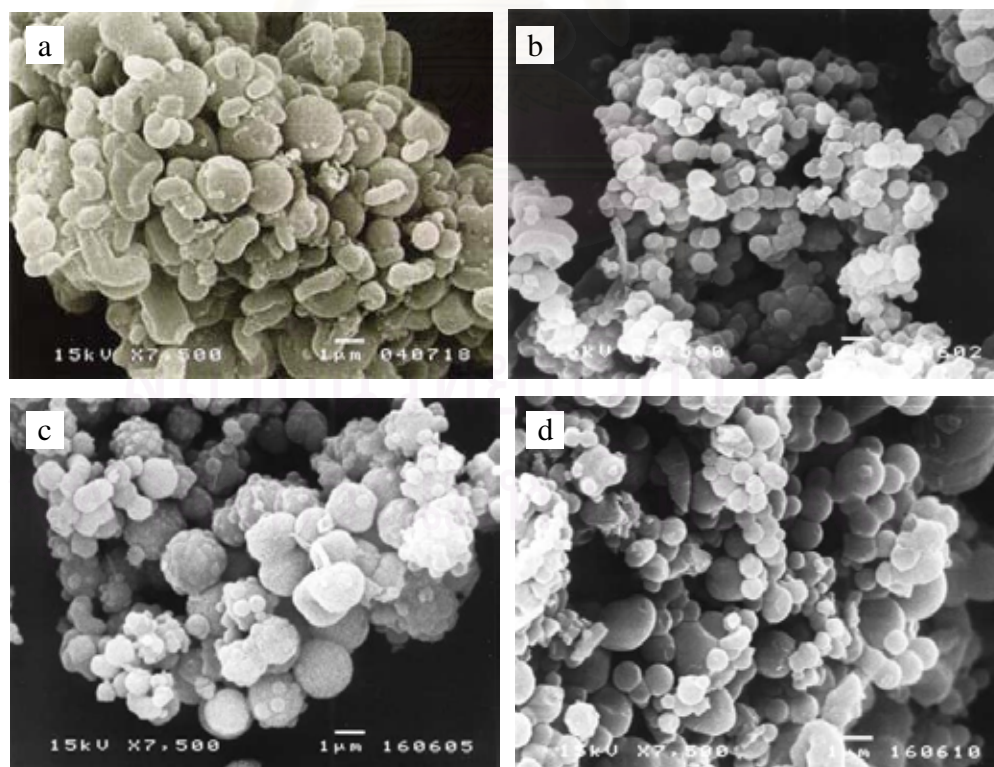


Figure 4.9 SEM images of silica synthesized from calcined mesoporous silica: (a) non-doped, (b) salen doped, (c) saltn doped and (d) haen doped mesoporous silica

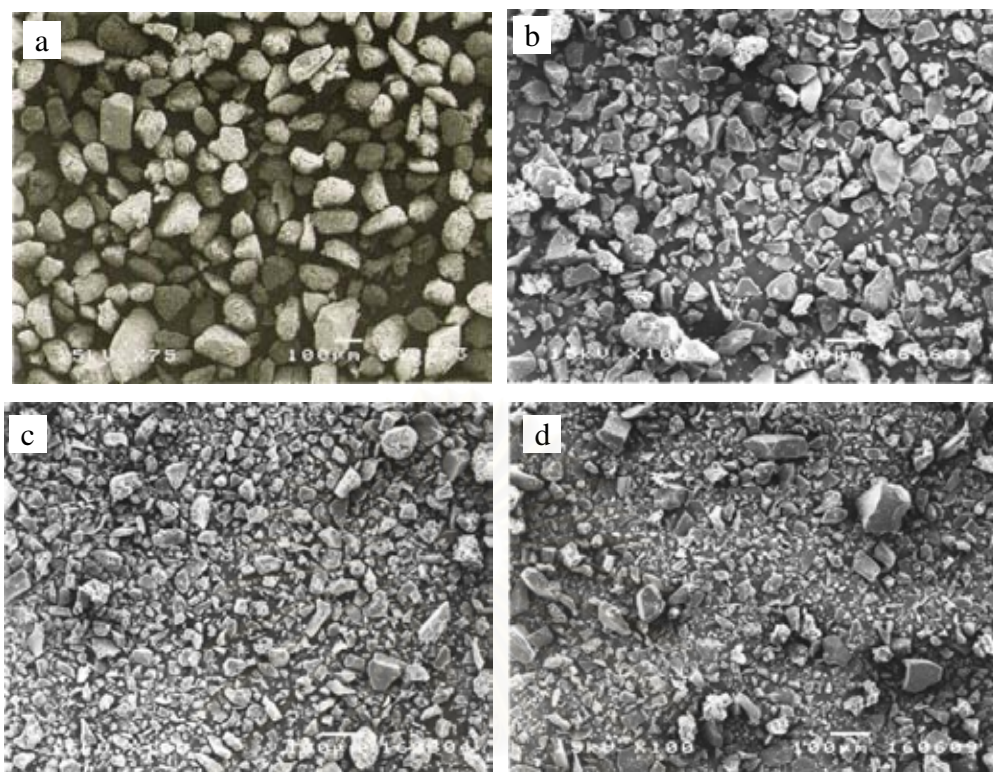


Figure 4.10 SEM images of silica synthesized from silica gel 60: (a) non-doped, (b) salen doped, (c) salt doped and (d) haen doped mesoporous silica

4.1.1.6 Determination of surface area and pore size

The porous nature of materials was evaluated by nitrogen sorption analysis. The specific surface area of as-synthesized samples with the pores filled with surfactant and ligand is about $10 - 20 \text{ m}^2 \text{ g}^{-1}$. In order to investigate the porous structure, all samples were calcined to remove the surfactant template. The results of calcined silica are shown in Figure 4.11.

All sample exhibit type IV isotherm according to IUPAC classification, which indicated the presence of mesopores. However, the capillary condensation step of silica prepared from silica gel 60 was found in the range of $0.7 < P/P_0 < 0.9$ which was due to capillary condensation inside the micropore. These results imply that the porous structure of silica synthesized from silica gel 60 were combined the characteristic of mesopore and micropore.

The results in Figure 4.12 show BJH pore sized distribution of modified silica synthesized from various precursors. The narrow pore size distribution was observed in all case. The BET surface area, pore volume and mesoporosity of modified silica are summarized in Table 4.5

As seen from Table 4.5, the large surface area of silica was obtained when TEOS or calcined mesoporous silica was using as silica precursor. Considering the pore diameter, it was found that the average pore diameter of modified silica synthesized from TEOS or calcined mesoporous silica confirmed the mesopore of these materials.

Table 4.5 Characterizations results of the Schiff's base doped mesoporous silica synthesized from various precursors

Precursor	Type of silica	S ($\text{m}^2 \text{g}^{-1}$)	V_p ($\text{cm}^3 \text{g}^{-1}$)	APD (nm)	d_{100} (nm)	a_0 (nm)	w (nm)
TEOS	Non-doped	1087	0.79	2.90	3.27	11.33	8.43
	Salen doped	830	0.79	3.82	3.68	12.74	8.92
	Saltn doped	623	0.66	4.26	3.53	12.24	7.98
	Haen doped	791	1.44	3.93	3.62	12.53	8.60
Calcined mesoporous silica	Non-doped	659	0.58	3.50	3.25	11.26	7.76
	Salen doped	1060	0.99	3.73	4.16	14.42	10.69
	Saltn doped	932	0.74	3.20	3.32	11.50	8.30
	Haen doped	999	0.91	3.65	3.27	11.32	7.67
Silica gel 60	Non-doped	514	0.65	-	-	-	-
	Salen doped	293	0.87	-	-	-	-
	Saltn doped	294	0.91	-	-	-	-
	Haen doped	338	1.05	-	-	-	-

S , BET surface area ($\text{m}^2 \text{g}^{-1}$) obtained from N_2 sorption; V_p , Total pore volume ($\text{cm}^3 \text{g}^{-1}$) obtained from single-point volume at $P/P_0 = 0.99$; APD , average pore diameter calculated from $4V_p/S$; d_{100} , d-value 100 reflections; a_0 = the lattice parameter, from the XRD data using the formula $a_0 = 2d_{100}\sqrt{3}$; w , pore wall thickness was equaled to a_0-APD .

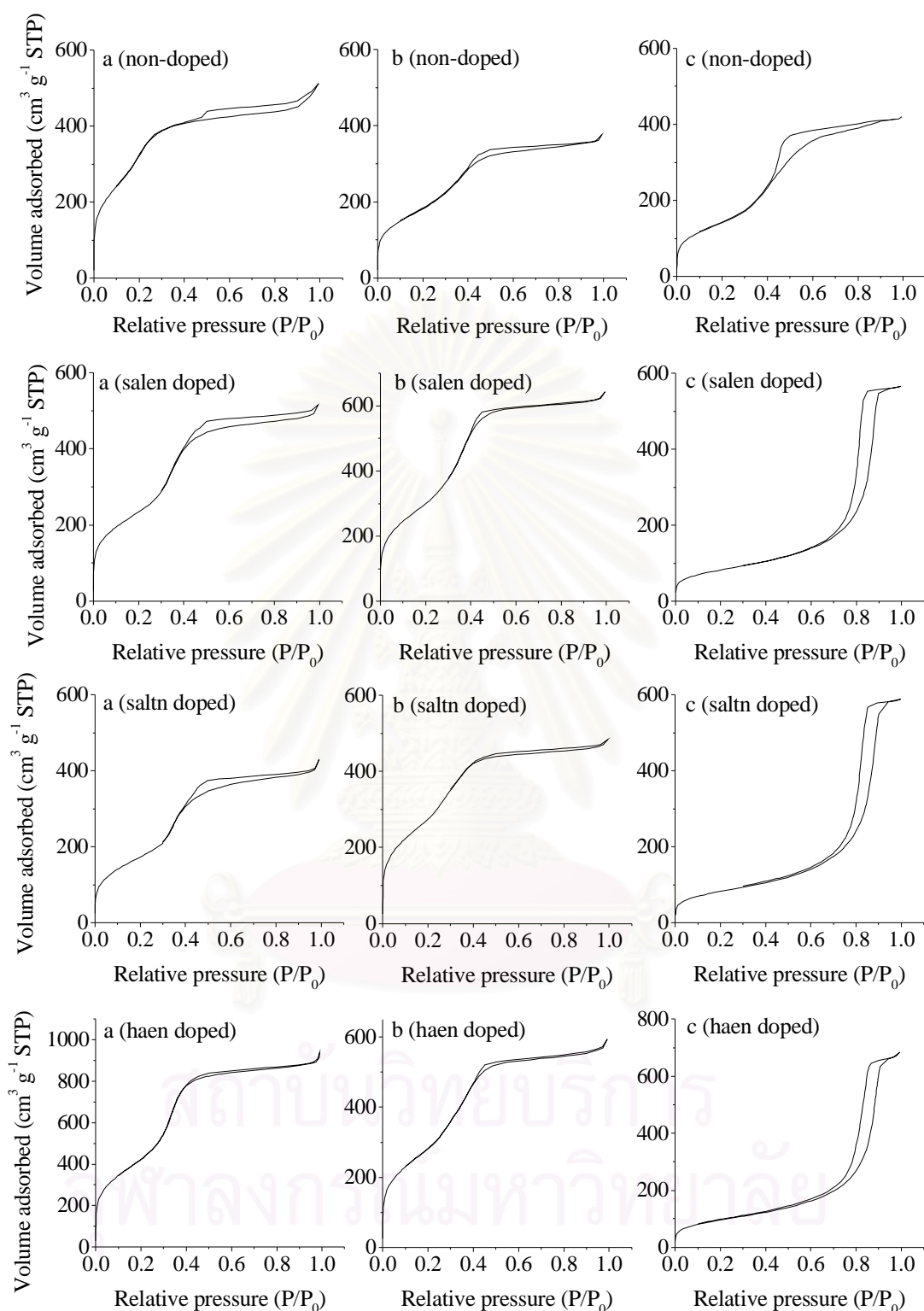


Figure 4.11 Nitrogen sorption isotherms of silica synthesized from various precursors: (a) TEOS (b) calcined mesoporous silica and (c) silica gel 60. The text in the parenthesis referred to the type of the Schiff's base doped silica.

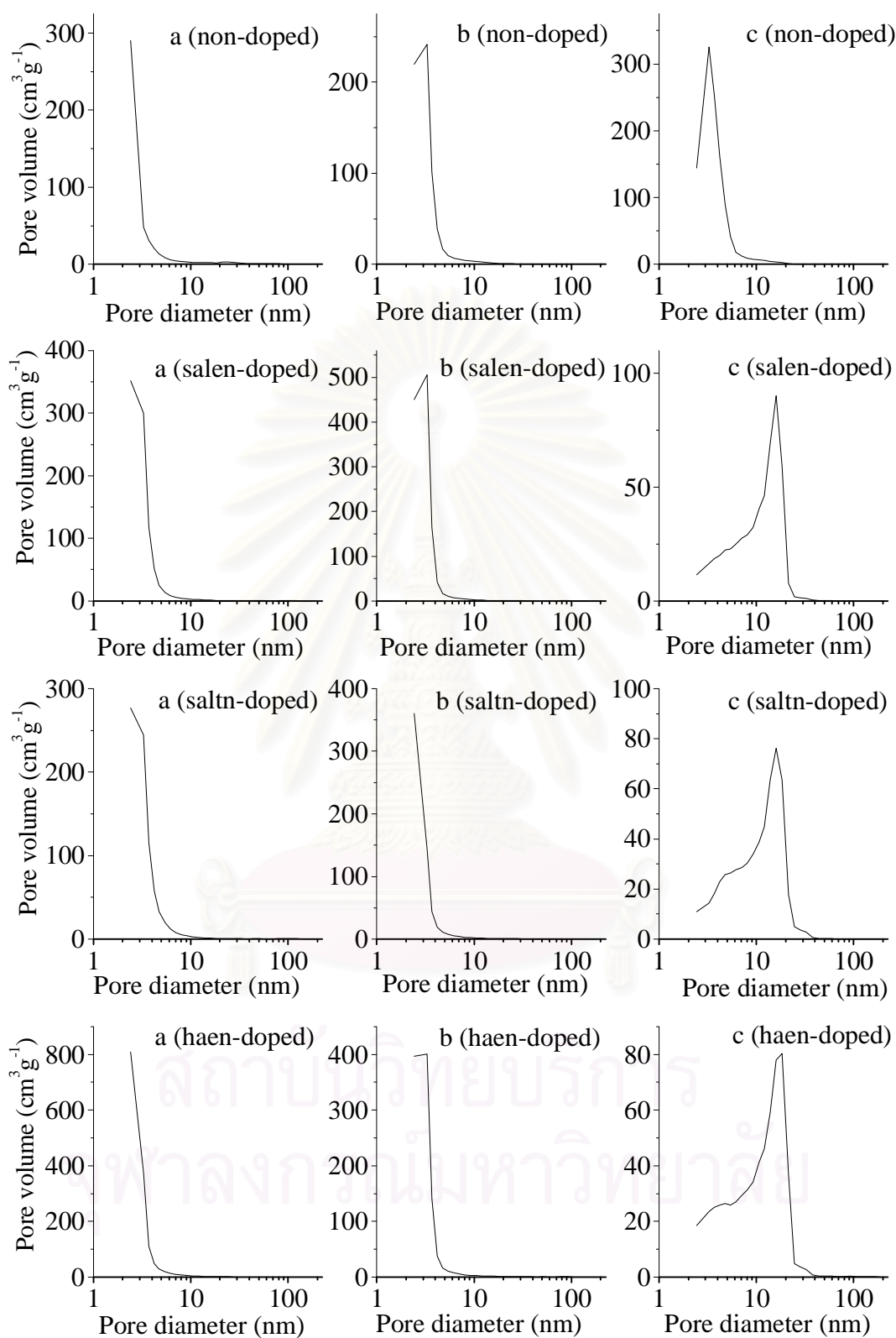


Figure 4.12 Pore size distribution of silica synthesized from various precursors: (a) TEOS (b) calcined mesoporous silica and (c) silica gel 60. The text in the parenthesis referred to the type of the Schiff's base doped silica.

4.1.2 Extraction properties of materials

The extraction properties of Schiff's base doped mesoporous silica synthesized from various silica precursors were conducted toward Cu(II), Fe(III) and Ni(II) in aqueous and 0.1 M NaNO₃ solution. The experiment was repeated three times. The results of each metal extraction were described as follows.

4.1.2.1 Extraction of Cu(II)

Form previous reported [47], the suitable condition for the extraction of Cu(II) by the Schiff's base doped mesoporous silica was pH 2.5. This condition was thus applied in this work. The results were plotted between the amount of Cu(II) extracted (mg g⁻¹) and type of precursor as presented in Figure 4.13.

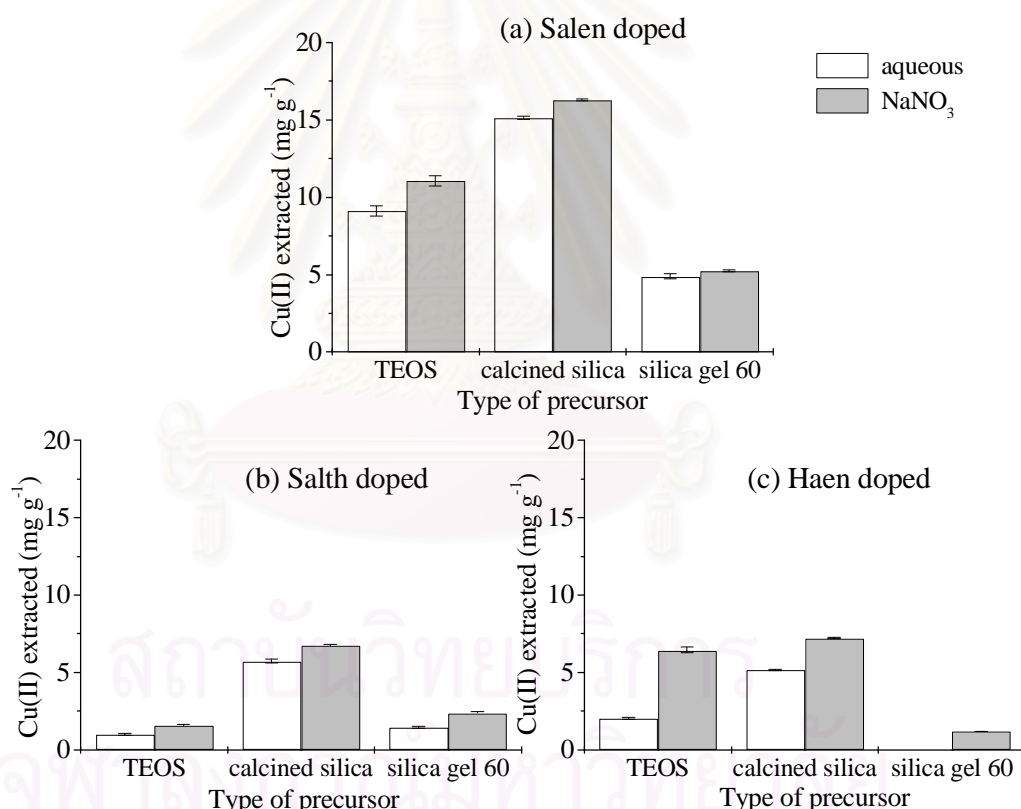


Figure 4.13 The amount of Cu(II) extracted by Schiff's base doped mesoporous silica: (a) salen doped, (b) saltn doped and (c) haen doped mesoporous silica

From the experimental results, it was found that non-doped mesoporous silica could not extract Cu(II) ions. As seen from Figure 4.13, the Cu(II) extractability of Schiff's base doped mesoporous silica synthesized from calcined mesoporous silica

higher than those of synthesized from TEOS or silica gel 60. This result could be explained by the silica prepared from the calcined mesoporous silica had higher surface area and amount of accessible Schiff's base. In addition, the Cu(II) ions extractability of all modified silica increased when the extraction was performed in NaNO₃ medium. The highest Cu(II) ion extracted value was found to be 16.29 ± 0.7 mg g⁻¹ which was obtained from salen doped mesoporous silica synthesized from calcined mesoporous silica. Interestingly, this Cu(II) extracted value was higher than 9.21 mg g⁻¹ which reported by Tarateerapap [54]. This phenomenon could be explained by the method used for the extraction. In fact, in this work, the extraction was performed via a magnetic stirrer. Whereas, in Tarateerapap's work, the experiment was carried out using an orbital shaker.

4.1.2.2 Extraction of Fe(III)

The influence of precursor on the Fe(III) extractability of Schiff's base doped mesoporous silica are displayed in Figure 4.14. According to the experimental results, non-doped mesoporous silica could not extract any Fe(III) ions in both media. On the contrary, all Schiff's bases doped mesoporous silica were capable of extracting these ions. This results indicated that Schiff's base ligands improve the Fe(III) extractability of silica. From the Figure 4.14, it was obviously seen that the amount of Fe(III) extracted was increased when NaNO₃ was present in metal solution. The comparison of the types of precursor, it was found that, in the NaNO₃ media, the salen doped mesoporous silica synthesized from calcined mesoporous silica had highest Fe(III) extractability. The highest extracted value was found to be 19.25 ± 0.36 mg g⁻¹. Considering the types of Schiff's base, it was found that salen doped mesoporous silica had the higher Fe(III) extractability than those of saltn doped or haen doped mesoporous silica.

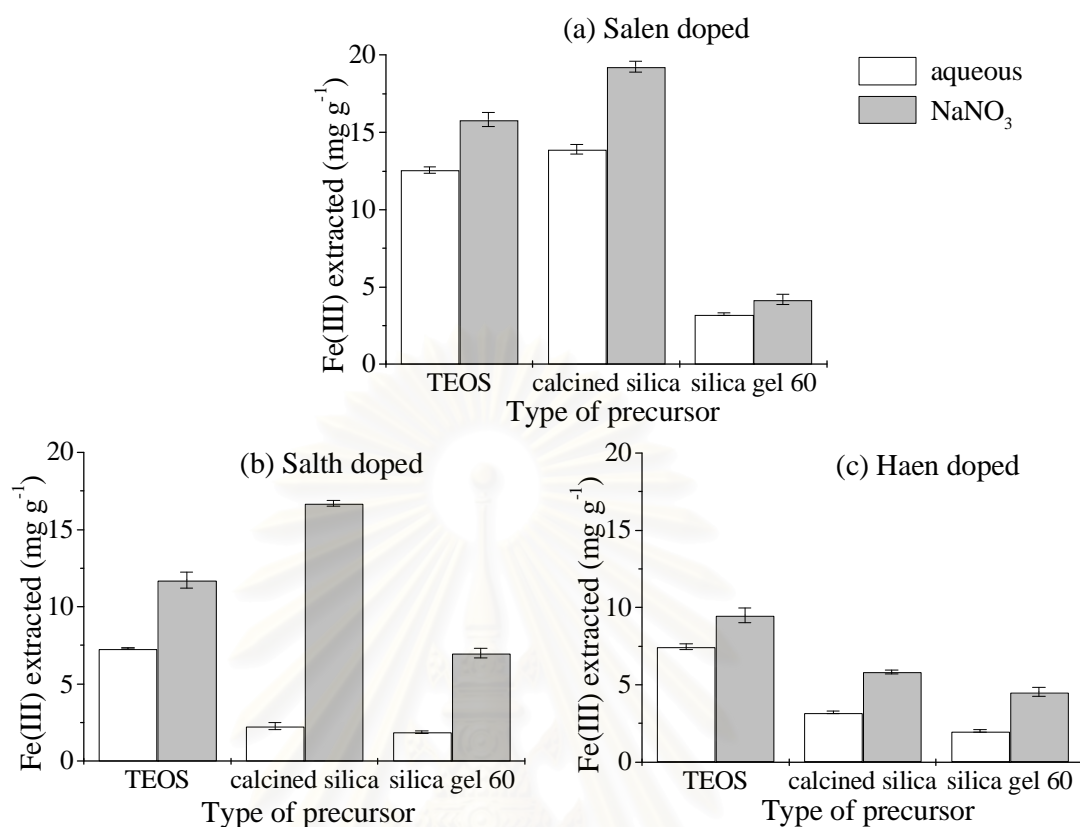


Figure 4.14 The amount of Fe(III) extracted by Schiff's base doped mesoporous silica: (a) salen doped, (b) saltn doped and (c) haen doped mesoporous silica.

4.1.2.3 Extraction of Ni(II)

The Ni(II) extractability of all silica synthesized from various precursors are shown in Figure 4.15. The Ni(II) extractability of all silica increased when the extraction performed in the NaNO₃ medium. In addition, the Ni(II) extractabilities of the non-doped and salen doped mesoporous silica were higher than those of saltn doped and haen doped mesoporous silica. These results implied that other Schiff's base doped mesoporous silica were not selective to the extraction of Ni(II).

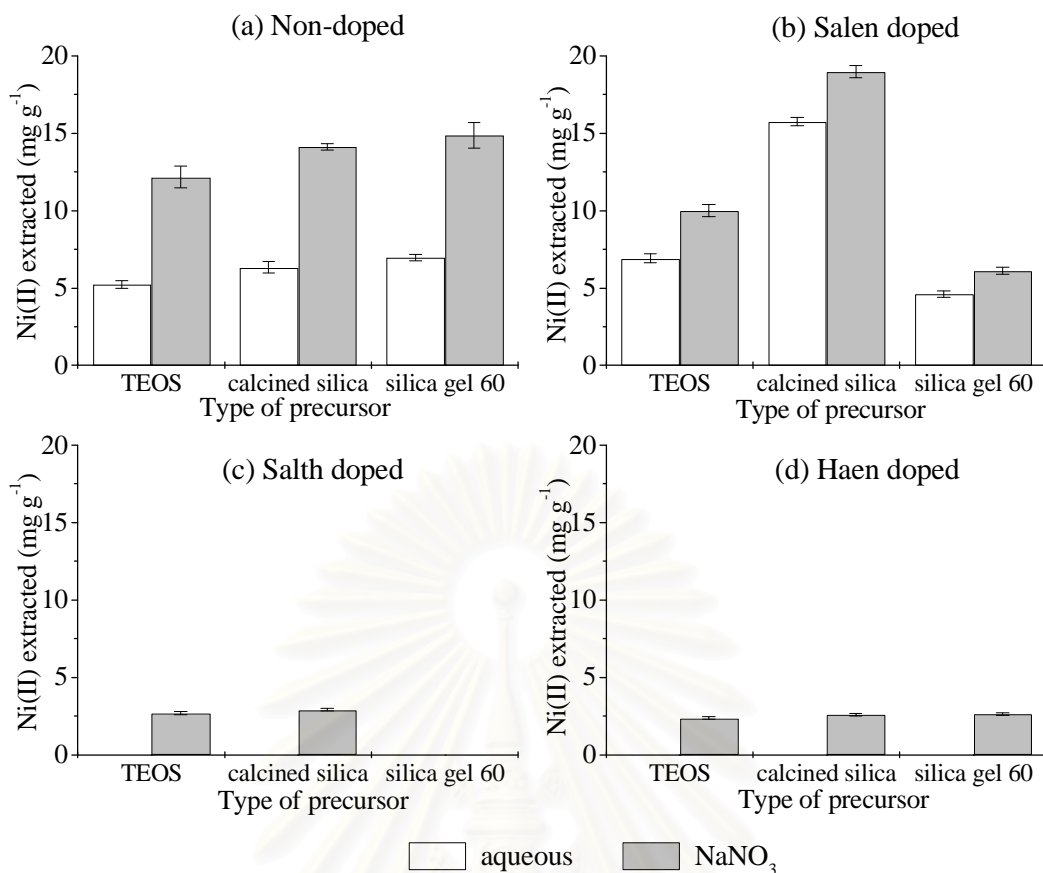


Figure 4.15 The amount of Ni(II) extracted by Schiff's base doped mesoporous silica: (a) salen doped, (b) saltn doped and (c) haen doped mesoporous silica

4.2 Synthesis and properties of silica synthesized from TEOS and co- precursor

The effect of silica co-precursor on the synthesis of Schiff's base doped mesoporous silica was also investigated in this work. Three different co-precursors are VTES, PTMS and ETES. The synthesis was performed in three replicated. The results are presented in Table 4.6 and Figure 4.16.

Table 4.6 The amount of incorporated Schiff's base in each Schiff's base doped mesoporous silica synthesized from TEOS and various co-precursors

Type of co-precursor	Amount of incorporated Schiff's base (mmol g ⁻¹)		
	Salen doped	Saltn doped	Haen doped
VTES	0.573 ± 0.011	0.385 ± 0.030	0.528 ± 0.006
PTMS	0.524 ± 0.009	0.351 ± 0.033	0.528 ± 0.012
ETES*	0.548	0.316	0.548

* Only one sample of each Schiff's base dope silica was synthesized since ETES is expensive.

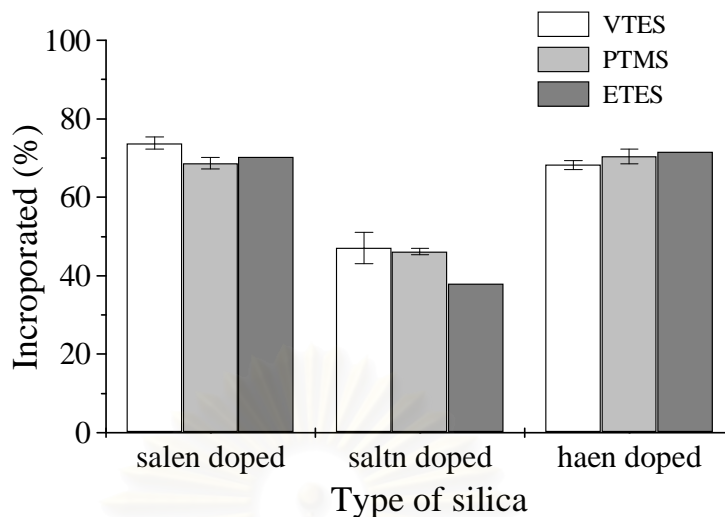


Figure 4.16 The percentage of incorporated Schiff's base in Schiff's base doped mesoporous silica synthesized by TEOS and different type of co-precursors.

As seen from Table 4.6 and Fig 4.16, the types of co-precursors did not significantly affect the amount of incorporated Schiff's base in the synthesized silica. To compared the amount of incorporated Schiff's base in Schiff's base doped mesoporous silica synthesized from TEOS and various co-precursors with those of silica synthesized from TEOS (Table 4.1), it was found that the Schiff's base doped silica synthesized from TEOS had higher amount of incorporated Schiff's base. These results might be due to the pendant groups of organosilane in the silica framework interfere the inclusion of Schiff's base molecules into the silica framework. Concerning the type of Schiff's base, the amount of incorporated Schiff's base in mesoporous silica was found to be in this order: salen > haen > saltn. This result was in accordance with the section 4.1.

4.2.1 Characterization of materials

4.2.1.1 Determination of organic matters

The organic matter content in silica synthesized from TEOS and various co-precursors are presented on Table 4.7. As seen, the organic matter contents obtained from the experiment were close to the theoretical values. For some minor difference might be explained by the amount of physisorbed and chemisorbed water as described previously.

Table 4.7 Organic matter content in mesoporous silica prepared from TEOS and various co-precursors.

Silica co-precursor	Type of silica	Organic matters (%)		Experimental value Theoretical value ^{× 100} (%)
		Experimental value	Theoretical value	
VTES*	non-doped	44.91 ± 0.75	39.01	115.13
	salen doped	51.17 ± 0.58	48.49	106.61
	saltn doped	47.75 ± 0.36	45.98	103.19
	haen doped	48.70 ± 0.53	48.51	100.39
PTMS*	non-doped	42.55 ± 0.88	37.81	112.54
	salen doped	52.15 ± 0.79	46.38	112.44
	saltn doped	46.13 ± 0.63	43.07	107.10
	haen doped	50.04 ± 0.67	47.66	105.00
ETES**	non-doped	43.46	38.74	112.10
	salen doped	50.44	47.80	105.50
	saltn doped	43.77	44.17	99.10
	haen doped	48.43	48.70	99.50

* Experimental values are calculated from three replicate data.

** Only one sample of each Schiff's base doped silica was calcined since ETES is expensive.

4.2.1.2 Determination of accessible Schiff's base

As described previously in section 4.1.1.2, the mixture of ethanol and H₂O with the volume ratio of 9:1 was used as an extracting solvent. The percentage of accessible Schiff's base in each modified silica is depicted in Figure 4.17. It was found that the percentage of accessible Schiff's base did not affected by types of co-precursors. Concerning the types of Schiff's base, it was found that the amount of accessible was found to be in this order: salen > saltn >> haen. This result may be explained by the inappropriate solvent for the haen ligands.

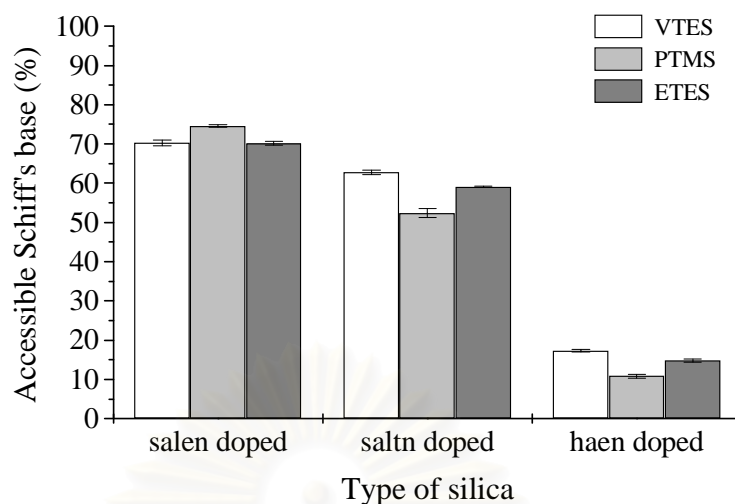


Figure 4.17 Percentage of accessible Schiff's base in modified silica synthesized from TEOS and various co-precursors.

4.2.1.3 Investigation of organic molecules using FTIR spectroscopy

As described previously in section 4.1.1.3. The presence of surfactant and Schiff's base molecules in the silica frameworks are shown in Figure 4.18-4.21. The details are given as follows: The major peaks of silica frameworks are absorption band of at 3400 cm^{-1} and 960 cm^{-1} . The absorption band around 2800 cm^{-1} , 2900 cm^{-1} and 1480 cm^{-1} are assigned to the C-H stretching of CTAB. The characteristic bands of C=N stretching at about 1600 cm^{-1} due to imine group of Schiff's base.

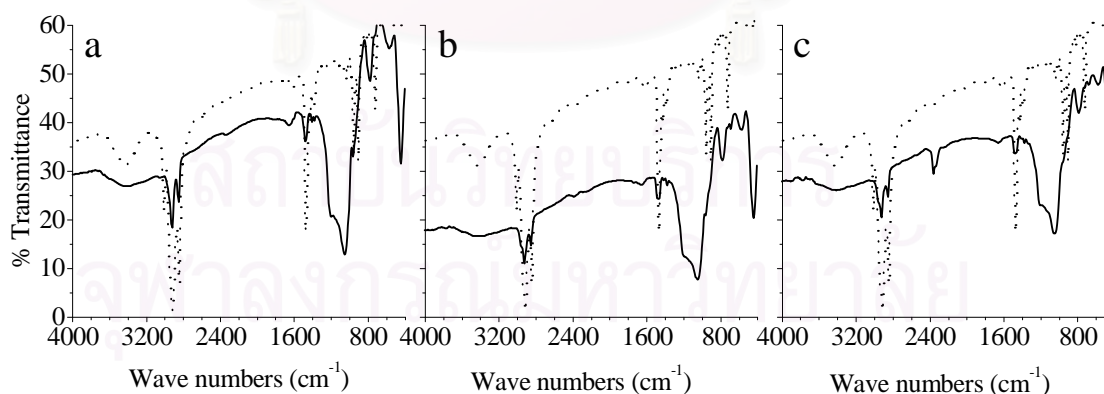


Figure 4.18 FT-IR spectra of CTAB and non-doped mesoporous silica synthesized from TEOS and various co-precursors: (a) VTES, (b) ETES and (c) PTMS. (Solid line: mesoporous silica, dot line: CTAB)

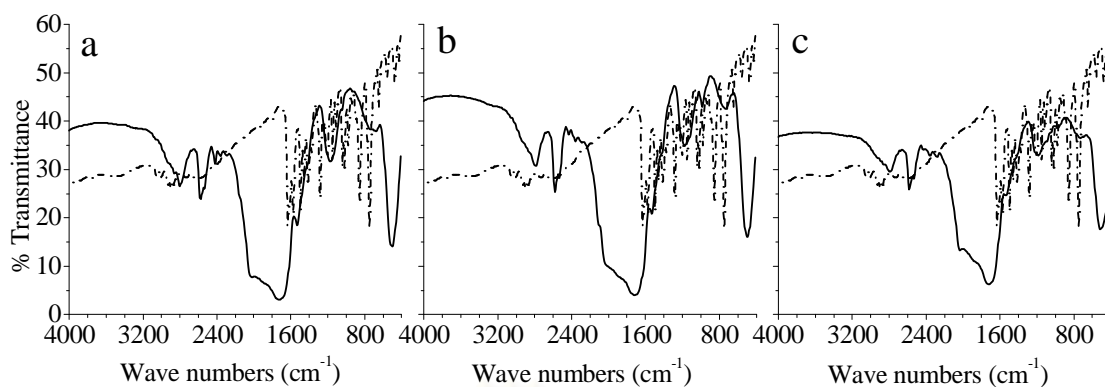


Figure 4.19 FT-IR spectra of salen and salen doped mesoporous silica synthesized from TEOS and various co-precursors: (a) VTES, (b) ETES and (c) PTMS. (Solid line: mesoporous silica and dash dot line: salen)

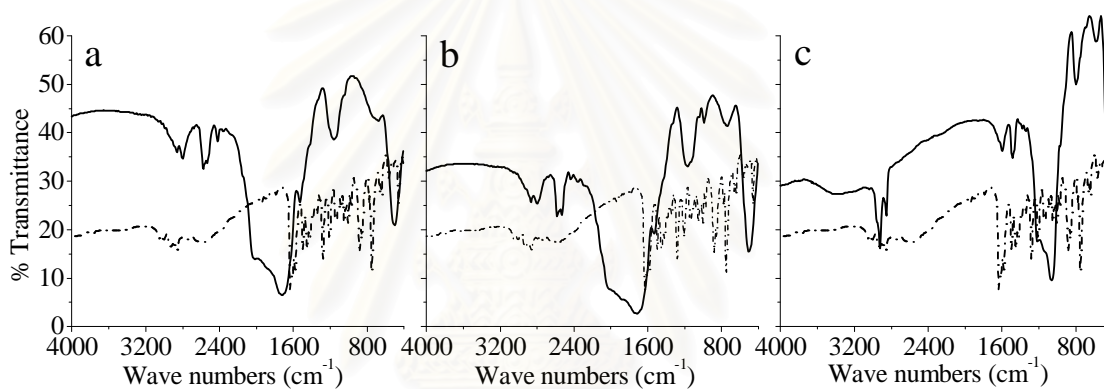


Figure 4.20 FT-IR spectra of saltn and saltn doped mesoporous silica synthesized from TEOS and various co-precursors: (a) VTES, (b) ETES and (c) PTMS. (Solid line: mesoporous silica and dash dot line: saltn)

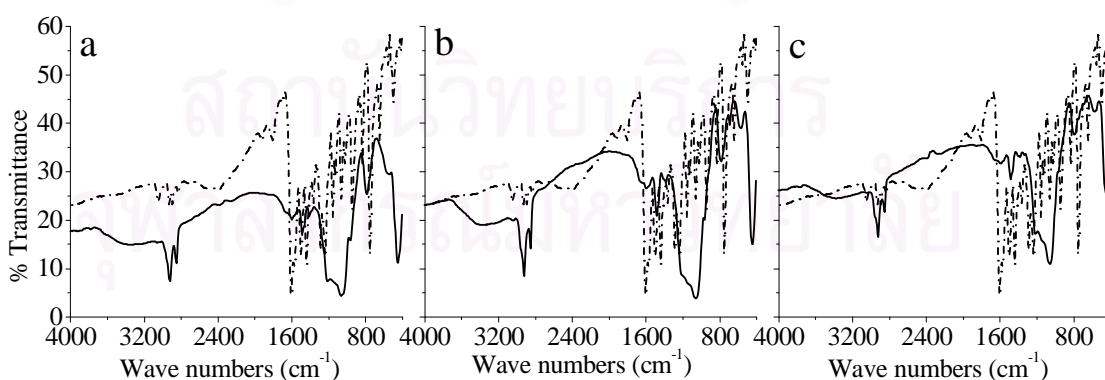


Figure 4.21 FT-IR spectra of haen and haen doped mesoporous silica synthesized from TEOS and various co-precursors: (a) VTES, (b) ETES and (c) PTMS. (Solid line: mesoporous silica and dash dot line: haen)

4.2.1.4 Determination of crystallinity of materials

The X-ray diffraction patterns obtained for the as-synthesized and calcined silica are displayed in Figure 4.22. All of the samples exhibited XRD reflection peak at 2θ around 2 degree. These patterns corroborated the occurrence of ordered mesostructured materials. Furthermore, the samples after calcinations revealed the increasing peak intensity. This indicated that the calcined samples were better structural ordering compare with the as-synthesized samples. These observed phenomena could be explained by that the calcination process promoted siloxane cross-linking led to the improving of ordering of the silica framework. The values of the structural parameters are listed in Table 4.8

As seen from Table 4.8, it was found that the d-spacing values of the calcined silica were significantly decreased in all case. This could be due to the occurrence of shrinkage in the lattice spacing after removal of surfactant as described earlier.

Table 4.8 XRD results of materials synthesized from TEOS and various co-precursors.

Co-precursor	Type of silica	as-synthesized silica		calcined silica	
		Two theta	d(nm)	Two theta	d(nm)
VTES	None-doped	2.540	3.48	2.920	3.02
	Salen doped	2.359	3.74	2.600	3.40
	Saltn doped	2.340	3.77	2.799	3.15
	Haen doped	2.359	3.74	2.560	3.45
PTMS	None-doped	2.500	3.53	2.602	3.39
	Salen doped	2.360	3.74	2.739	3.22
	Saltn doped	2.320	3.81	2.520	3.50
	Haen doped	2.360	3.74	2.620	3.37
ETES	None-doped	2.561	3.45	2.980	2.96
	Salen doped	2.301	3.84	2.619	3.37
	Saltn doped	2.300	3.84	2.719	3.25
	Haen doped	2.320	3.85	2.619	3.37

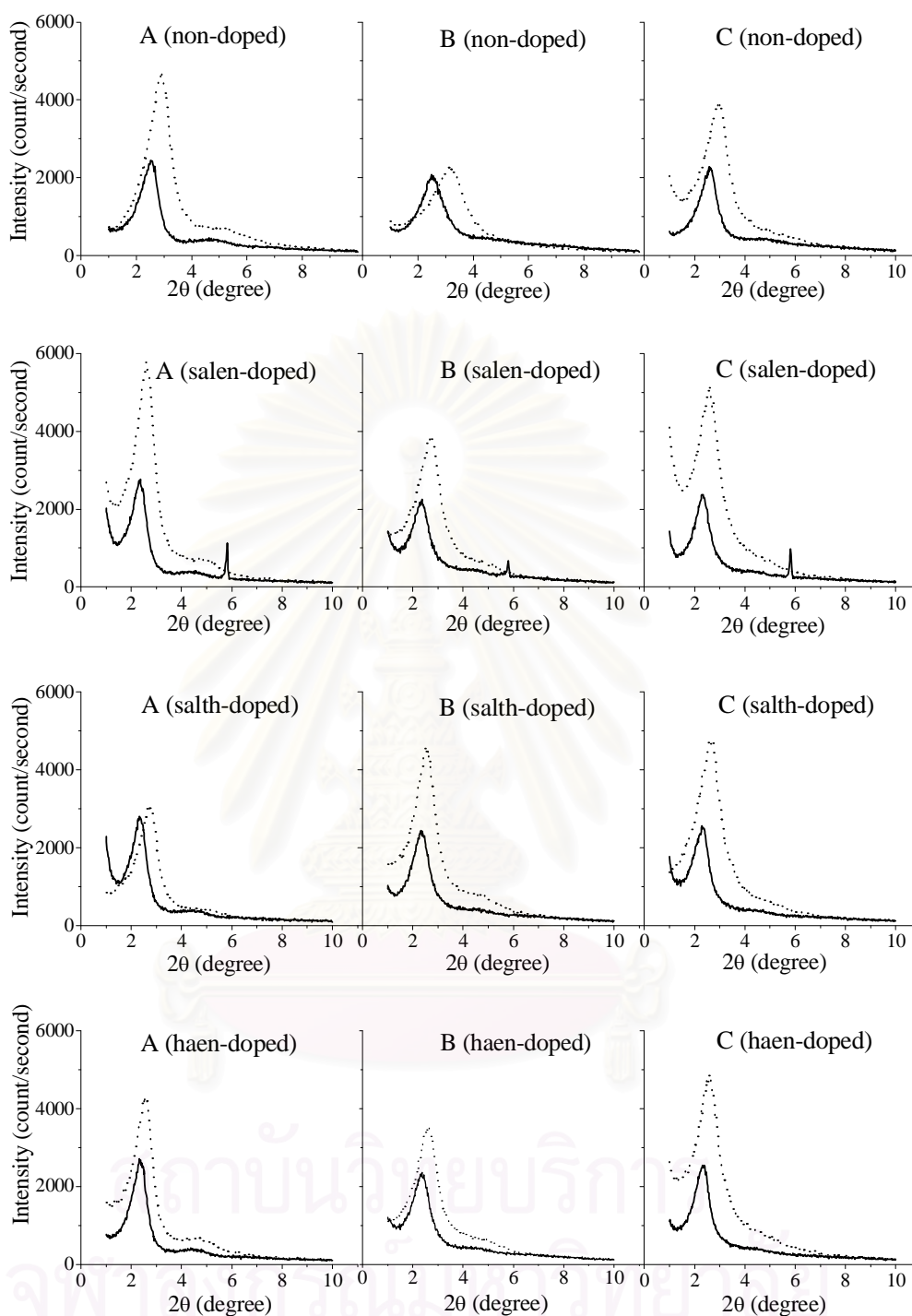


Figure 4.22 XRD patterns of silica synthesized from TEOS and various co-precursors: (A) VTES, (B) PTMS and (C) ETES (The text in the parenthesis referred to the type of the Schiff's base doped silica). Solid line: as-synthesized silica, dot line: calcined silica.

4.2.1.5 Morphology of materials

The well defined external morphologies of the samples synthesized from TEOS and various co-precursors are shown in Figure 4.23-4.25. The SEM micrograph reveals similar morphology. All of the samples illustrate agglomerates of spherical particles with smooth surface. The particle sizes of samples collected from SEM images were found in the range of 0.8 – 2.9 μm . In fact, the morphology of silica synthesized from TEOS and various co-precursors are similar to those of synthesized from TEOS without adding co-precursors (Figure 4.8). These results suggested that the addition of 20% mol co-precursors were not affect the morphology of synthesized silica. Moreover, the comparison of non-doped with Schiff's base doped mesoporous silica. It is interesting that the morphology of silica was not affected by the functionalization of Schiff's base ligand.

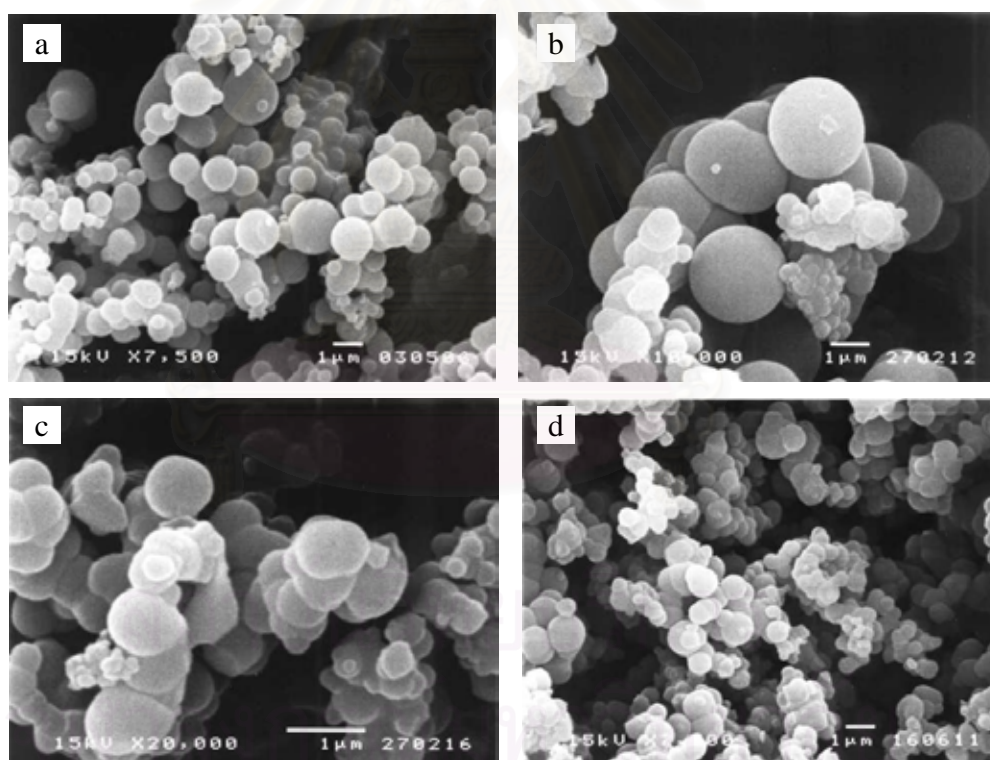


Figure 4.23 SEM images of silica synthesized from TEOS and VTES: (a) non-doped, (b) salen doped, (c) saltn doped and (d) haen doped mesoporous silica.

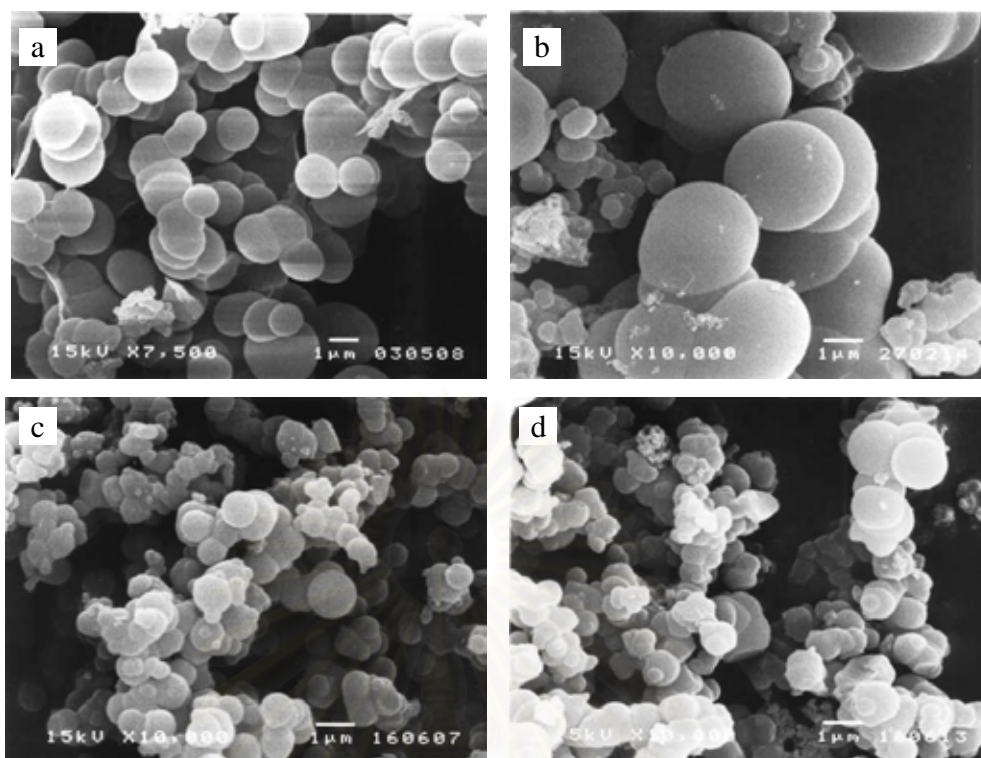


Figure 4.24 SEM images of silica synthesized from TEOS and PTMS: (a) non-doped, (b) salen doped, (c) saltn doped and (d) haen doped mesoporous silica

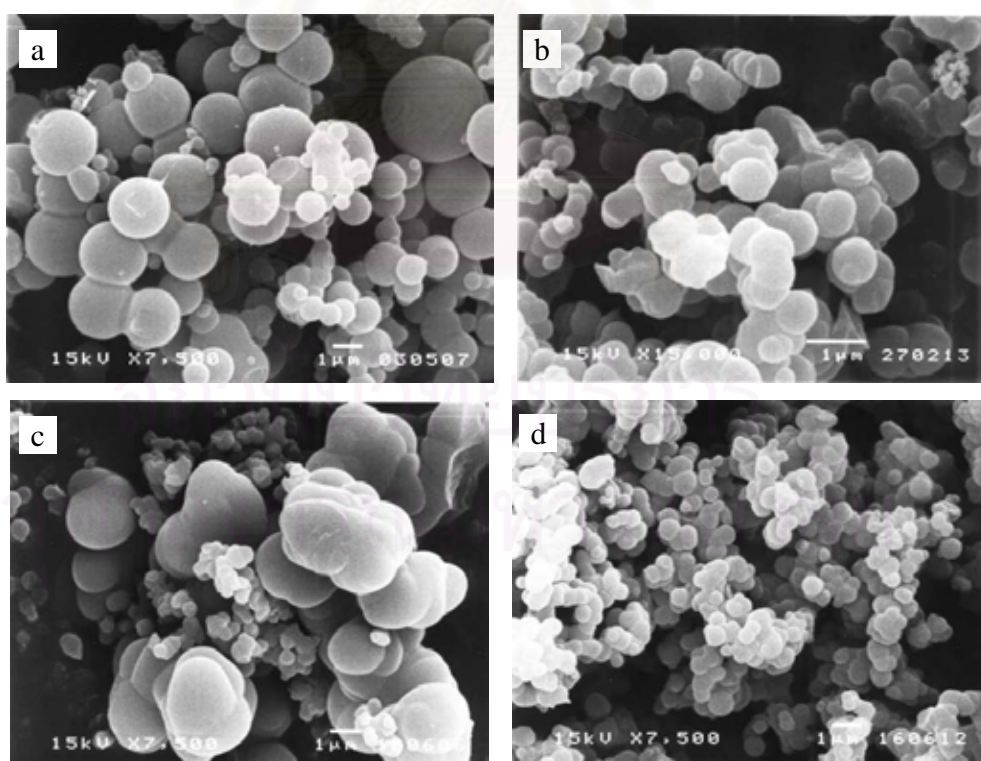


Figure 4.25 SEM images of silica synthesized from TEOS and ETES: (a) non-doped, (b) salen doped, (c) saltn doped and (d) haen doped mesoporous silica

4.2.1.6 Determination of surface area and pore size

The BET surface area of all as-synthesized silica were found in the range of 12 – 25 m² g⁻¹ which was very low due to the existence of the surfactant template in the silica framework. In order to conduct the porous structure of these materials, the surfactant template was removed by the calcinations. N₂ adsorption-desorption isotherms and pore size distribution of calcined silica synthesized from TEOS and various co-precursors are shown in Figure 4.26 and Figure 4.27, respectively. All samples were typical type IV isotherm with H4 hysteresis loop, which was characteristic of mesoporous material with slit-shaped pores. In addition, all sample synthesized by difference co-precursors presented the narrow pore size distribution, as shown in Fig 4.27.

The textural properties and mesoporosity were calculated using the isotherms and reported in Table 4.9. All modified silica were exhibited large BET surface area. The average pore diameters were in the range of 2.11 – 3.84 nm which were mesoporous materials. Considering the pore volume of silica synthesized from TEOS and various co-precursors with those of synthesized from TEOS without adding co-precursors (Table 4.5). It was found that the pore volume was decreased when co-precursor was added. This decreasing could be explained by the pore of silica was filled with the pendent group of organosilane therefore, the pore volume was reduced.

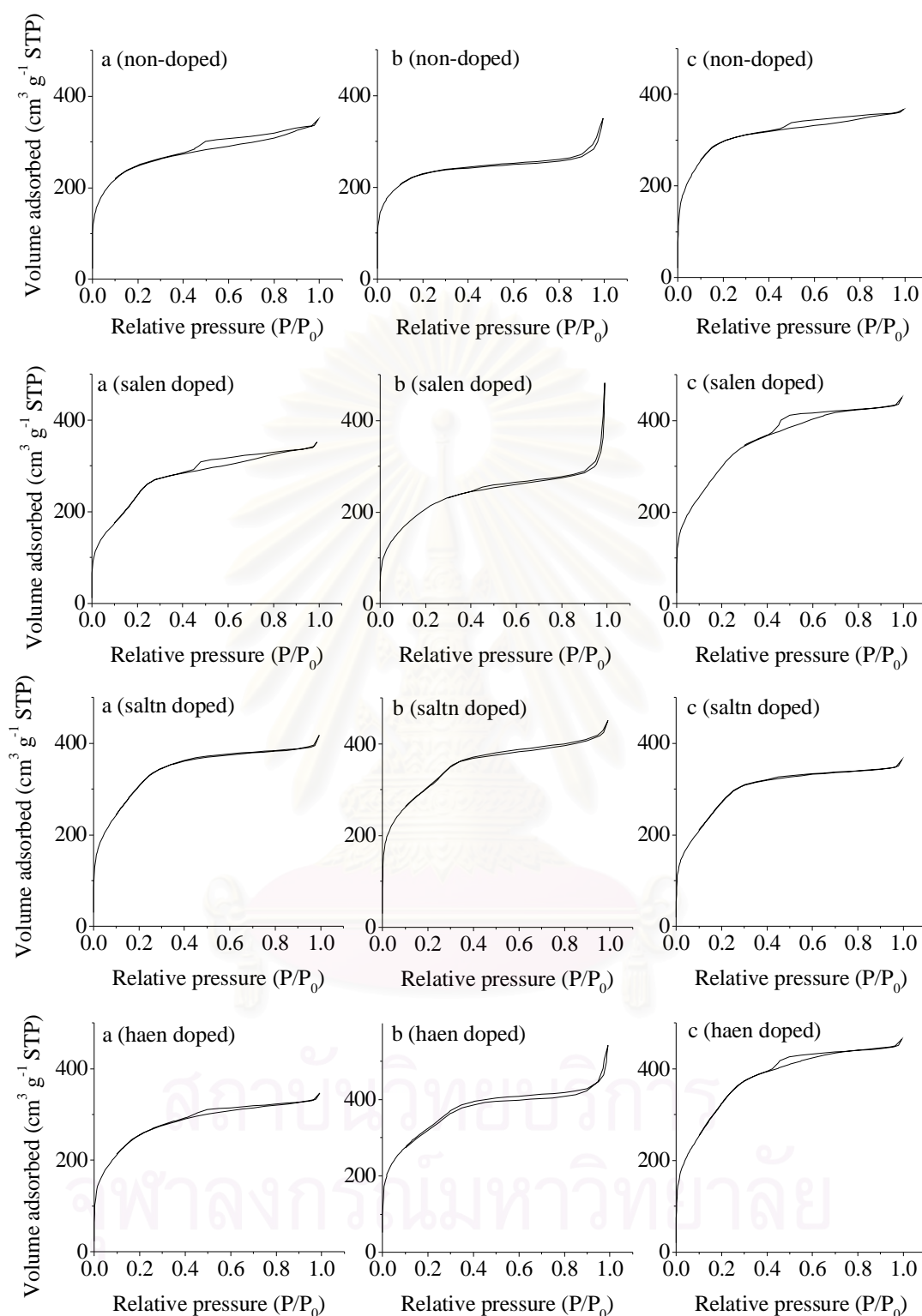


Figure 4.26 Nitrogen sorption isotherm of silica synthesized from TEOS and various co-precursors: (a) VTES, (b) PTMS and (c) ETES. The text in the parenthesis referred to the type of the Schiff's base doped silica.

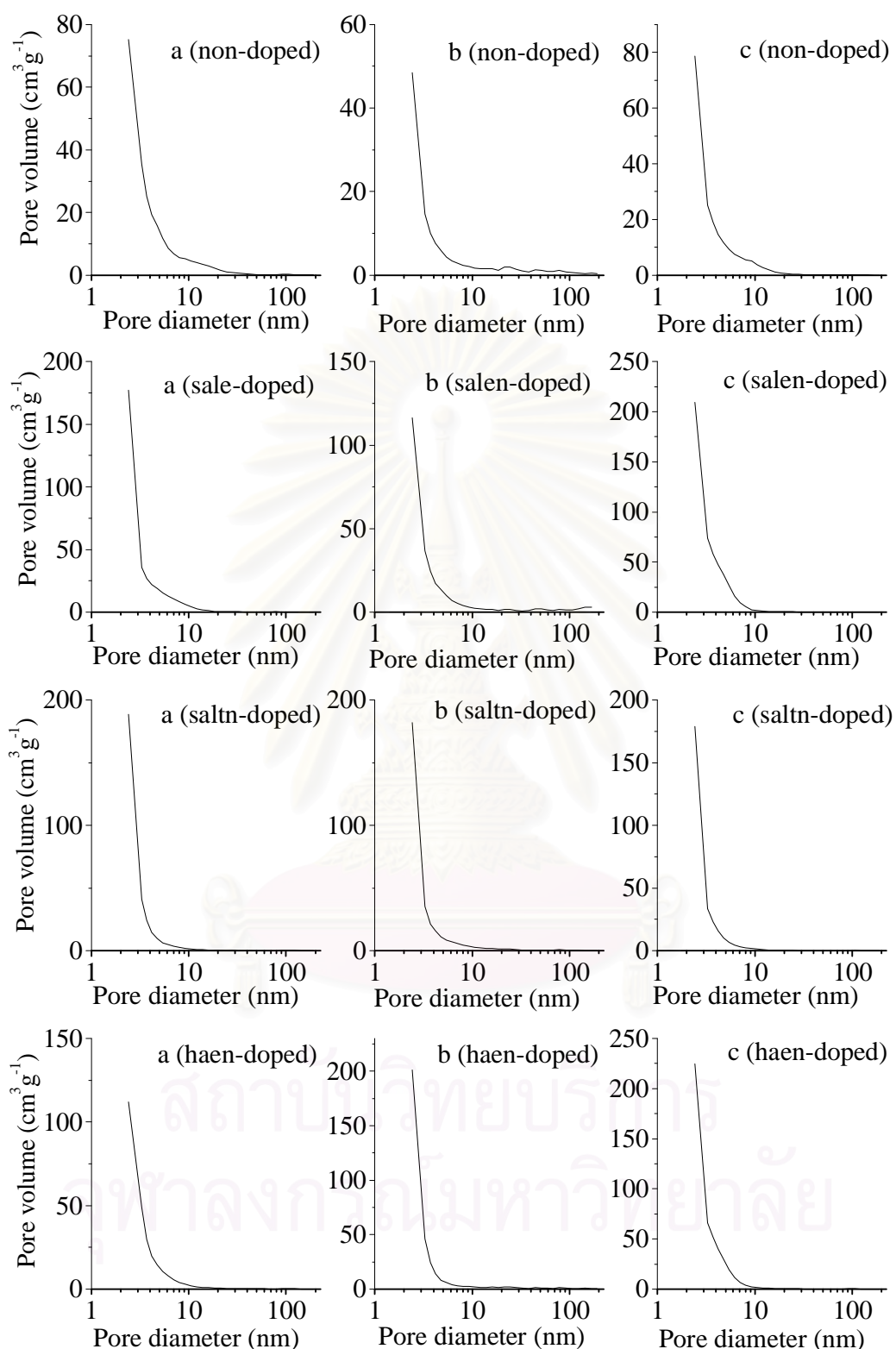


Figure 4.27 Pore size distribution of silica synthesized from TEOS and various co-precursors: (a) VTES, (b) PTMS and (c) ETES. The text in the parenthesis referred to the type of the Schiff's base doped silica.

Table 4.9 Characterizations results of the materials synthesized from TEOS and various co-precursors

Co-precursor	Type of silica	S (m^2g^{-1})	V_p (cm^3g^{-1})	APD (nm)	d_{100} (nm)	a_o (nm)	w (nm)
VTES	Non-doped	878	0.54	2.44	3.02	10.46	8.03
	Salen doped	707	0.54	3.07	3.40	11.76	8.69
	Saltn doped	1003	0.64	2.55	3.15	10.93	8.37
	Haen doped	930	0.53	2.29	3.45	11.94	9.65
PTMS	Non-doped	814	0.53	2.60	3.39	11.75	9.15
	Salen doped	756	0.75	3.94	3.22	11.16	7.22
	Saltn doped	1076	0.70	2.59	3.50	12.13	9.55
	Haen doped	1160	0.82	2.82	3.37	11.67	8.85
ETES	Non-doped	1071	0.57	2.11	2.96	10.26	8.15
	Salen doped	935	0.69	2.96	3.37	11.67	8.72
	Saltn doped	813	0.56	2.75	3.25	11.24	8.49
	Haen doped	1215	0.71	2.35	3.37	11.67	9.32

S , BET surface area (m^2g^{-1}) obtained from N_2 sorption; V_p , Total pore volume (cm^3g^{-1}) obtained from single-point volume at $P/P_o = 0.99$; APD , average pore diameter calculated from $4V_p/S$; d_{100} , d-value 100 reflections; a_o = the lattice parameter, from the XRD data using the formula $a_o = 2d_{100}\sqrt{3}$; w , pore wall thickness was equaled to a_o-APD .

4.2.2 Extraction properties of materials

To study the influence of co-precursor on the metal extraction properties of non-doped and Schiff's base doped mesoporous silica, the metal extractability of non-doped and Schiff's base doped mesoporous silica synthesized from TEOS and various co-precursors were compared with the silica synthesized from TEOS without adding co-precursor (The results are come from the section 4.1.2). The experiment were also performed using Cu(II), Fe(III) and Ni(II) in aqueous and 0.1 M NaNO_3 . The extractions were done in three replicates. The results of each metal extraction were described as follows.

4.2.2.1 Extraction of Cu(II)

As described previously in section 4.1.2.1. The Cu(II) extraction was also conducted at pH 2.5. The obtained results are presented in Figure 4.28. The experimental results found that non-doped mesoporous silica is not able to extract

Cu(II). It was seen from Figure 4.28 that the presence of NaNO_3 in metal solution cause the increasing of the Cu(II) sorption capacity of Schiff' base doped mesoporous silica. Consider the influence of co-precursor on the Cu(II) extractability, it was found that the amount of Cu(II) extracted increase when silica synthesized from TEOS and various co-precursors were used as sorbent, except haen doped mesoporous silica. For the later ligand, the Cu(II) extracted value not significantly different.

For the comparison of the type of Schiff's base, it was found that the Cu(II) extractability of Schiff base doped mesoporous silica had shown the following trend: salen doped > haen doped > saltn doped. This order was consistent with the amount of incorporated Schiff's base in the silica.

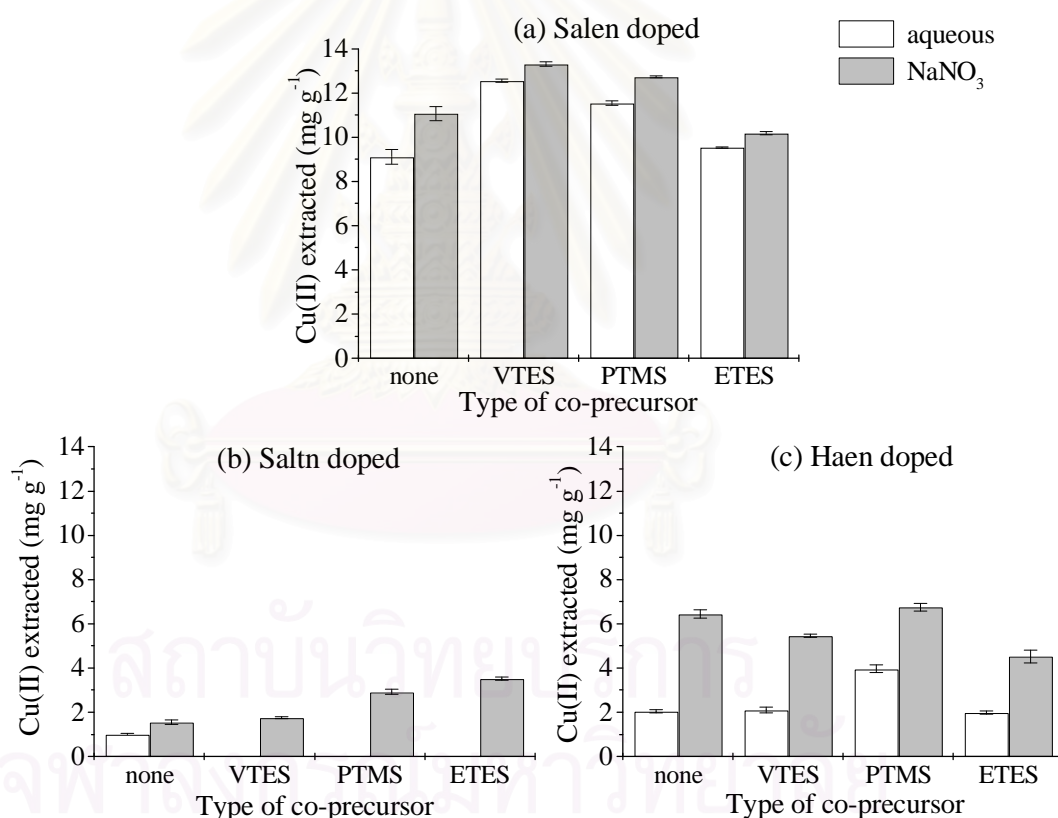


Figure 4.28 The Cu(II) extracted by Schiff's base doped mesoporous silica synthesized from TEOS and various co-precursor: (a) salen doped, (b) saltn doped and (c) haen doped

4.2.2.2 Extraction of Fe(III)

The influence of co-precursor on the Fe(III) extraction were also conduct in aqueous and 0.1 M NaNO₃ medium. The obtained results were depicted in Figure 4.29. the Fe(III) extraction capacity were increased when the extraction were performed in the NaNO₃ medium. For the salen doped and haen doped mesoporous silica, it was found that the Fe(III) extractability of modified silica obtained from TEOS and co-precursor were lower than those of silica synthesized from TEOS. This decreasing of Fe(III) sorption capacity was probably due to the steric hindrance of organic group from organosilane on the surface of silica.

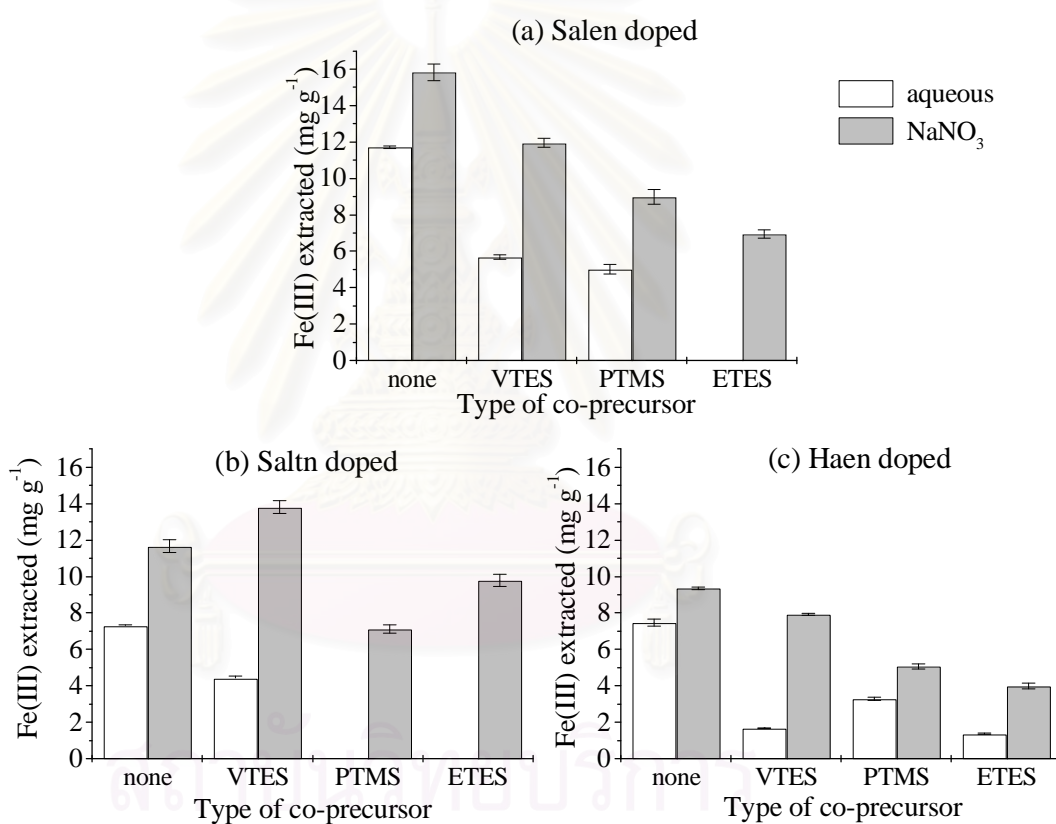


Figure 4.29 The Fe(III) extracted by Schiff's base doped mesoporous silica synthesized from TEOS and various co-precursors: (a) salen doped, (b) saltn doped and (c) haen doped

4.2.2.3 Extraction of Ni(II)

The amount of Ni(II) extracted using non-doped and Schiff's base doped mesoporous silica as sorbent are shown in Figure 4.30. As seen, the presence of NaNO₃ in metal solution enhanced the Ni(II) extractability of all silica. In addition, the Ni(II) extracted values of non-doped and salen doped mesoporous silica were higher than these of saltn doped or haen doped silica. These results meant that the other Schiff's base doped mesoporous silica were not selective to the extraction of Ni(II). For the comparison of Ni(II) extractability of silica synthesized with or without co-precursor, it was found that the presence of co-precursor did not significantly affect the Ni(II) extractability of Schiff's base doped mesoporous silica.

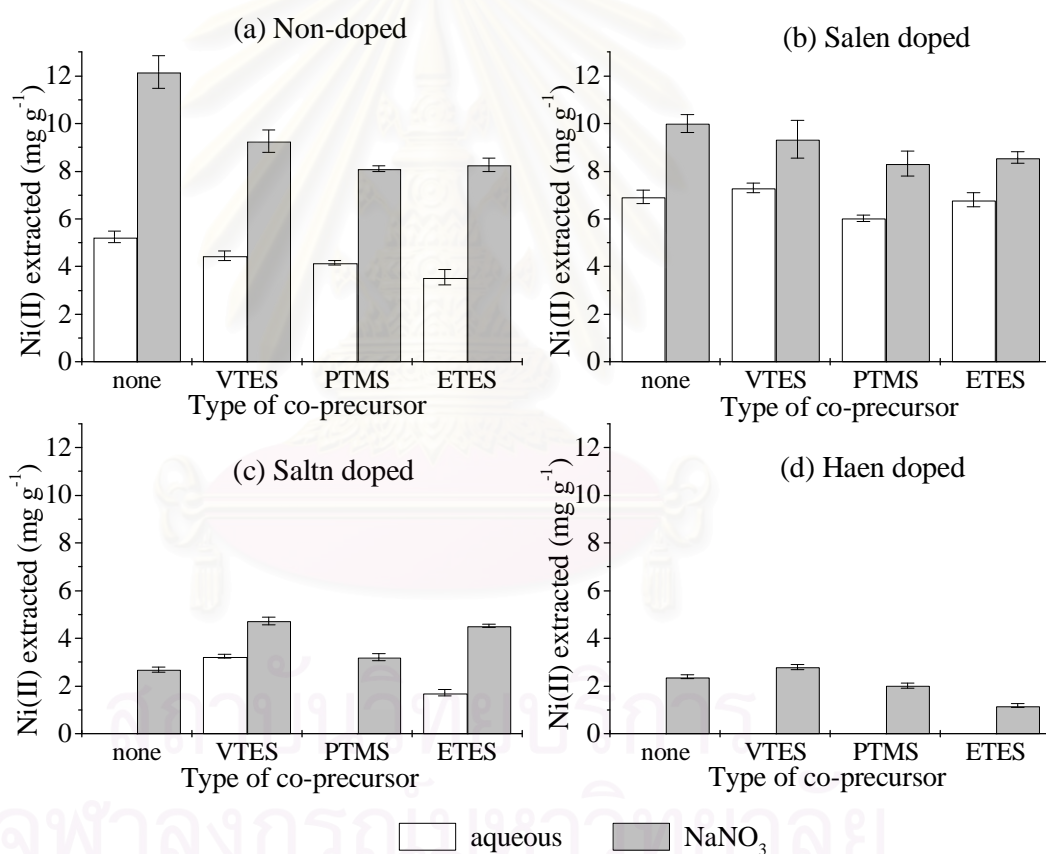


Figure 4.30 The Ni(II) extracted by Non-doped and Schiff's base doped mesoporous silica synthesized from TEOS and various co-precursor: (a) salen doped, (b) saltn doped and (c) haen doped

4.3 Influence of Schiff's base content on the synthesis and extraction properties of Schiff's base doped silica

The amount of incorporated Schiff's base in modified silica is a crucial factor that could influence the synthesis and sorption properties of the modified silica. Therefore, the synthesis and sorption properties of silica synthesized from various mole ratios of Schiff's base/TEOS were investigated.

4.3.1 Synthesis of material

In this part, the materials were prepared by keeping mole ratio of TEOS : H₂O : CTAB : C₂H₅OH equal to 1 : 140 : 0.18 : 13 and varying the mole ratios of Schiff's base/TEOS to 0.12, 0.15 and 0.18. The maximum mole ratio of Schiff's base/TEOS was limited at 0.18 due to the restriction of the solubility of Schiff's base. From the synthesis result, the similar phenomenon of leaching Schiff's base was observed as described previously in section 4.1. The amount of incorporated Schiff's base in mmol g⁻¹ of each Schiff's base doped mesoporous silica base on three replicate syntheses are presented in Table 4.10.

Table 4.10 The amount of incorporated Schiff's bases in each Schiff's base doped mesoporous silica synthesized from various mole ratios of Schiff's base/TEOS.

Mole ratio Schiff's base/TEOS	Amount of incorporated Schiff's base (mmol g ⁻¹)		
	Salen doped	Saltn doped	Haen doped
0.12	0.670 ± 0.009	0.490 ± 0.013	0.608 ± 0.022
0.15	0.874 ± 0.009	0.678 ± 0.018	0.814 ± 0.004
0.18	1.009 ± 0.001	0.856 ± 0.029	0.964 ± 0.007

From Table 4.10, the amount of incorporate Schiff's base was increased with the increasing of the Schiff's base/TEOS mole ratio. Concerning the type of Schiff's base, all silica synthesized from various mole ratios of Schiff's base/TEOS, the amount of incorporated Schiff's base was found to be in this order: salen > haen > salth. In addition, it is interestingly that the amounts of incorporated of Schiff's base were found higher than the previously reported by Khamloet [47]. The higher incorporated Schiff's base due to the mixing time of Schiff's base and ethanol was prolonged then the solubility of Schiff's base ligands are improved. Consequence, the starting mole

ratios of Schiff's base/TEOS could be extend to 0.18, thus the amounts of incorporated of Schiff's base are increased.

4.3.2 Characterization of materials

4.3.2.1 Determination of organic matters

The organic matter content in silica synthesized from various Schiff's base/TEOS mole ratios are shown in Table 4.11. It was found in all cases that the organic matter content obtained from experiment were close to the values calculated from the starting materials. The minor different could be explained by the amounts of the physisorbed and chemisorbed water as described previously.

Table 4.11 The organic matter contents in silica synthesized from different mole ratios of Schiff's base/TEOS.

Mole ratio of Schiff's base/TEOS	Type of silica	Organic matters (%)		$\frac{\text{experimental value}}{\text{theoretical value}} \times 100$ (%)
		Experimental value*	Theoretical value	
0.12	salen doped	55.52 ± 0.38	55.61	99.83
	saltn doped	51.73 ± 0.54	53.67	96.39
	haen doped	54.09 ± 0.13	55.88	96.80
0.15	salen doped	61.68 ± 0.44	58.75	104.98
	saltn doped	56.93 ± 0.49	56.42	100.90
	haen doped	60.28 ± 0.89	59.03	102.12
0.18	salen doped	62.31 ± 0.35	60.67	102.70
	saltn doped	60.62 ± 1.35	59.12	102.54
	haen doped	62.45 ± 1.60	61.46	101.62

* The experimental value base on three replicate experimental data.

4.3.2 Extraction properties of materials

4.3.2.1 Extraction of Fe(III)

To study the effect of the amount of Schiff's base ligand in the Schiff's base doped mesoporous silica on the metal sorption capacity of these silica. Thus, in this section, the silica synthesized from various Schiff's base/TEOS mole ratios were used as sorbent. The results from previous section reveals that Schiff's base doped mesoporous silica had show the excellent sorbent for the extraction of Fe(III) ions in

0.1 M NaNO_3 , so this condition was applied in this study. The extraction results are shown in Figure 4.32.

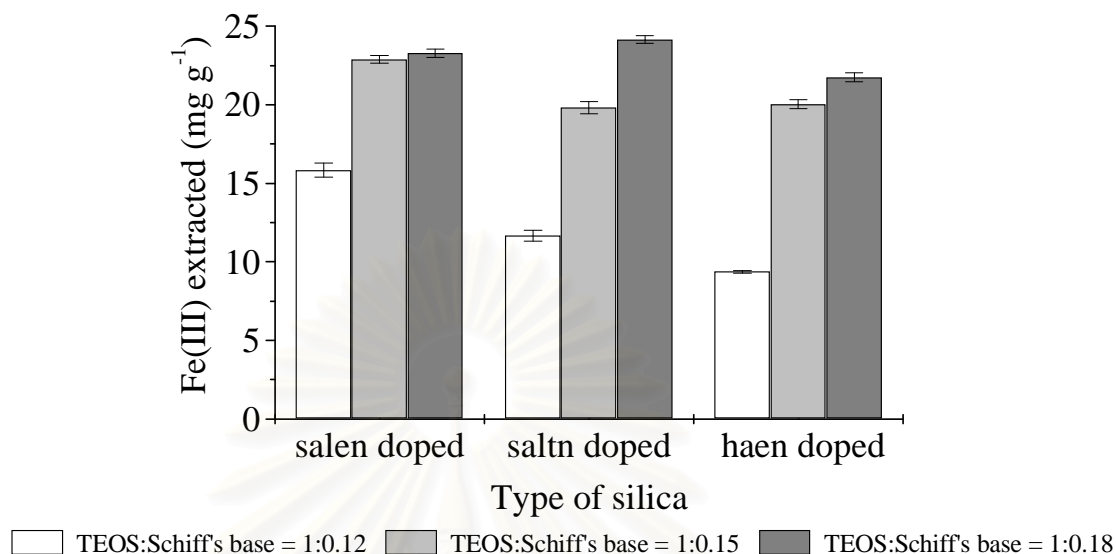


Figure 4.32 The Fe(III) extractability of Schiff's base doped mesoporous silica synthesized from various Schiff's base/TEOS mole ratios.

As seen from Figure 4.32, The amount of Fe(III) extracted was found to increase with the increasing of Schiff's base/TEOS mole ratio. This result imply that the amount of Schiff's base play the important role for the extraction of Fe(III). The comparison between type of Schiff's base, it was found that the Fe(III) sorption capacity of salen doped mesoporous silica higher than saltn doped or haen doped mesoporous silica when Schiff's base/TEOS mole ratio was 0.12 or 0.15. However, the Fe(III) extractability were slightly different for silica synthesized from Schiff's base/TEOS mole ratio equal 0.18.

4.4 Profound extraction study on appropriated Schiff's base modified sorbents

From previous sections (4.1-4.2), the salen doped mesoporous silica synthesized from TEOS or calcined mesoporous silica was shown the excellent extraction properties due to its high surface area, crystallinity and the amount of accessible salen. Thus, this silica was selected as a sorbent for profound extraction experiment.

4.4.1 Reproducibility

The reproducibility of metal extraction of salen doped mesoporous silica synthesized from TEOS or calcined mesoporous silica was studied towards Fe(III) in 0.1 M NaNO₃ medium since both materials showed good extractability. The obtained results are tabulated in Table 4.12. The reproducibility was good.

Table 4.12 The reproducibility results of Fe(III) extracted by salen doped mesoporous silica synthesized from TEOS or calcined mesoporous silica

Extraction number	Amount of Fe(III) extracted (mg g ⁻¹) by each silica	
	TEOS	Calcined mesoporous silica
1	15.32	19.01
2	16.06	19.66
3	16.15	19.08
4	15.00	19.02
5	14.72	19.22
6	14.61	19.33
7	15.48	19.42
8	15.13	19.17
9	15.44	19.68
10	15.59	-
11	15.80	-
12	15.66	-
13	15.32	-
14	16.06	-
15	16.15	-
Average	15.41	19.29
SD.	0.49	0.26
%RSD	3.15	1.33

4.4.2 Kinetic extraction

Kinetic of adsorption is one of the most important characteristic to be responsible for the efficiency of adsorption. The kinetic sorption of salen doped mesoporous silica synthesized from TEOS or calcined mesoporous silica were studies towards Cu(II) and Fe(III) in 0.1 M NaNO₃ medium. The amounts of extracted metal as a function of time for metal extraction of modified silica are displayed in Figure 4.33.

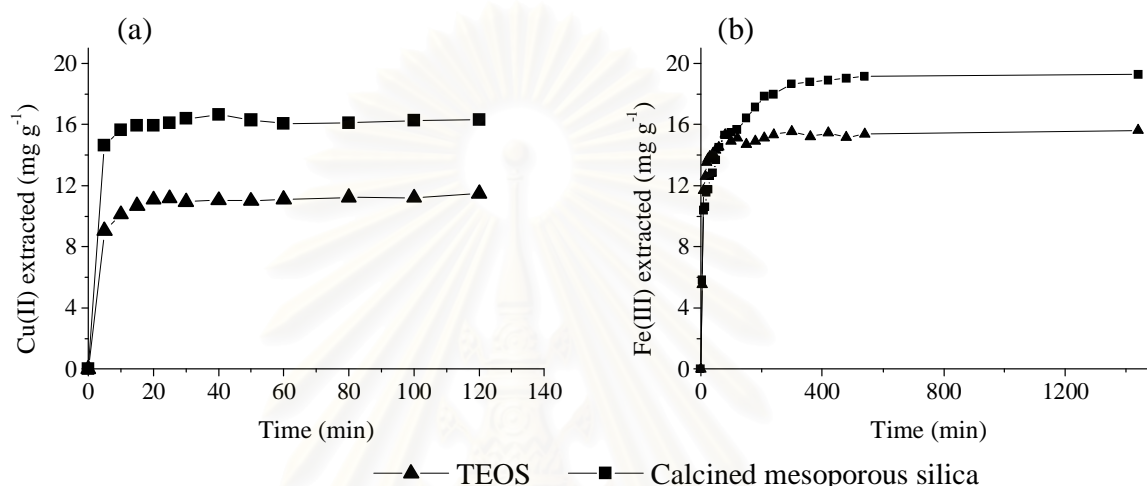


Figure 4.33 The sorption rate of metal onto salen doped mesoporous silica synthesized from TEOS or calcined mesoporous silica: (a) Cu(II) extraction and (b) Fe(III) extraction.

From the Figure 4.33, the metals extraction of modified silica was extremely rapid in the first few minutes and remained saturated until the end of the experimental. The equilibrium time of Cu(II) and Fe(III) extraction were found to be approximately 40 min and 420 min, respectively. These results implied that the experiment time (24 hrs.) used for all previous extraction of Cu(II) and Fe(III) was sufficient to achieve the extraction equilibrium. In addition the Cu(II) and Fe(III) extraction capacity obtained from kinetic extraction were in accordance with batch experiment.

In order to investigate the metal sorption mechanism of salen doped mesoporous silica synthesized from TEOS or calcined mesoporous silica, the three kinetic models were used, including the intra-particle diffusion, the pseudo-first-order and the pseudo-second-order kinetic models [51-53].

Intra-particle diffusion model

$$q_t = k_{dif} \sqrt{t} + C \quad (4.1)$$

where q_t is the amount of adsorbate adsorbed at time t (mg g^{-1}), k_{dif} is intra-particle diffusion rate constant ($\text{mg g}^{-1} \text{min}^{1/2}$)

The pseudo-first-order kinetic model is a simple of kinetic adsorption. This kinetic model is represented by the following equation:

$$\ln \frac{(q_e - q_t)}{q_e} = -k_1 t \quad (4.2)$$

where q_e is the adsorption capacity in equilibrium and k_1 is the rate constant of pseudo-first-order adsorption. The plot of $\ln((q_e - q_t)/q_e)$ versus t give a straight line for the pseudo-first-order kinetic. The value of pseudo-first-order rate constant k_1 was obtained from the slope of the straight line.

The pseudo-second-order model can be represented in the following form:

$$\frac{t}{q_t} = \frac{1}{k_2 q_e^2} + \frac{1}{q_e} t \quad (4.3)$$

where k_2 is the rate constant for the pseudo-second-order adsorption kinetics. The slope of plot t/q_t versus t give the value of q_e , and intercept k_2 can be calculated.

The obtained experimental data were plotted in linearised form of intra-particle diffusion, pseudo-first-order and pseudo-second-order kinetic model. The results are presented in Figure 4.34-4.36.

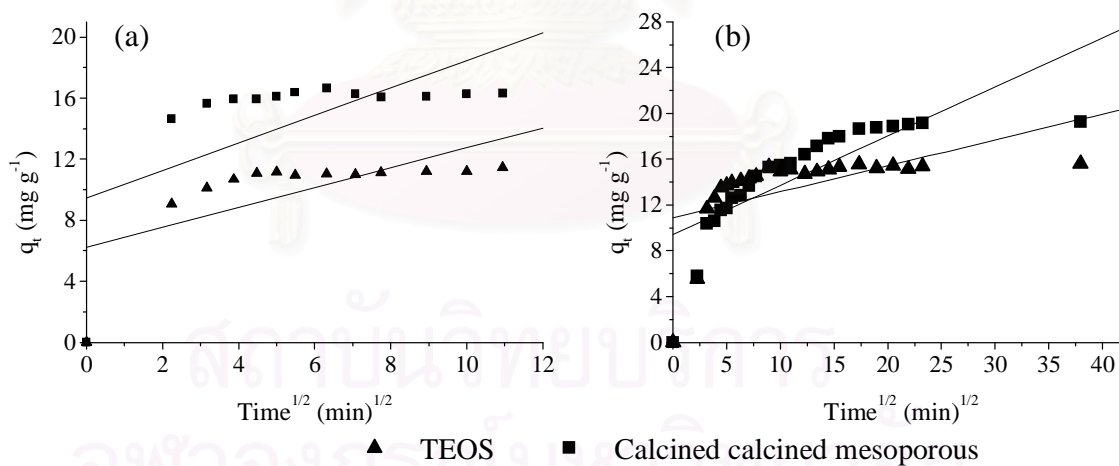


Figure 4.34 The intra-particle diffusion kinetic for adsorption of metals onto salen doped mesoporous silica synthesized from TEOS or calcined mesoporous silica: (a) Cu(II) extraction and (b) Fe(III) extraction.

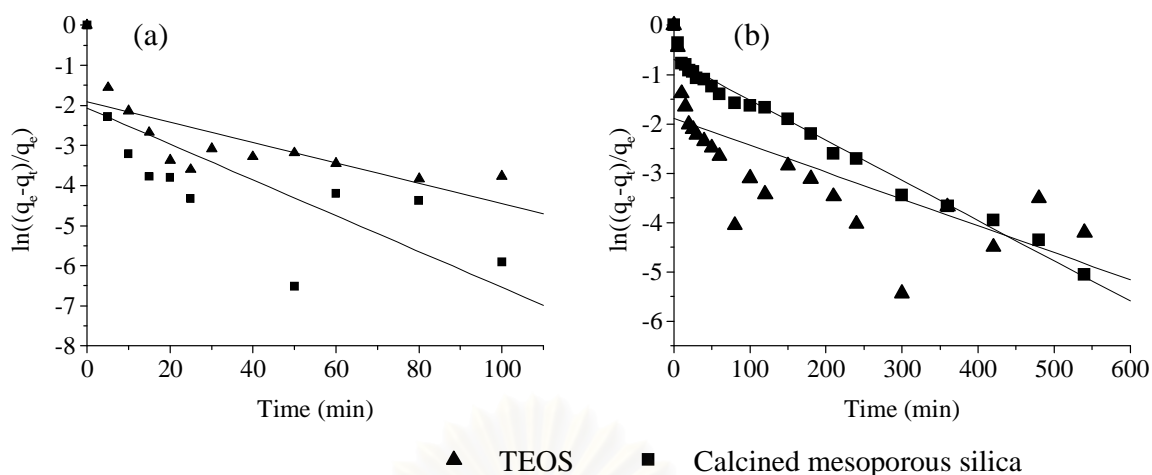


Figure 4.35 The pseudo-first-order kinetic for metal sorption of salen doped mesoporous silica synthesized from TEOS or calcined mesoporous silica: (a) Cu(II) extraction and (b) Fe(III) extraction.

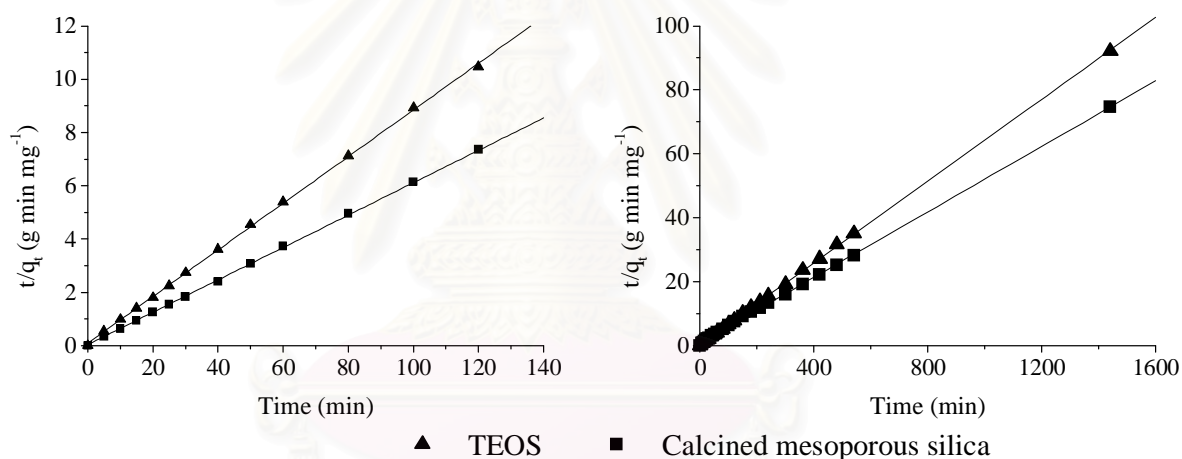


Figure 4.36 The pseudo-second-order kinetic for metal sorption of salen doped mesoporous silica synthesized from TEOS or calcined mesoporous silica: (a) Cu(II) extraction and (b) Fe(III) extraction.

The values parameters for intra-particle diffusion, pseudo-first-order and pseudo-second-order kinetic models are tabulated in Table 4.13-4.14. As seen, since the calculated correlation coefficients of pseudo-second-order kinetic models are closer to unity, and the theoretical q_e values are accordance with the experimental q_e values (Table 4.15). Therefore the kinetic adsorption could be approximated more favorable by the pseudo-second-order kinetic model for all metals extracted by salen doped mesoporous silica synthesized from TEOS or calcined mesoporous silica. It can be concluded that the modified silica behaves as the chelating exchanger because of

the salen functionality presence on it. Since, it is general understanding that pseudo-second-order kinetic model provide the best fits to the experimental data for the sorption systems where the chemisorptions are significant in the rate controlling step [52].

Table 4.13 The comparison of kinetic models for the adsorption of Cu(II) onto the salen doped mesoporous silica synthesized from TEOS or calcined mesoporous silica.

Type of precursor	Intra-particle diffusion			Pseudo-first-order		Pseudo-second-order		
	R ²	k _{dif}	C (mg g ⁻¹)	R ²	k ₁	R ²	k ₂	q _e (mg g ⁻¹)
TEOS	0.4456	0.6503	6.2413	0.5026	-0.0255	0.9996	0.0815	11.4155
Calcined mesoporous silica	0.3652	0.8570	9.8330	0.2993	-0.0387	0.9998	0.2600	16.2866

Table 4.14 The comparison of kinetic models for the adsorption of Fe(III) onto the salen doped mesoporous silica synthesized from TEOS or calcined mesoporous silica.

Type of precursor	Intra-particle diffusion			Pseudo-first-order		Pseudo-second-order		
	R ²	k _{dif}	C (mg g ⁻¹)	R ²	k ₁	R ²	k ₂	q _e (mg g ⁻¹)
TEOS	0.2964	0.2262	10.8930	0.5345	-0.0057	0.9999	0.0126	15.6250
Calcined mesoporous silica	0.6230	0.4287	9.4405	0.9974	-0.0082	0.9995	0.0030	19.5313

Table 4.15 The experimental value of amount of adsorbed metal at equilibrium (q_e) by the salen doped mesoporous silica synthesized from TEOS or calcined mesoporous silica.

Type of precursor	The experimental value of q _e (mg g ⁻¹)	
	Cu (II) extracted	Fe(III) extracted
TEOS	11.3478	15.6175
Calcined mesoporous silica	16.3097	19.2650

4.4.3 Effect of salt present in metal solution

The applications of sorbent are the most concern for the extraction of metal from various aqueous samples such as natural water, seawater or industrial wastewater, which contain several salts. Thus, the influences of salts presence in the metal solution on the metal extractability of modified silica synthesized from TEOS

or calcined mesoporous silica were investigated. Four salts including NaNO_3 , NaCl , KNO_3 and KCl with 0.1 M concentration of each are studied. The results were displayed in Figure 4.37.

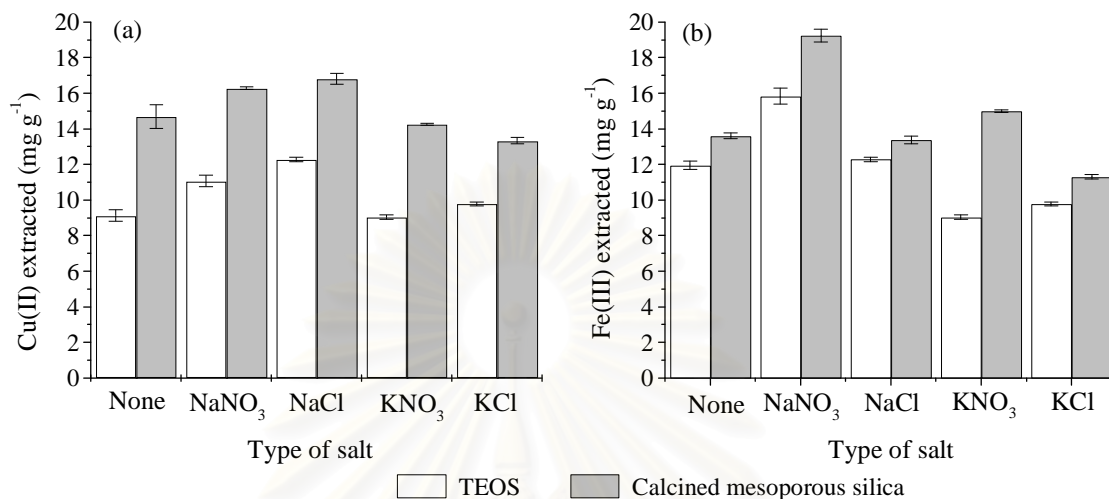


Figure 4.37 Effect of salt presence in the metal solution on the metal extraction: (a) Cu(II) extracted and (b) Fe(III) extracted.

From Figure 4.37, the maximum value of Cu(II) and Fe(III) extracted of both modified silica were obtained when the extraction was performed in NaCl and NaNO_3 , respectively. In addition, the metal extractability of modified silica in the present of Na^+ is better than K^+ . These results were probably due to the replacement of cetyltrimethylammonium ion (CTA^+) on the surface of silica by the Na^+ or K^+ ions present in solution. Since the size of Na^+ ion is smaller than that of K^+ ion then the replacement of CTA^+ by Na^+ is probably easier than the other one. Consequently, the steric hindrance on the surface was decreased and the extraction efficiency was promoted. Therefore, the following experiment were carried out at 100 ppm of Cu(II) in 0.1 M NaCl pH 2.5 and 100 ppm of Fe(III) in 0.1 M NaNO_3 .

For the comparison of metal extractability of both materials, it was found that the sorption capacity of salen doped mesoporous silica synthesized from calcined mesoporous silica were higher than those of synthesized from TEOS for all medium studied. This result might be due to the surface area and crystallinity of calcined mesoporous silica as previously stated.

4.4.4 Determination of sorbent capacity

Adsorption isotherm studies are of fundamental importance in determining the metal sorption capacity of modified silica and to understand the nature of adsorption. In this work, the metal sorption capacity of modified silica was evaluated using Cu(II) in 0.1 M NaCl at pH 2.5 and Fe(III) in 0.1 M NaNO₃. The metal concentration was varied from 75 ppm to 200 ppm. The results plotted between the initial metal concentration and the amounts of metal extracted are presented in Figure 4.38.

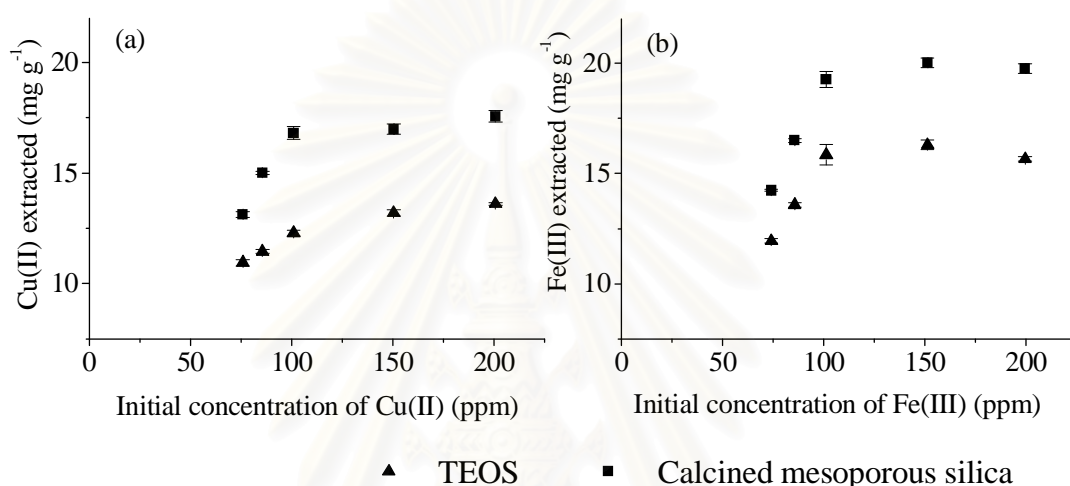


Figure 4.38 The amounts of metal extracted by the modified silica as a function of initial concentration of metal: (a) Cu(II) extracted and (b) Fe (III) extracted

As seen from Figure 4.38, the metal adsorption capacity of modified silica increased with the increasing initial concentration of metal until saturation. This result may be due to the active sites of modified silica become saturated and then adding more metal concentration cannot increase adsorption capacity because no more active sites are available. In addition, it was also found that the metal extraction of both modified silica were saturated when the concentration of metal was greater than or equal 100 ppm.

The adsorption isotherms are presented in Figure 4.39. The obtained adsorption data at equilibrium have been analyzed with two adsorption models, which are Langmuir isotherm equation (eq. 2.13) and Freundlich isotherm equation (eq. 2.15). The linearized Langmuir and Freundlich adsorption isotherm are illustrated in Figure 4.40 – 4.41, respectively. The Langmuir and Freundlich parameter for metal sorption of modified silica are listed in Table 4.16.

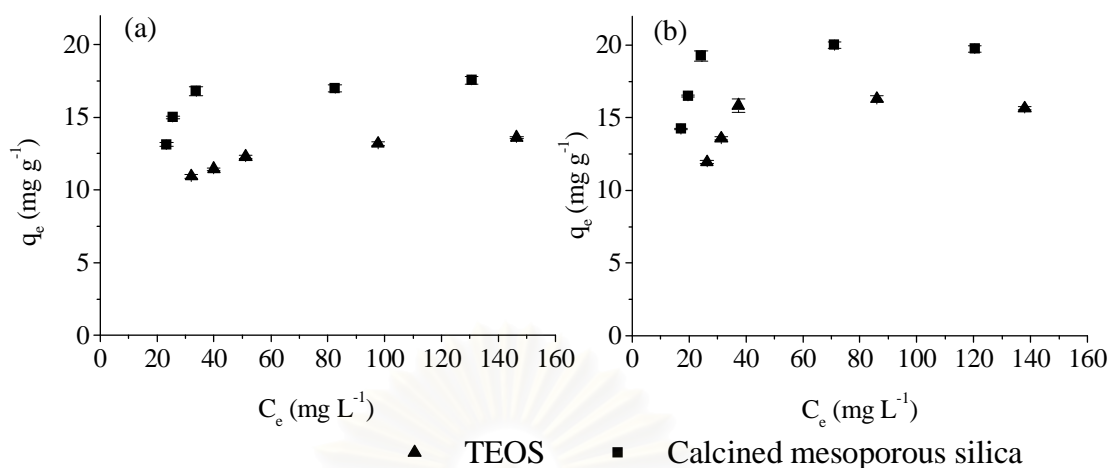


Figure 4.30 Equilibrium adsorption isotherm of metal adsorption on salen doped mesoporous silica synthesized from TEOS or calcined mesoporous silica: (a) Cu (II) and (b) Fe(III).

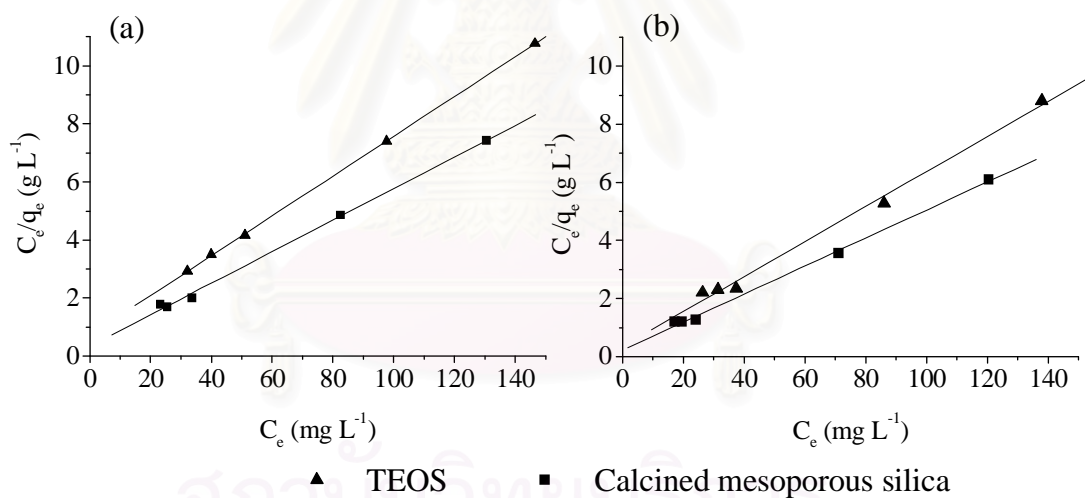


Figure 4.40 The linearization of Langmuir adsorption isotherm for metal adsorption by salen doped mesoporous silica synthesized from TEOS or calcined mesoporous silica: (a) Cu(II) adsorption and (b) Fe(III) adsorption.

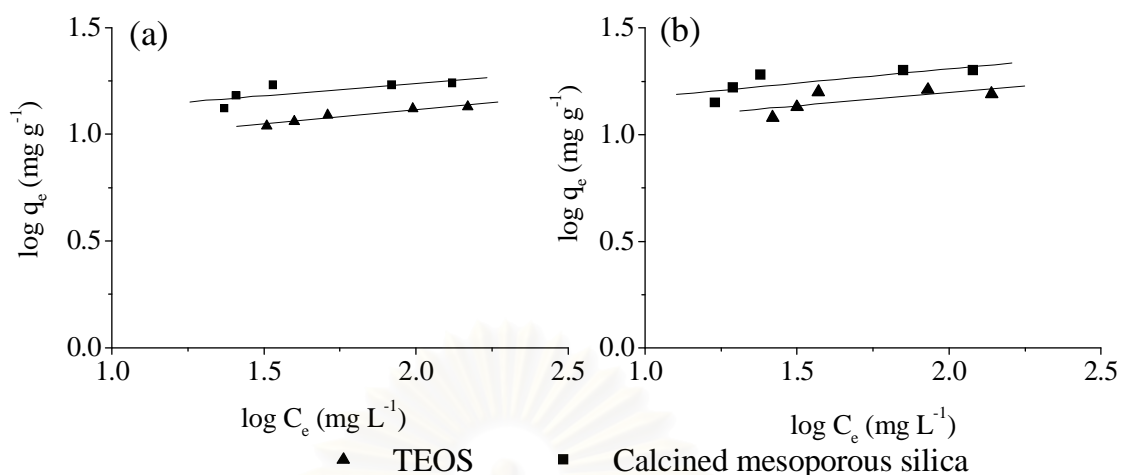


Figure 4.41 The linearization of Freundlich adsorption isotherm for metal adsorption by salen doped mesoporous silica synthesized from TEOS or calcined mesoporous silica: (a) Cu(II) adsorption and (b) Fe(III) adsorption.

Table 4.16 Langmuir and Freundlich constants for the metal sorption of salen doped mesoporous silica synthesized from TEOS or calcined mesoporous silica

Metal	Type of precursor	Langmuir constants			Freundlich constants		
		q_m (mg g ⁻¹)	K_L (L mg ⁻¹)	R^2	K_F (mg g ⁻¹)	n	R^2
Cu(II)	TEOS	14.58	0.0961	0.9999	6.84	7.0922	0.9488
	Calcined mesoporous silica	18.42	0.1582	0.9977	9.82	8.0645	0.6269
Fe(III)	TEOS	16.61	0.1730	0.9934	8.66	7.5758	0.5166
	Calcined mesoporous silica	20.70	0.2166	0.9970	11.17	7.7519	0.5771

It can be seen from Table 4.16 that all the correlation coefficient values (R^2) obtained from Langmuir isotherm is more than those from Freundlich isotherm. This indicated that the metal sorption of modified silica is best fitted to the Langmuir adsorption isotherm. This result suggested that the metals adsorption of modified silica are monolayer adsorption and homogeneous of the adsorbent surface. The maximum adsorption capacity of Cu(II) are 14.58 mg g⁻¹ and 18.42 mg g⁻¹ for salen

doped mesoporous silica synthesized from TEOS and calcined mesoporous silica, respectively. It was interesting that Cu(II) adsorption capacity of calcined-salen was higher than the value reported for the XAD-4 resin grafted with salen [42]. For the Fe(III) extraction, the maximum adsorption capacity were found to be 16.61 mg g⁻¹ and 20.70 mg g⁻¹ for TEOS-salen and calcined-salen, respectively. The Cu(II) and Fe(III) sorption capacity of salen doped mesoporous silica synthesized from calcined mesoporous silica were higher than that synthesized from TEOS.

4.4.5 Selectivity

From previous sections, it was found that salen doped mesoporous silica had shown the selective extraction towards the Cu(II) and Fe(III). Therefore, the selectivity of the salen doped mesoporous silica synthesized from TEOS or calcined mesoporous silica were performed using 25 mL of solution containing Cu(II) and Fe(III) with 100 ppm concentration of each. The results of each extracted ion expressed in mol kg⁻¹ are presented in Table 4.17.

Table 4.17 The amounts of each metal ion extracted from mixture solution using salen doped mesoporous silica synthesized from TEOS or calcined mesoporous silica as a sorbent

Type of precursor	Medium	Metal extracted (mol kg ⁻¹)	
		Cu(II)	Fe(III)
TEOS	aqueous	0.1291 ± 0.0008	0.0000 ± 0.0000
	NaNO ₃	0.1331 ± 0.0007	0.0256 ± 0.0012
	NaCl	0.0498 ± 0.0012	0.0426 ± 0.0007
Calcined mesoporous silica	aqueous	0.1467 ± 0.0016	0.0729 ± 0.0008
	NaNO ₃	0.1729 ± 0.0023	0.0894 ± 0.0025
	NaCl	0.0860 ± 0.0005	0.0480 ± 0.0008

As seen, both modified sorbent had selectivity for the extraction of Cu(II). These results were inconsistent with those reported by Khamloet [47]. However, in all case, the amount of Cu(II) extracted in each medium studied was found to be in this order: NaNO₃ > aqueous > NaCl. Furthermore, the metal extractability of salen doped mesoporous silica synthesized from calcined mesoporous silica was higher than that of silica synthesized from TEOS for all medium studied.

4.4.6 Effect of amount of silica

The amount of sorbent is an important parameter in the metal ion extraction. In order to elucidate the influence of this parameter, the experiment were carried out using 100 ppm of Cu(II) solution in 0.1 M NaCl at pH 2.5 and 100 ppm of Fe(III) in 0.1 M NaNO₃ as metal solution. The amount of modified sorbent were varied from 0.05 to 0.25 g. From the experimental results, it was found that the precipitation of Cu(OH)₂ and Fe(OH)₃ was formed at pH 5.5 and 7.0, respectively, when 0.20 g of salen doped mesoporous silica synthesized from TEOS was used as sorbent. Hence, the amount of salen doped mesoporous silica synthesized from TEOS was varied from 0.05 to 0.15 g. The precipitation of Cu(OH)₂ was also detected in the extraction of Cu(II) with 0.25 g of salen doped mesoporous silica synthesized from calcined mesoporous silica. Thus, the extraction of Cu(II), the amount modified silica synthesized from calcined mesoporous was varied from 0.05 to 0.20 g. The percentage of metal extracted with varying amount of modified silica is presented in Figure 4.42

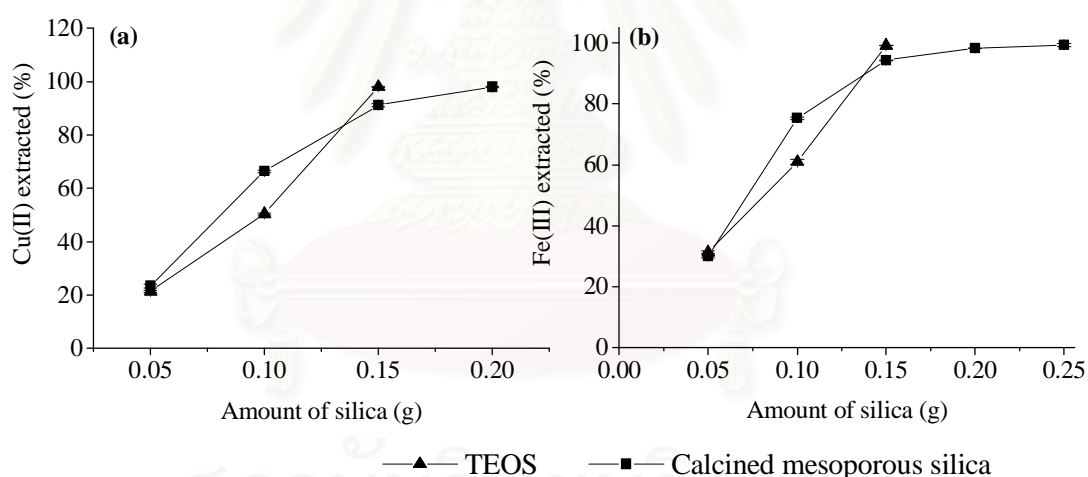


Figure 4.42 Effect of amount of salen doped mesoporous silica synthesized from different precursor on the metal extraction: (a) Cu(II) extracted and (b) Fe(III) extracted.

As seen from Figure 4.42, an increase in the percentage of metal extracted with increasing amount of modified silica was observed in all case. The increase in the adsorption capacity with the increasing amount of sorbent can be attributed to increased sorbent surface area and the availability of active site of modified silica. Furthermore, the Cu(II) and Fe(III) extracted were reached to 98% extracted value when the amount of modified sorbent were 0.15 g and 0.20 g for the salen doed

mesoporous silica synthesized from TEOS and calcined mesoporous silica, respectively.

4.4.7 Desorption and Reusability

To make the adsorption economical and reduce the waste disposal, the study of sorbent reusability is one of the interested subjects. In order to find out a proper eluent for the metal desorption, after initial extraction of 100 ppm Fe(III) in 0.1 M NaNO₃ by the salen doped mesoporous silica synthesized from TEOS, the Fe(III) were desorped with 10 ml of varying concentration of HNO₃ to 0.1, 0.075 and 0.05 M. Then, the same sorbent was repeated adsorption of cycle 2nd. The results are present in Table 4.18. It was obviously seen that 0.075 M of HNO₃ was the appropriate eluent since it provided high percentage of desorption. Furthermore, after the desorption with this eluent, the desorped silica could readsorp the Fe(III) ion. Thus 0.075 M of HNO₃ was selective for further desorption experiment.

Table 4.18 Effect of concentration of HNO₃ on the desorption of Fe(III) from salen doped mesoporous silica synthesized by TEOS and the comparison of adsorption and readsorption of such silica.

Concentration of HNO ₃ (M)	Desorption (%)	Adsorption (mg g ⁻¹)	Readsorption (mg g ⁻¹)
0.100	100.00	15.41	0.00
0.075	96.39	15.41	15.46
0.050	71.69	15.41	13.34

The reusability of salen doped mesoporous silica synthesized from TEOS or calcined mesoporous silica were performed. The adsorption-desorption cycle was repeated for three times. The adsorption was carried out with 25 mL of 100 ppm of Fe(III) in 0.1 M NaNO₃ medium. The desorption was performed using 10 mL of 0.075 M HNO₃ as eluent. The results of each cycle are summarized in Table 4.19

Table 4.19 The amount of Fe(III) extracted by salen doped silica synthesized from TEOS or calcined mesoporous silica in each cycle.

Cycle	Amount of Fe(III) extracted (mg g^{-1}) by silica	
	TEOS	Calcined mesoporous silica
1	15.26 ± 0.22	18.99 ± 0.22
2	13.87 ± 0.29	13.48 ± 0.07
3	10.88 ± 0.12	11.84 ± 0.19

As seen from Table 4.19, both modified silica could be successfully reused at least three times. However, the amount of Fe(III) extracted by both modified silica were slightly decreased when the sorbent was reused. These results may be due to the progressive lost of salen during the acid treatment for releasing the sorped metal ions. In addition, the Fe(III) extractability of salen doped silica synthesized from calcined mesoporous silica was higher than that of silica synthesized from TEOS.

CHAPTER V

CONCLUSIONS

Different Schiff's base doped mesoporous silica could be successfully synthesized from various silica precursors. All the Schiff's base doped mesoporous silica, except the silica synthesized from silica gel 60 had large surface, narrow pore size distribution and crystalline structure.

The study of metal extraction properties of the as-synthesized Schiff's base doped mesoporous silica had shown the capability of these modified silica towards the extraction of Cu(II), Fe(III) and Ni(III). On the contrary, the non-doped mesoporous silica could not extract any Cu(II) and Fe(III) ions. The presence of NaNO₃ in metal solution improved significantly the metal sorption capacity of Schiff's base doped mesoporous silica. The comparison of metal extractability of Schiff's base doped mesoporous silica synthesized from different silica precursors revealed that the Schiff's doped mesoporous silica synthesized from TEOS or calcined mesoporous silica had more metal extraction capacity than the silica prepared from other sources did due to their ordered structure.

The investigation of Schiff's base/TEOS ratio on the synthesis and sorption properties of Schiff's base doped mesoporous silica had shown that the amount of incorporated Schiff's base increased with the increase of Schiff's base/TEOS ratio used in the synthesis. The maximum amounts of incorporated Schiff's base were found to be 1.00, 0.86, and 0.96 mmol g⁻¹ for salen, saltn, and haen doped mesoporous silica, respectively. The amount of incorporated Schiff's base affected the Fe(III) extraction of modified silica.

The profound extraction studies including kinetic extraction, effect of amount of sorbent, selectivity, and reusability were carried out using salen doped mesoporous synthesized from TEOS or calcined mesoporous silica due to their remarkable physical and chemical properties. The sorption process of these materials followed the pseudo-second order kinetic. The sorption isotherm correlated well with the Langmuir model. The maximum Cu(II) and Fe(III) extraction capacity of salen doped mesoporous silica synthesized from calcined mesoporous silica was found to be 18.42 and 20.70 mg g⁻¹ respectively. The modified silica had high selectivity to the Cu(II)

extraction. The reusability of these sorbent was successfully performed at least three times.



สถาบันวิทยบริการ
จุฬาลงกรณ์มหาวิทยาลัย

REFERENCES

1. R. K. Iler. *The chemistry of silica*. New York: John Wiley & Sons, 1979, 186, 467, 510-511.
2. J. Nawrocki. The silanol group and its role in liquid chromatography. *J. Chromatogr. A*. 779 (1997): 29-71.
3. A. Berthod. Silica: backbone material of liquid chromatographic column packing. *J Chromatogr.* 549 (1991): 1-28.
4. O. Lev. Diagnostic applications of organically doped sol-gel porous glass. *Analisis.* 20 (1992): 543-553.
5. M. S.- Niasari, M. H.- Kabutarkhani and F. Davar. Alumina-supported Mn(II), Co(II), Ni(II) and Cu(II) N,N-bis(salicylidene)-2,2-dimethylpropane-1,3-diamine complexes: Synthesis, characterization and catalytic oxidation of cyclohexane with tert-butylhydroperoxide and hydrogen peroxide. *Catal. Commun.* 7 (2006): 955-962.
6. S. Oshma, N. Hirayama, K. Kubono, H. Kokusen and T. Honjo. Structure control of Schiff base ligands for selective extraction of copper(II). *Anal. Sci.* 18 (2002): 1351-1355.
7. S. Dadfarnia, A. Mohammed, H. Shabani, F. Tamaddon and M. Rezaei. Immobilized salen (N,N'-bis(salicylidene) ethylenediamine) as a complexing agent for on-line sorbent extraction/peconcentration and flow injection-flame atomic absorption spectrometry. *Anal. Chim. Acta.* 539 (2005): 69-75.
8. M. A. Wahab, I. Imae, Y. Kawakami and C. Ha. Periodic mesoporous organosilica materials incorporating various organic functional group: synthesis, structural characterization, and morphology. *Chem. Mater.* 17 (2005): 2165-2174.
9. D. A. Loy, B. M. Baugher, C. R. Baugher, D. A. Schneider and K. Rahimina. Substituent effect on the sol-gel chemistry of organotrialkoxysilanes. *Chem. Mater.* 12 (2000): 3624-3632.
10. E. M. Thurman and M. S. Mills. *Solid-phase extraction*. New York: John Wiley & Sons, 1998, 29.

11. K. S. W. Sing, D. H. Everett, R. A. W. Haul, L. Moscou, R. A. Pierotti, J. Rouquerol and T. Siemieniewska. Reporting physisorption data for gas/solid systems with special reference to the determination of surface area and porosity. *Pure Appl. Chem.* 57 (1985): 603-619.
12. C. J. Brinker. Hydrolysis and condensation of silicates: effects on structure. *J. Non-Cryst. Solids.* 100 (1998): 31-50.
13. B. Hatton, K. Landskron, W. Whitnall, D. Perovic and G. A. Ozin. Past, present and future of periodic mesoporous organosilicas – The PMOs. *Acc. Chem. Res.* 38 (2005): 305-312.
14. M. M. Collinson. Recent trends in analytical of organically modified silicate materials. *Trend Analytical Chem.* 21 (2002): 30-38.
15. M. A. Markowitz, J. Klaehn, R. A. Hendel, S. B. Qadriq. S. L. Golledge, D. G. Castner and B. P. Gaber. Direct synthesis of metal-chelating mesoporous silica: Effect of added organosilanes on silicate formation and adsorption properties. *J. Phy. Chem. B.* 104 (2000): 10820-10826.
16. J. S. Beck, J. C. Vartuli, W. J. Roth, M. E. Leonowicz, C. T. Kresge, K. D. Schmitt, C. T. W. Chu, D. H. Olsen, E. W. Sheppard, S. B. McCullen, J. B. Higgins, J. L. Schlenker. A new family of mesoporous molecular sieves prepared with liquid crystal templates. *J. Am. Chem. Soc.* 114 (1992): 10835-10842.
17. A. Vinu, T. Mori, and K. Ariga. Review: New families of mesoporous materials. *Sci. and Tech. of Adv. Mater.* 7 (2006): 753-771.
18. P. Selvam, S. K. Bhatia, and C. G. Sonwane. Recent advances in processing and characterization of periodic mesoporous MCM-41 silicate molecular sieves. *Ind. Eng. Chem.* 40 (2001): 3237-3261.
19. Q. Huo, D. I. Margolese, U. Ciesla, D. G. Demuth, P. Feng, T. E. Gier, P. Sieger, A. Firouzi, B. F. Chmelka, F. Schuth, and G. D. Stucky. Organization of organic molecules with inorganic molecular species into nanocomposites biphasic arrays. *Chem. Mater.* 6 (1994): 1176-1191.
20. S. Inagaki, Y. Sakamoto, Y. Fukushima, and O. Terasaki. Pore Wall of a Mesoporous Molecular Sieve Derived from Kanemite. *Chem. Mater.* 8 (1996): 2089-2095.

21. M. E. Davis and S. L. Burkett. Towards the rational design and synthesis of microporous and mesoporous silica containing materials. *Zeolites* 12 (1995): 33.
22. R. J. Hodgson, Y. Chen, Z. Zhang, D. Tleugabulova, H. Long, X. Zhao, M. Organ, M. A. Brook and J. D. Brennan. Protein-doped monolithic silica columns for capillary liquid chromatography prepared by the sol-gel method: applications to frontal affinity chromatography. *Anal. Chem.* 76 (2004): 2780-2790.
23. C. R. Ringenbach, S. R. Livingston, D. Kumar and C. C. Landry. Vanadium-doped acid-prepared mesoporous silica: synthesis, characterization, and catalytic studies on the oxidation of a mustard gas analogue. *Chem. Mater.* 17 (2005): 5580-5586.
24. C. Xu, K. Wygladacz, Y. Qin, R. Retter, M. Bell and E. Bakker. Microsphere optical ion sensors based on doped silica gel templates. *Anal. Chim. Acta* 537 (2005): 135-143.
25. P. P.-Tofino, J. M. B.-Moreno and M. C. P.-Conde. Analysis of isoproturon at trace level by solid phase extraction competitive fluoroimmunosensing after enrichment in a sol-gel immunosorbent. *Anal. Chim. Acta.* 562 (2006): 122-127.
26. G. Leofanti, M. Padovan, G. Tozzola and B. Venturelli. Surface area and pore texture of catalysts. *Catalysis Today.* 41 (1998): 207-219.
27. J. Zýka, *Instrumentation in analytical chemistry II*. New York: Ellis Horwood, 1994, 281-283.
28. S. Cook, Electron microscopy [online]., Available from: http://www.steve.gb.com/science/electron_microscopy.html [2006, April 4].
29. D. A. Skoog and J. J. Leary. *Principle of instrumental analysis*. 4th ed. New York: Saunders College, 1992, 128, 363-364.
30. Y. Shiraishi, G. Nishimuru, T. Hirai, I. Komasa. Separation of transition metals using inorganic adsorbents modified with chelating ligands. *Ind. Eng. Chem. Res.* 41 (2002): 5065-5070.
31. A. Özer. Removal of Pb(II) ions from aqueous solution by sulphuric acid-treated wheat bran. *J. Hazard. Mater.* 141 (2007): 753-761.

32. I. Langmuir. The constitution and fundamental properties of solids and liquids. *J. Am. Chem. Soc.* 38 (1916): 2221-2295.
33. H. M. F. Freundlich. Über die adsorption in losungen. *Z. Phy. Chem. A.* 57 (1906): 385-470.
34. S. Yamada. Advancement on stereochemical aspects of Schiff base metal complex. *Coord. Chem. Rev.* 190-192 (1999): 537-555.
35. S. Abe, J. Mochizuki, T. Sone. Liquid-liquid extraction of iron(III) and gallium(III) with macrocyclic Schiff bases containing bisphenol A subunits. *Anal. Chim. Acta.* 319 (1996): 387-392.
36. M. S.- Niasari, M. H.- Kabutarkhani and F. Davar. Alumina-supported Mn(II), Co(II), Ni(II) and Cu(II) *N,N*-bis(salicylidene)-2,2-dimethylpropane-1,3-diamine complexes: Synthesis, characterization and catalytic oxidation of cyclohexane with *tert*-butylhydroperoxide and hydrogen peroxide. *Catal. Commun.* 7 (2006): 955-962.
37. S. Oshma, N. Hirayama, K. Kubono, H. Kokusen and T. Honjo. Structure control of Schiff base ligands for selective extraction of copper(II). *Anal. Sci.* 18 (2002): 1351-1355.
38. M. Shamsipur, A. R. Ghiasvand, H. Sharghi and H. Naeimi. Solid phase extraction of ultra trace copper(II) using octadecyl silica membrane disks modified by a naphthol-derivative Schiff's base. *Anal. Chim. Acta.* 408 (2000): 271-277.
39. E. F. Murphy, L. Schmid, T. Bürgi, M. Maciejewski and A. Baiker. Nondestructive sol-gel immobilization of metal(salen) catalysts in silica aerogels and xerogels. *Chem. Mater.* 13 (2001): 1296-1304.
40. A. K. Jain, V. K. Gupta, P. A. Ganeshpure and J. R. Raison. Ni(II)-selective ion sensors of salen type Schiff base chelates. *Anal. Chim. Acta.* 553 (2005): 177-184.
41. S. Dadfarnia, A. Mohammed, H. Shabani, F. Tamaddon and M. Rezaei. Immobilized salen (*N,N'*-bis(salicylidene) ethylenediamine) as a complexing agent for on-line sorbent extraction/preconcentration and flow injection-flame atomic absorption spectrometry. *Anal. Chim. Acta.* 539 (2005): 69-75.

42. Y.- S. Kim, G. In, C.- W. Han and J.- M. Choi. Studies on synthesis and application of XAD-4-salen chelate resin for separation and determination of trace elements by solid phase extraction. *Microchem. J.* 80 (2005): 151-157.
43. R. Mokaya. On the extended recrystallisation of mesoporous silica characterization of restructured pure silica MCM-41. *J. Mater. Chem.* 12 (2002): 3027-3033.
44. A. S. M. Chong, X. S. Zhao. Functionaled nanoporous silicas for the immobilization of penicillin acylase. *Appl. Surf. Sci.* 237 (2004): 398-404.
45. Z. Wu, H. Joo, I. – S. Ahn, S. Haam, J. – H. Kim and K. Lee. Organic dye adsorption on mesoporous hybrid gels. *Chem. Eng. J.* 102 (2004): 277-282.
46. A. R. Khorrami, H. Naeimi and A. R. Fakhari. Determination of nickel in natural waters by FAAS after sorption on octadecyl silica membrane disk modified with a recently synthesized Schiff's base. *Talanta.* 64 (2004): 13-17.
47. P. Khamloet. Synthesis and characterization of Schiff's base doped mesoporous silica and application to solid-phase extraction of metal. Master's Thesis, Department of Chemistry, Faculty of Science, Chulalongkorn University, 2004.
48. A. Boos, A. Intasiri, J. Brunette and M. J. F. Leroy. Surfactant-templated silica doped 1-phenyl-3-methyl-4-stearoylpyrazol-5-one (HPMSP) as a new sorbent. *J. Mater. Chem.* 12 (2002): 886-889.
49. L. H. Larry and J. K. West. The Sol-Gel process. *Chem. Rev.* 90 (1990): 33-72.
50. X. Wang, T. Dou and Y. Xiao. Synthesis of double-mesopore silica using aqueous ammonia as catalyst. *Chem. Commun.* 9 (1998): 1035-1036.
51. I. D. Mall, V. C. Srivastava, N. K. Agarwal. Removal of Orange-G and Methyl Violet dyes by adsorption onto bagasse fly ash – kinetic study and equilibrium isotherm analysis. *Dyes Pigments.* 69 (2006): 210-223.
52. Y. S. Ho, G. McKay. Pseudo-second order model for sorption processes. *Process Biochem.* 34 (1999): 451-465.

53. S. Azizian. Kinetic models of sorption: a theoretical analysis. *J. Colloid Interface Sci.* 276 (2004): 47-52.
54. T. Tarateerapap. Metal extraction from aqueous solution using Schiff's base functionalized mesoporous silica. Master's Thesis, Environmental Science, Graduate school Chulalongkorn University. 2004.



สถาบันวิทยบริการ
จุฬาลงกรณ์มหาวิทยาลัย



APPENDICES

สถาบันวิทยบริการ
จุฬาลงกรณ์มหาวิทยาลัย

APPENDIX I

SYNTHESIS OF SCHIFF'S BASE LIGAND

Three Schiff's base ligands illustrated in Figure I.1 were prepared by slowly adding interested primary diamines (1 mol-equiv.) to an interested aldehyde or ketone (2 mol-equiv.). The resulting mixture was stirred at room temperature until precipitate occurred. The solid was then filtered off, washed and recrystallized by ethanol. The type of starting substrate used for the synthesis of each Schiff's base is shown in Table I.1

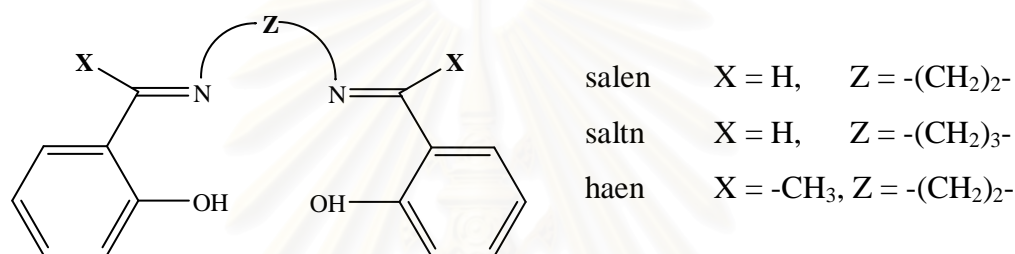


Figure I.1 The structure of Schiff's base ligand.

Table I.1 Starting substrate used for the synthesis of various Schiff's bases.

Type of Schiff's base	Type of starting substrate	
	aldehyde or ketone	diamine
Salen	salicylaldehyde	ethylenediamine
Saltn	salicylaldehyde	2-propylenediamine
Haen	2-hydroxyacetophenone	ethylenediamine

The physical properties of all obtained Schiff's bases are displayed as follows.

2,2'-(ethane-1,2-diylbis[nitrilo(*E*)methylylidene]diphenol (salen): Bright yellow crystal 95% yield; m. p. 125-126 °C; IR (KBr): 3500 (w), 3010-3050 (w), 2860-2950 (w), 1790-2040 (w), 1640 (s), 1460-1610 (w), 1280 (s) and 1150 (s) cm⁻¹; ¹H-NMR (CDCl₃) δ (ppm): 3.94 (s, 4H), 6.85 (dt, J = 7.99, 1.20 Hz, 2H), 6.94 (d, J = 8.00 Hz, 2H), 7.22 (dd, J = 8.00, 1.604 Hz, 2H), 7.25-7.31 (m, 2H) 8.36 (s, 2H) and 13.22 (s, 2H)

2,2'-{propane-1,3-diylbis[nitrilo(*E*)methylylidene]}diphenol (saltn):

Yellow needle crystal 28% yield; m. p. 52-53 °C; IR (KBr): 3500 (w), 3000-3060 (w), 2870-2590 (w), 1630 (s), 1627, 1580, 1500 (m), 1280 (m) and 750 (s) cm^{-1} ; $^1\text{H-NMR}$ (CDCl_3) δ (ppm): 2.09-2.14 (quintet, 2H, $J = 7.02$), 3.72 (dt, $J = 8.00, 0.80$ Hz, 2H), 6.88 (dt, $J = 8.00, 1.20$ Hz, 2H), 6.96 (d, $J = 8.00$, 2H), 7.25 (dd, $J = 6.00, 1.20$ Hz, 2H) 7.29 – 7.33 (m, 2H) 8.38 (s, 2H) and 13.44 (s, 2H)

2,2'-{ethane-1,2-diylbis[nitrilo(*1E*)eth-1-yl-1-ylidene]}diphenol (haen):

Yellow needle crystal 81% yield; m. p. 197-198 °C; IR (KBr): 3500 (w), 3010-3050 (w), 3050 (w), 2840-2930 (w), 1800 (w), 1440-1600 (s), 1240 (s) and 750 (s) cm^{-1} ; $^1\text{H-NMR}$ (CDCl_3) δ (ppm): 2.38 (s, OH), 3.98 (s, 4H), 6.79 (dt, $J = 7.60, 0.40$, 2H), 6.91 (dd, $J = 8.00, 0.80$, 2H), 7.26 – 7.30 (m, 2H), 7.52 (dd, $J = 8.00, 1.56$, 2H) and 12.31 (s, 2H)



สถาบันวิทยบริการ
จุฬาลงกรณ์มหาวิทยาลัย

APPENDIX II
¹H NMR SPECTRUM OF SCHIFF'S BASE LIGAND

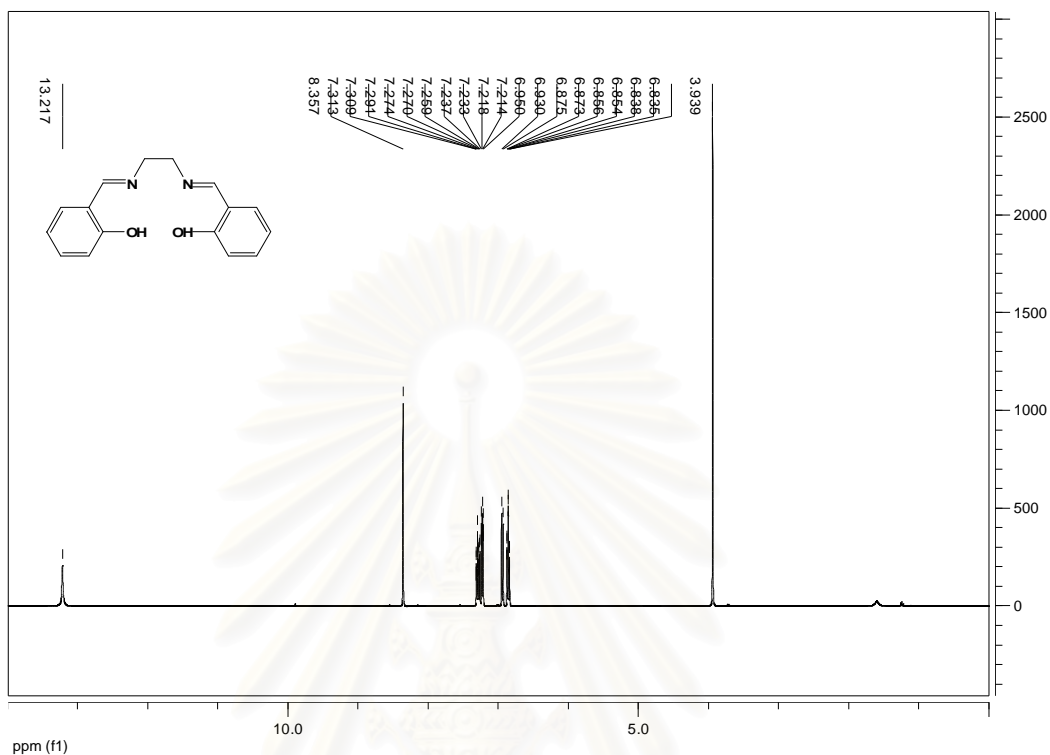


Figure II.1 ¹H NMR spectrum of Salen in CDCl₃ at 400 MHz

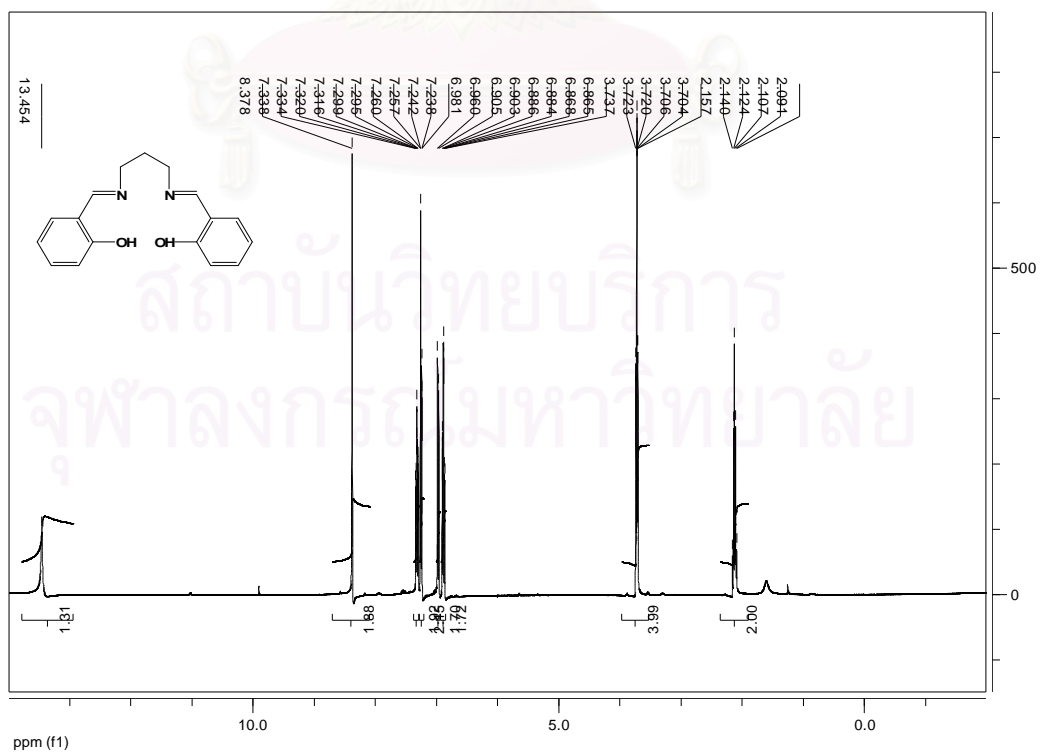


Figure II.2 ¹H NMR spectrum of Saltn in CDCl₃ at 400 MHz

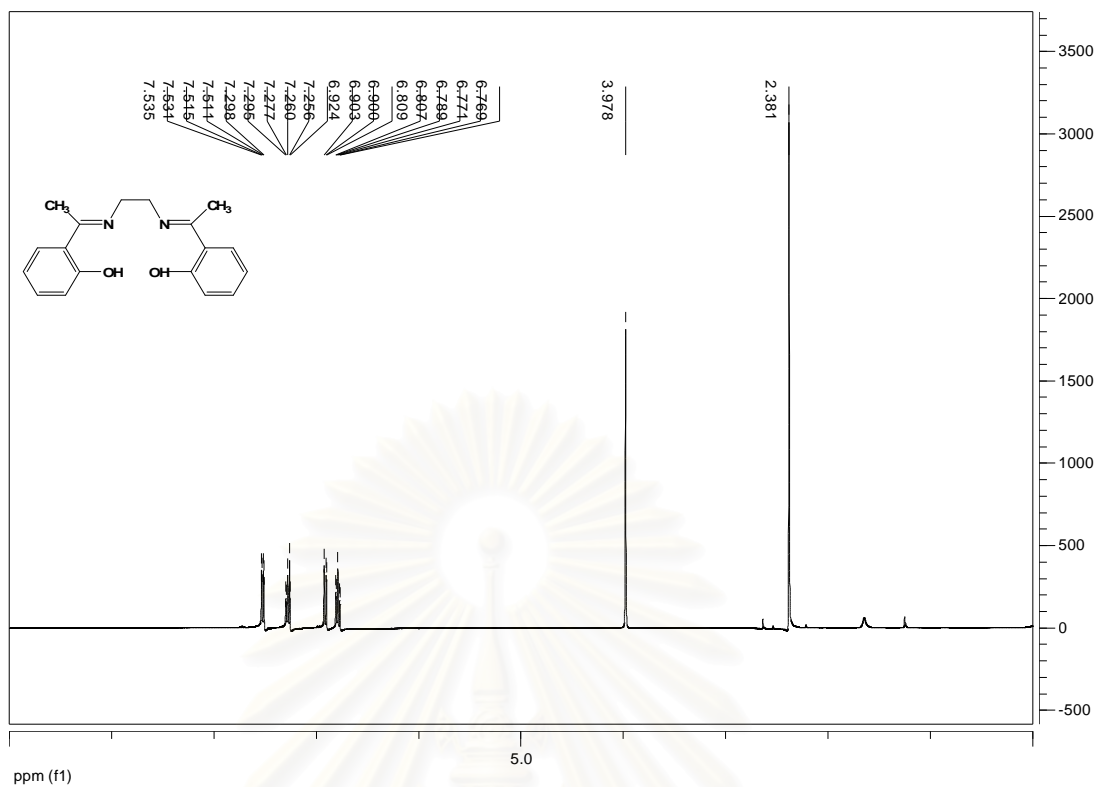


Figure II.3 ^1H NMR spectrum of Haen in CDCl_3 at 400 MHz

สถาบันวิทยบริการ
จุฬาลงกรณ์มหาวิทยาลัย

APPENDIX III

SYNTHESIS OF CALCINED MESOPOROUS SILICA

The preparation of calcined mesoporous silica is as follows: CTAB was dissolved in an aqueous solution of 0.1 M NaOH. The mixture was stirred at 60 °C for 1 hour. The ethanol and TEOS were then added. The mole composition of the final gel was 1 TEOS : 140 H₂O : 0.18 CTAB : 13 C₂H₅OH. The mixture was kept stirring at 60 °C for 1 hour and at room temperature for 23 hours. The synthesized silica was filtered, washed with water copiously and HNO₃. This silica was then dried at 110 °C overnight. The obtained silica was calcined at 540 °C for 10 hours.



สถาบันวิทยบริการ
จุฬาลงกรณ์มหาวิทยาลัย

APPENDIX IV

THE XRD PATTERNS AND N₂ SORPTION ISOTHERMS OF CALCINED MESOPOROUS SILICA AND SILICA GEL 60

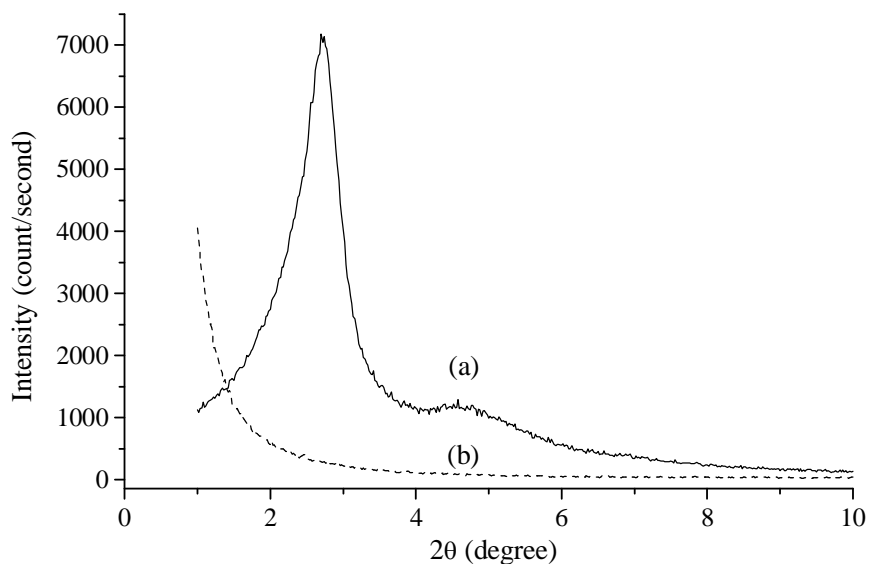


Figure IV.1 The XRD patterns of (a) calcined mesoporous silica and (b) silica gel 60

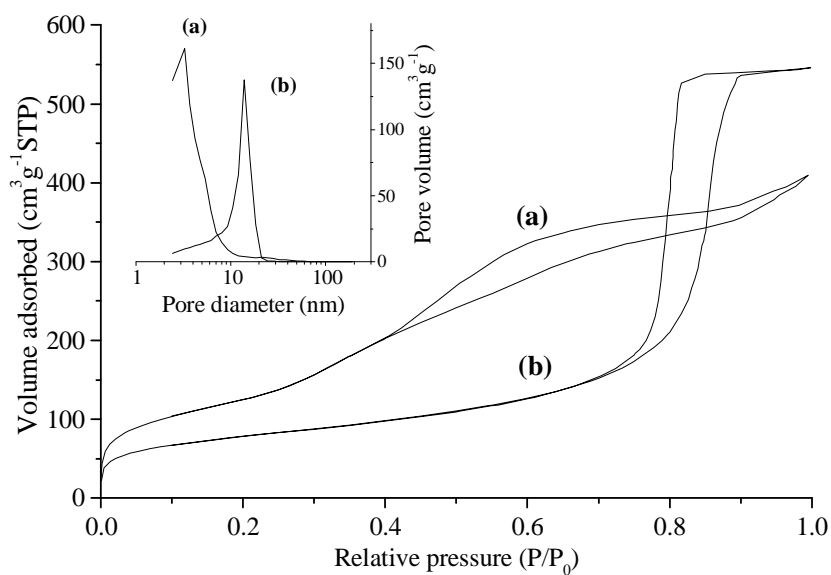


Figure IV.2 N₂ adsorption-desorption isotherms and pore-size distribution plot (insert) of (a) Calcined mesoporous silica and (b) Silica gel 60

Table IV.1 The textural properties of calcined mesoporous silica and silica gel 60

Sample	S (m ² /g)	V_p (cm ³ /g)	APD (nm)	d_{100} (nm)	a_0 (nm)	w (nm)
Calcined mesoporous	454	0.62	5.46	3.27	11.32	5.86
Silica gel 60	442	0.84	12.22	-	-	-

S , BET surface area (m²/g) obtained from N₂ sorption; V_p , Total pore volume (cm³/g) obtained from single-point volume at P/P₀ = 0.99; APD , average pore diameter calculated from $4V_p/S$; d_{100} , d-value 100 reflections; a_0 = the lattice parameter, from the XRD data using the formula $a_0 = 2d_{100}\sqrt{3}$; w , pore wall thickness was equaled to a_0-APD .

APPENDIX V
CALCULATION OF ORGANIC MATTER CONTENTS
IN MESOPOROUS SILICA

V.1 The silica synthesized from single silica precursor

V.1.1 Mesoporous silica synthesized from TEOS

Table V.1 The amount of starting materials for the synthesis of silica using TEOS as silica precursor

Modified silica		Starting materials				
		TEOS	H ₂ O	CTAB	EtOH	Incorporated Schiff's base
Non-doped	(g)	5.2001	63.01	1.6414	14.9574	-
	(mole)	0.0250	3.5006	0.0045	0.3274	-
Salen doped	(g)	5.2165	63.20	1.6413	14.9570	-
	(mole)	0.0250	3.5111	0.0045	0.3247	2.24×10^{-3}
Saltn doped	(g)	5.1901	62.97	1.6395	14.9615	-
	(mole)	0.0249	3.4983	0.0045	0.3248	1.63×10^{-3}
Haen doped	(g)	5.2029	63.00	1.6407	14.9386	-
	(mole)	0.0250	3.5000	0.0045	0.3243	2.10×10^{-3}

The calculation of organic matter contents in each modified silica is shown below:

V.1.1.1 Non-doped silica

TEOS 0.0250 mole provided SiO₂ 0.0250 mole = $0.0250 \times 60.0843 = 1.5021$ g

CTAB 0.0045 mole provided CTA⁺ 0.0045 mole = $0.0045 \times 284.56 = 1.2805$ g

The mass of non-doped silica = $1.5021 + 1.2805 = 2.7826$ g

Therefore, the percentage of organic matters in non-doped silica

$$= (1.2805/2.7806) \times 100 = 46.05 \%$$

V.1.1.2 Salen doped silica

TEOS 0.0250 mole provided SiO₂ 0.0250 mole = $0.0250 \times 60.0843 = 1.5021$ g

CTAB 0.0045 mole provided CTA⁺ 0.0045 mole = $0.0045 \times 284.56 = 1.2805$ g

The amount of salen in silica = $2.24 \times 10^{-3} \times 268.32 = 0.6010$ g

The organic matters in salen doped silica = $1.2805 + 0.6010 = 1.8815$ g

The mass of salen doped silica = $1.5021 + 1.2805 + 0.6010 = 3.3836$ g

Therefore, the percentage of organic matters in salen doped silica

$$= (1.8815/3.3836) \times 100 = 55.61 \%$$

V.1.1.3 Saltn doped silica

TEOS 0.0249 mole provided SiO₂ 0.0249 mole = $0.0249 \times 60.0843 = 1.5021$ g

CTAB 0.0045 mole provided CTA⁺ 0.0045 mole = $0.0045 \times 284.56 = 1.2805$ g

The amount of saltn in silica = $1.63 \times 10^{-3} \times 282.34 = 0.4602$ g

The organic matters in saltn doped silica = $1.2805 + 0.4602 = 1.7407$ g

The mass of saltn doped silica = $1.5021 + 1.2805 + 0.4602 = 3.2428$ g

Therefore, the percentage of organic matters in saltn doped silica

$$= (1.7407/3.2428) \times 100 = 53.67 \%$$

V.1.1.4 Haen doped silica

TEOS 0.0250 mole provided SiO₂ 0.0250 mole = $0.0250 \times 60.0843 = 1.5021$ g

CTAB 0.0045 mole provided CTA⁺ 0.0045 mole = $0.0045 \times 284.56 = 1.2805$ g

The amount of haen in silica = $2.10 \times 10^{-3} \times 296.36 = 0.6223$ g

The organic matters in haen doped silica = $1.2805 + 0.6223 = 1.9028$ g

The mass of haen doped silica = $1.5021 + 1.2805 + 0.6223 = 3.4049$ g

Therefore, the percentage of organic matters in haen doped silica

$$= (1.9028/3.4049) \times 100 = 55.88 \%$$

V.1.2 Mesoporous silica synthesized from Calcined mesoporous silica

Table V.2 The amount of starting materials for the synthesis of silica using calcined mesoporous silica as silica precursor

Modified silica		Starting materials				
		Calcined silica	H ₂ O	CTAB	EtOH	Incorporated Schiff's base
Non-doped	(g)	1.5075	63.01	1.6443	14.9613	-
	(mole)	0.0251	3.5006	0.0045	0.3248	-
Salen doped	(g)	1.5063	63.04	1.6405	15.0001	-
	(mole)	0.0251	3.5022	0.0045	0.3256	1.83×10^{-3}
Saltn doped	(g)	1.4989	63.02	1.6437	14.9745	-
	(mole)	0.0249	3.5011	0.0045	0.3250	7.17×10^{-4}
Haen doped	(g)	1.5069	63.04	1.6418	14.9520	-
	(mole)	0.0251	3.5022	0.0045	0.3245	2.09×10^{-3}

The calculation of organic matter contents in each modified silica is shown below:

V.1.2.1 Non-doped silica

Calcined mesoporous silica 1.5075 g provided SiO₂ = 1.5075 g

CTAB 0.0045 mole provided CTA⁺ 0.0045 mole = 0.0045×284.56 = 1.2805 g

The mass of non-doped silica = $1.5075 + 1.2805$ = 2.7880 g

Therefore, the percentage of organic matters in non-doped silica

$$= (1.2805/2.7880) \times 100 = 45.93 \%$$

V.1.2.2 Salen doped silica

Calcined mesoporous silica 1.5063 g provided SiO₂ = 1.5063 g

CTAB 0.0045 mole provided CTA⁺ 0.0045 mole = 0.0045×284.56 = 1.2805 g

The amount of salen in silica = $1.83 \times 10^{-3} \times 268.32$ = 0.4910 g

The organic matters in salen doped silica = $1.2805 + 0.4910$ = 1.7706 g

The mass of salen doped silica = $1.5063 + 1.2805 + 0.4910$ = 3.2778 g

Therefore, the percentage of organic matters in salen doped silica

$$= (1.7706/3.2778) \times 100 = 54.01 \%$$

V.1.2.3 Saltn doped silica

Calcined mesoporous silica 1.4989 g provided SiO₂ = 1.4989 g

$$\begin{aligned}
 \text{CTAB } 0.0045 \text{ mole provided CTA}^+ 0.0045 \text{ mole} &= 0.0045 \times 284.56 = 1.2805 \text{ g} \\
 \text{The amount of saltn in silica} &= 7.17 \times 10^{-4} \times 282.34 = 0.2024 \text{ g} \\
 \text{The organic matters in saltn doped silica} &= 1.2805 + 0.2024 = 1.4829 \text{ g} \\
 \text{The mass of saltn doped silica} &= 1.4989 + 1.2805 + 0.2024 = 2.9818 \text{ g} \\
 \text{Therefore, the percentage of organic matters in saltn doped silica} &= (1.4829/2.9818) \times 100 = 49.73 \%
 \end{aligned}$$

V.1.2.4 Haen doped silica

$$\begin{aligned}
 \text{Calcined mesoporous silica } 1.5069 \text{ g provided SiO}_2 &= 1.5069 \text{ g} \\
 \text{CTAB } 0.0045 \text{ mole provided CTA}^+ 0.0045 \text{ mole} &= 0.0045 \times 284.56 = 1.2805 \text{ g} \\
 \text{The amount of haen in silica} &= 2.09 \times 10^{-3} \times 296.36 = 0.6193 \text{ g} \\
 \text{The organic matters in haen doped silica} &= 1.2805 + 0.6193 = 1.8998 \text{ g} \\
 \text{The mass of haen doped silica} &= 1.5069 + 1.2805 + 0.6193 = 3.4067 \text{ g} \\
 \text{Therefore, the percentage of organic matters in haen doped silica} &= (1.8998/3.4067) \times 100 = 55.76 \%
 \end{aligned}$$

V.1.3 Mesoporous silica synthesized from silica gel 60

Table V.3 The amount of starting materials for the synthesis of silica using silica gel 60 as silica precursor

Modified silica		Starting materials				
		silica gel 60	H ₂ O	CTAB	EtOH	Incorporated Schiff's base
Non-doped	(g)	1.5073	63.01	1.6426	14.9936	-
	(mole)	0.0251	3.5006	0.0045	0.3255	-
Salen doped	(g)	1.5071	63.01	1.6422	14.9969	-
	(mole)	0.0250	3.5006	0.0045	0.3255	9.67×10^{-4}
Saltn doped	(g)	1.5084	63.03	1.6434	14.9774	-
	(mole)	0.0251	3.5017	0.0045	0.3251	2.90×10^{-4}
Haen doped	(g)	1.4859	62.91	1.6417	15.0100	-
	(mole)	0.0247	3.4950	0.0045	0.3258	7.77×10^{-4}

The calculation of organic matter contents in each modified silica is shown below:

V.1.3.1 Non-doped silica

Silica gel 60 1.5073 g provided SiO₂ = 1.5073 g

CTAB 0.0045 mole provided CTA⁺ 0.0045 mole = 0.0045 x 284.56 = 1.2805 g

The mass of non-doped silica = 1.5073 + 1.2805 = 2.7878 g

Therefore, the percentage of organic matters in non-doped silica
= (1.2805/2.7878) x 100 = 45.93 %

V.1.3.2 Salen doped silica

Silica gel 60 1.5071 g provided SiO₂ = 1.5071 g

CTAB 0.0045 mole provided CTA⁺ 0.0045 mole = 0.0045 x 284.56 = 1.2805 g

The amount of salen in silica = 9.67 x 10⁻⁴ x 268.32 = 0.2596 g

The organic matters in salen doped silica = 1.2805 + 0.2596 = 1.5401 g

The mass of salen doped silica = 1.5071 + 1.2805 + 0.2596 = 3.0482 g

Therefore, the percentage of organic matters in salen doped silica
= (1.5401/3.0482) x 100 = 50.52 %

V.1.3.3 Saltn doped silica

Silica gel 60 1.5084 g provided SiO₂ = 1.5084 g

CTAB 0.0045 mole provided CTA⁺ 0.0045 mole = 0.0045 x 284.56 = 1.2805 g

The amount of saltn in silica = 2.91 x 10⁻⁴ x 282.34 = 0.0821 g

The organic matters in saltn doped silica = 1.2805 + 0.0821 = 1.3626 g

The mass of saltn doped silica = 1.5084 + 1.2805 + 0.0821 = 2.8710 g

Therefore, the percentage of organic matters in saltn doped silica
= (1.3626/2.8710) x 100 = 47.46 %

V.1.3.4 Haen doped silica

Silica gel 60 1.4859 g provided SiO₂ = 1.4859 g

CTAB 0.0045 mole provided CTA⁺ 0.0045 mole = 0.0045 x 284.56 = 1.2805 g

The amount of haen in silica = 7.77 x 10⁻⁴ x 296.36 = 0.2304 g

The organic matters in haen doped silica = 1.2805 + 0.2304 = 1.5109 g

The mass of haen doped silica = 1.4859 + 1.2805 + 0.2304 = 2.9968 g

Therefore, the percentage of organic matters in haen doped silica
= (1.5109/2.9968) x 100 = 50.41 %

V.2 The silica synthesized from TEOS and co-precursors

The calculation of organic matters contents in these materials are calculated according to the equations 2.2-2.5.

V.2.1 Mesoporous silica synthesized from TEOS and VTES

Table V.4 The amount of starting materials for the synthesis of silica using TEOS and VTES as silica precursors

Modified silica		Starting materials					
		TEOS	VTES	H ₂ O	CTAB	EtOH	Incorporated Schiff's base
Non-doped	(g)	5.1994	1.0219	63.01	1.6423	14.9663	-
	(mole)	0.0250	0.0063	3.5006	0.0045	0.3249	-
Salen doped	(g)	5.2151	1.2212	63.00	1.6427	14.9632	-
	(mole)	0.0250	0.0064	3.5000	0.0045	0.3248	2.28×10^{-3}
Salt n doped	(g)	5.2213	1.1949	62.98	1.6425	14.9772	-
	(mole)	0.0251	0.0063	3.4989	0.0045	0.3251	1.51×10^{-3}
Haen doped	(g)	5.2105	1.2001	63.05	1.6373	14.9637	-
	(mole)	0.0250	0.0063	3.5028	0.0045	0.3248	2.04×10^{-3}

The calculation of organic matter contents in each modified silica is shown below:

V.2.1.1 Non-doped silica

$$\text{TEOS } 0.0250 \text{ mole provided SiO}_2 \text{ } 0.0250 \text{ mole} = 0.0250 \times 60.0843 = 1.5021 \text{ g}$$

$$\begin{aligned} \text{VTES } 0.0063 \text{ mole provided CH}_2\text{=CHSiO}_{1.5} \text{ } 0.0063 \text{ mole} \\ = 0.0063 \times 79.1308 = 0.4997 \text{ g} \end{aligned}$$

$$\text{CTAB } 0.0045 \text{ mole provided CTA}^+ \text{ } 0.0045 \text{ mole} = 0.0045 \times 284.56 = 1.2805 \text{ g}$$

$$\text{The mass of non-doped silica} = 1.5021 + 0.4997 + 1.2805 = 3.3823 \text{ g}$$

$$\begin{aligned} \text{Therefore, the percentage of organic matters in non-doped silica} \\ = (1.2805/3.2823) \times 100 = 39.01. \% \end{aligned}$$

V.2.1.2 Salen doped silica

$$\text{TEOS } 0.0250 \text{ mole provided SiO}_2 \text{ } 0.0250 \text{ mole} = 0.0250 \times 60.0843 = 1.5021 \text{ g}$$

$$\begin{aligned} \text{VTES } 0.0064 \text{ mole provided CH}_2\text{=CHSiO}_{1.5} \text{ } 0.0064 \text{ mole} \\ = 0.0064 \times 79.1308 = 0.5077 \text{ g} \end{aligned}$$

$$\text{CTAB } 0.0045 \text{ mole provided CTA}^+ \text{ } 0.0045 \text{ mole} = 0.0045 \times 284.56 = 1.2805 \text{ g}$$

The amount of salen in silica $= 2.28 \times 10^{-3} \times 268.32 = 0.6118 \text{ g}$
 The organic matters in salen doped silica $= 1.2805 + 0.6118 = 1.8923 \text{ g}$
 The mass of salen doped silica $= 1.5021 + 0.5077 + 1.2805 + 0.6118 = 3.9021 \text{ g}$
 Therefore, the percentage of organic matters in salen doped silica
 $= (1.8923/3.9021) \times 100 = 48.49 \%$

V.2.1.3 Saltn doped silica

TEOS 0.0251 mole provided SiO_2 0.0251 mole $= 0.0250 \times 60.0843 = 1.5081 \text{ g}$
 VTES 0.0063 mole provided $\text{CH}_2=\text{CH}-\text{SiO}_{1.5}$ 0.0063 mole
 $= 0.0063 \times 79.1308 = 0.4968 \text{ g}$
 CTAB 0.0045 mole provided CTA^+ 0.0045 mole $= 0.0045 \times 284.56 = 1.2805 \text{ g}$
 The amount of saltn in silica $= 1.51 \times 10^{-3} \times 282.34 = 0.4263 \text{ g}$
 The organic matters in saltn doped silica $= 1.2805 + 0.4263 = 1.7068 \text{ g}$
 The mass of saltn doped silica $= 1.5081 + 0.4968 + 1.2805 + 0.4263 = 3.7117 \text{ g}$
 Therefore, the percentage of organic matters in saltn doped silica
 $= (1.7068/3.7117) \times 100 = 45.98 \%$

V.2.1.4 Haen doped silica

TEOS 0.0250 mole provided SiO_2 0.0250 mole $= 0.0250 \times 60.0843 = 1.5021 \text{ g}$
 VTES 0.0063 mole provided $\text{CH}_2=\text{CH}-\text{SiO}_{1.5}$ 0.0063 mole
 $= 0.0063 \times 79.1308 = 0.4989 \text{ g}$
 CTAB 0.0045 mole provided CTA^+ 0.0045 mole $= 0.0045 \times 284.56 = 1.2805 \text{ g}$
 The amount of haen in silica $= 2.04 \times 10^{-3} \times 296.36 = 0.6045 \text{ g}$
 The organic matters in haen doped silica $= 1.2805 + 0.6045 = 1.8851 \text{ g}$
 The mass of haen doped silica $= 1.5021 + 0.4989 + 1.2805 + 0.6045 = 3.8861 \text{ g}$
 Therefore, the percentage of organic matters in haen doped silica
 $= (1.8851/3.8861) \times 100 = 48.51 \%$

V.2.2 Mesoporous silica synthesized from TEOS and PTMS

Table V.5 The amount of starting materials for the synthesis of silica using TEOS and PTMS as silica precursors

Modified silica		Starting materials					
		TEOS	PTMS	H ₂ O	CTAB	EtOH	Incorporated Schiff's base
Non-doped	(g)	5.2183	1.0412	62.97	1.6418	14.9927	-
	(mole)	0.0250	0.0063	3.4983	0.0045	0.3254	-
Salen doped	(g)	5.2090	1.0436	62.99	1.6425	14.9771	-
	(mole)	0.0250	0.0064	3.4994	0.0045	0.3251	2.02×10^{-3}
Saltn doped	(g)	5.2181	1.0494	62.96	1.6426	14.9760	-
	(mole)	0.0250	0.0064	3.4978	0.0045	0.3251	1.12×10^{-3}
Haen doped	(g)	5.2150	1.0420	63.04	1.6441	14.9939	-
	(mole)	0.0250	0.0063	3.5022	0.0045	0.3255	2.15×10^{-3}

The calculation of organic matter contents in each modified silica is shown below:

V.2.2.1 Non-doped silica

$$\text{TEOS } 0.0250 \text{ mole provided SiO}_2 \text{ } 0.0250 \text{ mole} = 0.0250 \times 60.0843 = 1.5021 \text{ g}$$

$$\text{PTMS } 0.0063 \text{ mole provided CH}_3(\text{CH}_2)_2\text{SiO}_{1.5} \text{ } 0.0063 \text{ mole} \\ = 0.0063 \times 95.1729 = 0.6032 \text{ g}$$

$$\text{CTAB } 0.0045 \text{ mole provided CTA}^+ \text{ } 0.0045 \text{ mole} = 0.0045 \times 284.56 = 1.2805 \text{ g}$$

$$\text{The mass of non-doped silica} = 1.5021 + 0.6032 + 1.2805 = 3.3858 \text{ g}$$

$$\text{Therefore, the percentage of organic matters in non-doped silica} \\ = (1.2805/3.3858) \times 100 = 37.81 \%$$

V.2.2.2 Salen doped silica

$$\text{TEOS } 0.0250 \text{ mole provided SiO}_2 \text{ } 0.0250 \text{ mole} = 0.0250 \times 60.0843 = 1.5021 \text{ g}$$

$$\text{PTMS } 0.0064 \text{ mole provided CH}_3(\text{CH}_2)_2\text{SiO}_{1.5} \text{ } 0.0064 \text{ mole} \\ = 0.0064 \times 95.1729 = 0.6046 \text{ g}$$

$$\text{CTAB } 0.0045 \text{ mole provided CTA}^+ \text{ } 0.0045 \text{ mole} = 0.0045 \times 284.56 = 1.2805 \text{ g}$$

$$\text{The amount of salen in silica} = 2.02 \times 10^{-3} \times 268.32 = 0.5420 \text{ g}$$

$$\text{The organic matters in salen doped silica} = 1.2805 + 0.5420 = 1.8225 \text{ g}$$

$$\text{The mass of salen doped silica} = 1.5021 + 0.6046 + 1.2805 + 0.5420 = 3.9292 \text{ g}$$

Therefore, the percentage of organic matters in salen doped silica

$$= (1.8225/3.9292) \times 100 = 46.38 \%$$

V.2.2.3 Saltn doped silica

TEOS 0.0250 mole provided SiO₂ 0.0250 mole = 0.0250 x 60.0843 = 1.5021 g

PTMS 0.0064 mole provided CH₃-CH₂-CH₂-SiO_{1.5} 0.0064 mole
= 0.0064 x 95.1729 = 0.6080 g

CTAB 0.0045 mole provided CTA⁺ 0.0045 mole = 0.0045 x 284.56 = 1.2805 g

The amount of saltn in silica = 1.12 x 10⁻³ x 282.34 = 0.3162 g

The organic matters in saltn doped silica = 1.2805 + 0.3162 = 1.5967 g

The mass of saltn doped silica = 1.5021 + 0.6080 + 1.2805 + 0.3162 = 3.7068 g

Therefore, the percentage of organic matters in saltn doped silica

$$= (1.5967 / 3.7068) \times 100 = 43.07 \%$$

V.2.2.4 Haen doped silica

TEOS 0.0250 mole provided SiO₂ 0.0250 mole = 0.0250 x 60.0843 = 1.5021 g

PTMS 0.0063 mole provided CH₃-CH₂-CH₂-SiO_{1.5} 0.0063 mole
= 0.0063 x 95.1729 = 0.6037 g

CTAB 0.0045 mole provided CTA⁺ 0.0045 mole = 0.0045 x 284.56 = 1.2805 g

The amount of haen in silica = 2.15 x 10⁻³ x 296.36 = 0.6371 g

The organic matters in haen doped silica = 1.2805 + 0.6371 = 1.9177 g

The mass of haen doped silica = 1.5021 + 0.6037 + 1.2805 + 0.6371 = 4.0235 g

Therefore, the percentage of organic matters in haen doped silica

$$= (1.9177 / 4.0235) \times 100 = 47.66 \%$$

V.2.3 Mesoporous silica synthesized from TEOS and ETES

Table V.6 The amount of starting materials for the synthesis of silica using TEOS and ETES as silica precursors

Modified silica		Starting materials					
		TEOS	ETES	H ₂ O	CTAB	EtOH	Incorporated Schiff's base
Non-doped	(g)	5.2185	1.2386	63.01	1.6391	14.6478	-
	(mole)	0.0250	0.0064	3.5006	0.0045	0.3179	-
Salen doped	(g)	5.2166	1.2270	63.01	1.6411	14.9550	-
	(mole)	0.0250	0.0064	3.5006	0.0045	0.3246	2.12×10^{-3}
Salt doped	(g)	5.2306	1.2338	63.01	1.6360	14.9417	
	(mole)	0.0251	0.0064	3.5006	0.0045	0.3243	1.14×10^{-3}
Haen doped	(g)	5.2249	1.2343	63.03	1.6337	14.9509	
	(mole)	0.0250	0.0064	3.5017	0.0045	0.3245	2.16×10^{-3}

The calculation of organic matter contents in each modified silica is shown below:

V.2.3.1 Non-doped silica

TEOS 0.0250 mole provided SiO₂ 0.0250 mole = 0.0250 x 60.0843 = 1.5021 g

ETES 0.0064 mole provided CH₃CH₂SiO_{1.5} 0.0064 mole
= 0.0064 x 81.1461 = 0.5226 g

CTAB 0.0045 mole provided CTA⁺ 0.0045 mole = 0.0045 x 284.56 = 1.2805 g

The mass of non-doped silica = 1.5021 + 0.5226 + 1.2805 = 3.3052 g

Therefore, the percentage of organic matters in non-doped silica
= (1.2805/3.3052) x 100 = 38.74 %

V.2.3.2 Salen doped silica

TEOS 0.0250 mole provided SiO₂ 0.0250 mole = 0.0250 x 60.0843 = 1.5021 g

ETES 0.0064 mole provided CH₃CH₂SiO_{1.5} 0.0064 mole
= 0.0064 x 81.1461 = 0.5177 g

CTAB 0.0045 mole provided CTA⁺ 0.0045 mole = 0.0045 x 284.56 = 1.2805 g

The amount of salen in silica = $2.12 \times 10^{-3} \times 268.32 = 0.5688$ g

The organic matters in salen doped silica = 1.2805 + 0.5688 = 1.8493 g

The mass of salen doped silica = 1.5021 + 0.5177 + 1.2805 + 0.5688 = 3.8691 g

Therefore, the percentage of organic matters in salen doped silica

$$= (1.8493/3.8691) \times 100 = 47.80 \%$$

V.2.3.3 Saltn doped silica

TEOS 0.0251 mole provided SiO₂ 0.0251 mole = 0.0251 x 60.0843 = 1.5081 g

ETES 0.0064 mole provided CH₃-CH₂-SiO_{1.5} 0.0064 mole

$$= 0.0064 \times 81.1461 = 0.5206 \text{ g}$$

CTAB 0.0045 mole provided CTA⁺ 0.0045 mole = 0.0045 x 284.56 = 1.2805 g

The amount of saltn in silica = 1.15 x 10⁻³ x 282.34 = 0.3246 g

The organic matters in saltn doped silica = 1.2805 + 0.3246 = 1.6052 g

The mass of saltn doped silica = 1.5081 + 0.5206 + 1.2805 + 0.3246 = 3.6338 g

Therefore, the percentage of organic matters in saltn doped silica

$$= (1.6052 / 3.6338) \times 100 = 44.17 \%$$

V.2.3.4 Haen doped silica

TEOS 0.0250 mole provided SiO₂ 0.0250 mole = 0.0250 x 60.0843 = 1.5021 g

ETES 0.0064 mole provided CH₃-CH₂-SiO_{1.5} 0.0064 mole

$$= 0.0064 \times 81.1461 = 0.5208 \text{ g}$$

CTAB 0.0045 mole provided CTA⁺ 0.0045 mole = 0.0045 x 284.56 = 1.2805 g

The amount of haen in silica = 2.16 x 10⁻³ x 296.36 = 0.6401 g

The organic matters in haen doped silica = 1.2805 + 0.6401 = 1.9206 g

The mass of haen doped silica = 1.5021 + 0.5208 + 1.2805 + 0.6401 = 3.9435 g

Therefore, the percentage of organic matters in haen doped silica

$$= (1.9206 / 3.9435) \times 100 = 48.70 \%$$

CURRICULUM VITAE

Kanokkarn Skulnee was born on November 18, 1977 in Bangkok, Thailand. She received a Bachelor's degree of Science, majoring in Chemistry from Chulalongkorn University in 2000. Since 2004, she has been a graduate student studying in Program of Petrochemistry and polymer Science, Faculty of Science, Chulalongkorn University, Bangkok, Thailand. Her current address is 641 M. 8 T. Bangpumai A. Murang Samutprakarn.